



THE UNIVERSITY OF QUEENSLAND
A U S T R A L I A

**Trajectory Optimisation of a Partially-Reusable
Rocket-Scramjet-Rocket Small Satellite Launch System**

Sholto O. Forbes-Spyratos

B.Eng. (Mechanical and Aerospace) (Hons. I) & B.Sc. (Physics)

A thesis submitted for the degree of Doctor of Philosophy at
The University of Queensland in 2018

School of Mechanical Engineering
Centre for Hypersonics

Abstract

Declaration by author

This thesis is composed of my original work, and contains no material previously published or written by another person except where due reference has been made in the text. I have clearly stated the contribution by others to jointly-authored works that I have included in my thesis.

I have clearly stated the contribution of others to my thesis as a whole, including statistical assistance, survey design, data analysis, significant technical procedures, professional editorial advice, and any other original research work used or reported in my thesis. The content of my thesis is the result of work I have carried out since the commencement of my research higher degree candidature and does not include a substantial part of work that has been submitted to qualify for the award of any other degree or diploma in any university or other tertiary institution. I have clearly stated which parts of my thesis, if any, have been submitted to qualify for another award.

I acknowledge that an electronic copy of my thesis must be lodged with the University Library and, subject to the policy and procedures of The University of Queensland, the thesis be made available for research and study in accordance with the Copyright Act 1968 unless a period of embargo has been approved by the Dean of the Graduate School.

I acknowledge that copyright of all material contained in my thesis resides with the copyright holder(s) of that material. Where appropriate I have obtained copyright permission from the copyright holder to reproduce material in this thesis.

Publications during candidature

Journal papers

Sholto O. Forbes-Spyratos, Michael P. Kearney, Michael K. Smart, and Ingo H. Jahn. “Trajectory Design of a Rocket-Scramjet-Rocket Multi-Stage Launch System”. In: *Journal of Spacecraft and Rockets - Under Consideration* TBD (2018)

Conference papers

S.O. Forbes-Spyratos, M.P. Kearney, M.K. Smart, and I.H. Jahn. “Trajectory design of a rocket-scramjet-rocket multi-stage launch system”. In: *21st AIAA International Space Planes and Hypersonics Technologies Conference, Hypersonics 2017*. Xiamen, China, 2017. ISBN: 9781624104633

Publications included in this thesis

This thesis comprises partly of publications, as allowed by University of Queensland Policy PPL 4.60.07. The papers that have been included have all been published in peer reviewed journals at the time of submission.

make this table more compact

Sholto O. Forbes-Spyratos, Michael P. Kearney, Michael K. Smart, and Ingo H. Jahn. “Trajectory Design of a Rocket-Scramjet-Rocket Multi-Stage Launch System”. In: *Journal of Spacecraft and Rockets - Under Consideration* TBD (2018)

Contributor	Contribution
Sholto O. Forbes-Spyratos	Performed simulations (%)
	Analysis of results (%)
	Wrote and edited paper (%)
Ingo H. Jahn	Analysis of results (%)
Michael P. Kearney	Analysis of results (%)
Michael K. Smart	Analysis of results (%)
	Wrote and edited paper (%)

Contributions by Others to the Thesis

Except for the contributions by others to publications above, there are no contributions by others to this thesis.

Statement of Parts of the Thesis Submitted to Qualify for the Award of Another Degree

None.

Acknowledgements

Keywords

keyword, keyword, keyword, keyword, keyword

Australian and New Zealand Standard Research Classification (ANZSRC)

ANZSRC code: 090107 Hypersonic Propulsion and Hypersonic Aerodynamics, 20%

ANZSRC code: 090106 Flight Dynamics, 20%

ANZSRC code: 090108, Satellite, Space Vehicle and Missile Design and Testing, 20%

ANZSRC code: 090104 Aircraft Performance and Flight Control Systems , 20%

ANZSRC code: 010303 Optimisation , 20%

Fields of Research (FoR) Classification

FoR code: 0901, Aerospace Engineering, 100%

CONTENTS

List of figures	xv
List of tables	xvii
1 Introduction	1
1.1 Research aims	3
1.2 Thesis outline	4
2 Literature review	7
2.1 Scramjets	7
2.2 Reusable Satellite Launch Systems	8
2.2.1 Small Satellite Launchers	9
2.2.2 Airbreathing Access to Space Systems	14
2.2.3 Small Airbreathing Launchers	15
2.3 The SPARTAN	16
2.3.1 Scramjet Engine Model	17
2.4 First Stage Rocket Booster	17
2.5 Exoatmospheric Rocket Engines	18
2.6 Partially-Airbreathing Launch Vehicle Ascent Trajectories	20
2.6.1 Single-Stage Vehicles	21
2.6.2 Multi-Stage Vehicles	22
2.7 Hypersonic Vehicle Flyback Trajectories	24
2.7.1 Examples of Optimised Fly-Back Trajectories	25
2.8 Optimal Control	28
2.8.1 The Single Shooting Method	30

CONTENTS

2.8.2	The Multiple Shooting Method	30
2.8.3	The Pseudospectral Method	32
2.8.4	Pseudospectral Examples	35
2.8.5	Available Solvers	36
2.9	Aerodynamic Analysis	38
2.9.1	HYPAERO	38
2.9.2	CART3D	39
2.9.3	Missile DATCOM	41
2.10	Summary	41
3	Launch Vehicle Design and Simulation	43
3.1	Second Stage Scramjet	46
3.1.1	The SPARTAN Accelerator	46
3.1.2	Propulsion	46
3.1.3	The Aerodynamics of the SPARTAN	49
3.2	First Stage Rocket	57
3.2.1	Aerodynamics Including First Stage	58
3.3	Third Stage Rocket - Baseline	59
3.3.1	Heat Shield Sizing	61
3.3.2	Fuel Tank Sizing	63
3.3.3	The Aerodynamics of the Third Stage Rocket	64
4	LODESTAR	67
4.1	Optimal Control	68
4.1.1	GPOPS-2 Example - Brachistochrone Problem	69
4.2	The Trajectory Optimal Control Problems	70
4.2.1	Dynamic Model	70
4.2.2	Trajectory Connection Points	71
4.2.3	First Stage Trajectory	73
4.2.4	Second Stage Trajectory	73
4.2.5	Second Stage Return Trajectory	76
4.2.6	Third Stage Trajectory	77
4.2.7	Combined Second Stage Ascent & Return Trajectory	77
4.2.8	Validation	77
5	Trajectories Involving Flyback	79
5.1	Flyback trajectories	79
5.2	Sensitivity Analysis	79

6 Full Trajectory Optimisation	81
7 Third Stage Sizing Study	87
7.1 Third Stage Sizing	87
8 Conclusions	89
8.1 Recommendations for future work	89
Library	91
A CART3D Results	99
A.1 Engine-On Plume Check	99
A.2 CART3D Results	99

LIST OF FIGURES

1.1	The scramjet-powered second stage of the SPARTAN CITATIONXX.	3
2.1	scramjet-CITE hypersonic airbreathing propulsion	7
2.2	Characteristic performance for airbreathing and rocket engines with Mach number[Fry2004].	8
2.3	cite blue origin	10
2.4	10
2.5	http://www.dailymail.co.uk/sciencetech/article-5361789/Ride-Elon-Musks-Starman-travels-space.html	11
2.6	The SKYLON spaceplane [70].	14
2.7	The airbreathing vehicle flight corridor [56].	15
2.8	An early design of the socket-scramjet-rocket launch system incorporating the SPARTAN [26].	16
2.9	The C-RESTM10 propulsion database, specific impulse.	18
2.10	An example of a constant gain PID controller, controlling the SPARTAN trajectory around a 50kPa dynamic pressure design point [46].	20
2.11	21
2.12	Powell	21
2.13	22
2.14	Wilhite	22
2.15	a) Airbreathing b) Airbreathing/Rocket	23
2.16	The trajectory of the launch system developed by Tsuchiya and Mori [68]	23
2.17	23
2.18	The trajectory of the launch system developed by Mehta and Bowles [37].	23
2.19	The flight path of a glide-back booster, developed by Tetlow et al. CITEXX.	26
2.20	The flight path of a powered fly-back booster, developed by Tetlow et al. CITEXX.	26

LIST OF FIGURES

2.21	28
2.22	An illustration of the subdivision associated with multiple shooting [38]. Dashed lines illustrate the initial trajectory guess and the solid line indicates the final trajectory once the joining conditions are met.	31
2.23	36
2.24	HYPAERO analysis surface grid [26].	38
2.25	SPARTAN aerodynamics, developed using HYPAERO [48].	39
2.26	The Skylon spaceplane, simulated using CART3D at Mach 12.189, $\alpha = 7.512^\circ$ [36]. Cell distribution produced by mesh adaption is shown.	40
3.1	The launch process of the rocket-scramjet-rocket launch system, presented in simplified form.	44
3.2	The rocket-scramjet-rocket launch system, top view, showing the SPARTAN and first stage.	45
3.3	The rocket-scramjet-rocket launch system, side view, showing the SPARTAN and fuel tanks, along with the third and first stages.	45
3.4	The locations of conditions relevant to C-REST engine simulation.	47
3.5	Flow conditions after the conical shock generated by the vehicle nose cone. Figure a) shows the Mach number, b) shows the pressure ratio, and c) shows the temperature ratio following the conical shock.	48
3.6	Specific impulse of the CRESTM10 engines with input temperature and Mach number. Available data points are indicated.	49
3.7	Operable equivalence ratio of the CRESTM10 engines with input temperature and Mach number. Available data points are indicated.	50
3.8	SPARTAN model showing control surfaces. Dimensions to be included.	51
3.9	The forces on the SPARTAN during flight.	51
3.10	Flap deflection required for trim of the SPARTAN. Negative up. Change colourmap to have same range	53
3.11	Process for generating aerodynamic databases.	54
3.12	Surface triangulation of the Baseline SPARTAN. Need to recolour this image.	55
3.13	Pointwise view of the SPARTAN showing engine outlet boundaries.	56
3.14	Engine-on CART3D simulation at Mach 7, 6° angle of attack, and 24km altitude. improve the quality of images - max quality when exporting from tecplot	57
3.15	Trimmed aerodynamic coefficients with the C-REST engines powered on. Coefficients correspond to a reference area of 62.77m^2 . NOTE: I need to run a new clic case for these plots without nozzle or boat tail	58
3.16	CART3D flow result for the SPARTAN, at Mach 7, 6° angle of attack.	59

3.17 Trimmed aerodynamic Characteristics of the SPARTAN with C-REST engine powered off. Coefficients correspond to a reference area of 62.77m^2	60
3.18 Unstarted scramjet engines. Placeholder Image, this will be improved.	61
3.19 CART3D result for the SPARTAN and first stage vehicles at Mach 2, -1° angle of attack.	61
3.20 Aerodynamic characteristics of the SPARTAN including the first stage rocket.	62
3.21 The third stage rocket, showing major internal features. note:labels to be added	62
3.22 Variation in coefficient of thrust with area ratio [64].	63
3.23 Aerodynamic characteristics of the baseline third stage rocket, for a reference area of 0.95m^2 .	65
3.24 Thrust vector force balance.	65
4.1	70
4.2	71
4.3	72
4.4	74
4.5	75
6.1	82
6.2	82
6.3	83
6.4	83
6.5	84
6.6	84
6.7	85
A.1	100
A.2 Mesh generated by CART3D around the SPARTAN and first stage vehicles.	100
A.3 CART3D flow result for the SPARTAN, at Mach 1.1, 6° angle of attack.	100
A.4 CART3D flow result for the SPARTAN, at Mach 3, 6° angle of attack.	101

LIST OF TABLES

2.1	Comparison of upper stage rocket engines.	19
2.2	Summary of programs capable of pseudospectral optimisation.	37
3.1	Mass breakdown of the modified SPARTAN vehicle.	46
3.2	First Stage Engine Properties [CITATIONXX].	59
3.3	Third stage heat shield breakdown.	63
3.4	Third stage fuel distribution.	64
4.1	72

CHAPTER 1

INTRODUCTION

focus on objectives and chapter outlines, give to Kearney to review first for thesis review - 1 page dot point with where im up to -refer to stated objectives from mid cand

In recent years, the space sector has seen a significant shift in the paradigm of space launch system design. The sector has moved towards privatisation, with new and innovative launch systems competing to offer the most cost-efficient and reliable launches. The sector has also seen a split between those who produce large or small satellite launchers. For large payload launchers, reusability is a major focus in the design of new launch systems, with the purpose of making a launch system cost efficient over multiple launches. For small payload launchers, reusability is more complex than for large launchers, as the additional systems necessary for reusability add a larger fraction of system mass, and require a proportionally larger fuel mass. Consequently, the focus of small launch system design is currently on producing expendable launch systems as cheaply and efficiently as possible, using state of the art technologies such as 3D printing to expedite the process. However, if reusability is able to be successfully integrated into small launch system design, it has the potential increase the cost efficiency and launch flexibility, potentially opening up the small satellite market significantly.

A potential candidate for integrating reusability into small satellite launch systems is the use of air-breathing engines. Airbreathing engines produce higher specific impulse than rockets, and require far less propellant to be carried on-board a launch vehicle. The use of airbreathing engines for reusability has particular applicability to small satellite launchers. The higher efficiency and reduced propellant mass of airbreathing vehicles allows the additional mass of the systems necessary for reusability to be mitigated. An airbreathing vehicle can be designed in a similar fashion to a conventional aircraft, with wings, stabilisers and ailerons.

The primary engines in consideration for launch vehicles are ramjet and scramjet engines. These engines offer good efficiency, and have operational regimes which allow them to effectively accelerate a launch vehicle over a range of Mach numbers. Ramjets and scramjets rely on the high velocity of

CHAPTER 1. INTRODUCTION

the aircraft to compress the flow of air entering the engine before combustion. Ramjets slow the air to subsonic speeds and are suited to operation at low Mach numbers, whereas scramjets keep the flow supersonic throughout, and operate within the hypersonic regime, above Mach 5. The strict operational regime of these engines means that a launch system cannot be solely powered by airbreathing engines. Rocket power is necessary for at least the exoatmospheric portion of the trajectory, and is necessary also to accelerate the ramjet or scramjet to minimum operational speed. As a result, the designs of airbreathing launch systems are necessarily partially-airbreathing, usually separated into multiple stages to increase weight efficiency.

The design of the trajectory of a partially-airbreathing launch system is extremely important to its performance. The airbreathing engines of a ramjet or scramjet-powered stage require high dynamic pressure to operate effectively, and airbreathing engines are generally designed for high lift-to-drag. Conversely, rocket-powered stages produce more thrust at higher altitude, and are generally designed for weight efficiency. For these launch systems, the various stages and engines involved during launch require trade-offs in engine efficiency and thrust generation, stage mass, and vehicle aerodynamics. These factors require the launch trajectory of the system to be thoroughly simulated and optimised, to ensure that the launch vehicle is operating effectively.

Calculating the optimal trajectory for a space launch system is an integral part of the preliminary vehicle and mission design process. An optimal trajectory calculated without predispositions can offer valuable insights into the performance of a launch vehicle, and drive future design decisions. Calculating the optimal trajectory profile for a launch system typically requires the use of optimal control theory. Optimal control theory is a general set of techniques which find a control law to maximise a given metric of a system. For a launch vehicle, optimal control allows the best possible payload-to-orbit to be calculated in simulations during design. Optimal control theory allows a trajectory to be calculated in which the flight path of each individual vehicle is considered simultaneously to produce a maximum-payload trajectory. Optimal control is particularly important for launch systems incorporating airbreathing engines, where the performance of each vehicle is thoroughly different. Optimal control is able to produce an optimised trajectory which satisfies equality or inequality constraints. These constraints allow for the physical limitations of the vehicle, such as heating and structural loading limits, to be imposed. These constraints also allow any necessary mission conditions to be established, such as orbital velocity and fly-back.

This study applies optimal control theory to a three stage rocket-scramjet-rocket launch system being developed by The University of Queensland, designated The SPARTAN. This launch system is designed to be partially reusable, with at least the second stage scramjet vehicle flying back to the initial launch site. In previous studies it has been assumed that the optimal trajectory for the scramjet powered vehicle is at its maximum dynamic pressure and all other trajectory stages have conformed to this assumption. This study will develop an optimal trajectory profile for The SPARTAN, with the aim of producing an optimal trajectory profile which may be applied to any rocket-airbreathing-rocket

system for delivering small satellites to Earth orbit.



Figure 1.1: The scramjet-powered second stage of the SPARTAN CITATIONXX.

Add image of the final trajectory

1.1 Research aims

The overall aim of this thesis is to apply state of the art numerical optimisation techniques to the trajectory of a rocket-scramjet-rocket small satellite launch system. The purpose of this optimised trajectory is to maximise the payload-to-orbit capabilities of the launch system, thereby also maximising the cost efficiency of the system.

add more, flexibility, turn around time, operability

This will be achieved through the following objectives: IJ - not objectives, redo

1.

2.

3.

4.

1.2 Thesis outline

Chapter 2 - Literature Review

This chapter presents a review of literature related to the different aspects of this thesis. The theory behind scramjet propulsion is presented, followed by a background of reusable and small satellite launch systems. A review of the trajectories of partially-airbreathing launch systems is presented, comparing the optimised trajectories of various conceptual vehicles. An overview of optimal control theory is presented, with particular emphasis on the pseudospectral method of optimal control which is employed within this study. Lastly, an overview of the optimal control and aerodynamic solvers which are used in this study is presented.

Chapter 3 - Launch Vehicle Baseline Design

This chapter provides details of the design, aerodynamics and engine models of all three stages. The SPARTAN scramjet-powered stage is presented first, followed by the first and third stages, due to the external scramjet vehicle design being taken from prior work. The design of each stage is presented, followed by the propulsion model, and finally the aerodynamic characteristics.

Chapter 4 - LODESTAR

This chapter details the method used for the simulation and optimisation of the trajectory, packaged within the trajectory analysis program LODESTAR, which has been created for this study. The specifics of the optimal control methodology used are presented, along with relevant examples. The simulation methodology is detailed, along with the construction of the optimal control simulation. The specific set-up of the optimal control program is detailed for each trajectory stage, specifying the costs and constraints which drive the optimal control solver. Finally, the methods for validating the final solutions are specified.

Chapter 5 - Optimised Trajectory

This chapter presents the results of the trajectory optimised using LODESTAR. The ascent of the SPARTAN and third stage rocket are optimised along with the fly-back of the SPARTAN, for maximum payload-to-orbit.

Chapter 6 - Trajectory Sensitivity Study

Chapter 7 - Third Stage Sizing Study

Conclusions

The body of this thesis concludes by summarising the most significant findings from

CHAPTER 2

LITERATURE REVIEW

KEEP THIS SECTION AS BROAD AS POSSIBLE

This chapter examines the relevant literature associated with the different aspects of the work conducted as part of this thesis.

Explain order of literature and what was examined.

2.1 Scramjets

make this section more general , move discussion of launchers later

explain mechanisms

add research exploring min/max speeds - expected thrust / Isp

point of section - understanding expected performance of scramjets

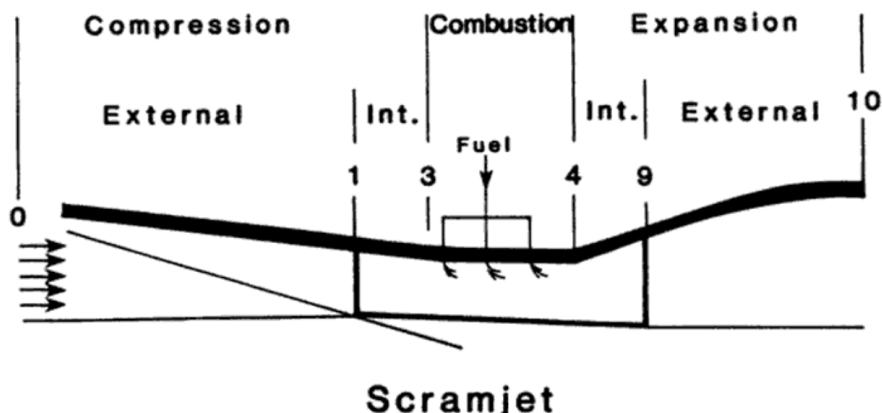


Figure 2.1: scramjet-CITE hypersonic airbreathing propulsion

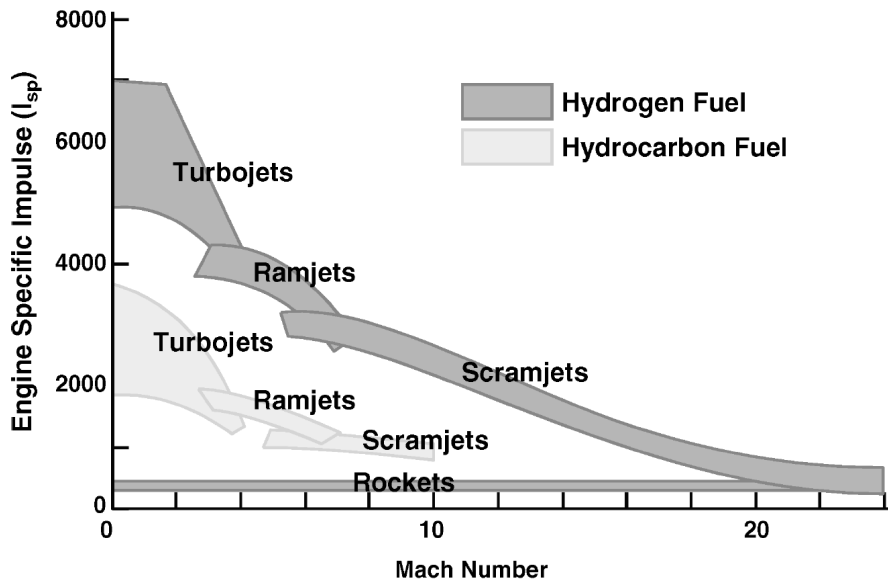


Figure 2.2: Characteristic performance for airbreathing and rocket engines with Mach number[Fry2004].

A Scramjet, or supersonic combustion ramjet, is an airbreathing engine design which combusts air at supersonic speeds and is capable of high Mach number operation. Scramjets compress air without moving parts, using geometry changes within the engine [Curran2001a], as well as on the forebody of the vehicle to create inlet shocks which provide the compression required for combustion[Smart2012]. This is similar in operation to a ramjet engine, however a scramjet does not generate a normal shock, allowing supersonic air to enter the combustor. Maintaining supersonic speeds throughout the engine allows scramjets to operate efficiently at Mach numbers of 5 and greater, with a large operable range. Scramjets were proposed in the 1940's [11] and found to be capable of positive net thrust in 1993 [44] but have yet to be developed to a level which would allow for commercial application.

Scramjets offer much higher specific impulse than rockets over their operating range [6] [10].

2.2 Reusable Satellite Launch Systems

Launch system technologies have progressed rapidly over the last 60 years. From the early vehicles based on intercontinental ballistic missile technology such as the Thor based launch systems, capable of launching 40-400kg to LEO in the 1960s, to the more modern Atlas V based systems of the 2000s capable of launching 9750-18500kg to LEO <http://www.aerospace.org/crosslinkmag/spring-2010/launch-vehicles-then-and-now-50-years-of-evolution/>. The materials, propulsion technology, aerodynamics and guidance algorithms have all improved significantly, enabling rockets to become more efficient, cheaper to produce, and more reliable. As the demand for satellite launches grows, and the cost of development of launchers becomes cheaper, the potential for profiting from space launches

increases. This has driven a large portion of the space flight industry to move towards privatisation, with a heavy focus on reusable technology.

Reusing launch vehicles allows the cost-over-time of the reused components to be reduced drastically, which subsequently allows the cost of individual launches to be reduced. Reduced costs minimises the barrier of entry for space launches, improving the diversity of space-based enterprises. Reusing launch system components also allows faster turnaround times for launches, as refurbishment of stages is much faster than manufacturing stages from scratch. Reduced turnaround times are key for improving mission scheduling, allowing satellites to be launched sooner, on a more flexible time frame.

Reusable launch technology is the focus of many of the largest private launch companies. The SpaceX Falcon 9 and Falcon Heavy have been demonstrated on multiple occasions, landing booster stages successfully, and re-flying reused boosters multiple times. In the near future the Blue Origin New Glenn is planned, with potentially the Airbus Adeline to follow (to be used on the Ariane 6).

For a launch vehicle to be reusable, it must necessarily have the ability to come back to Earth safely, without damage to major system components. This return flight requires the addition of system components which allow the reusable stage to fly to a specified landing point. Control surfaces, structural components, additional fuel, and in the case of the Adeline, additional engines, must be incorporated within a reusable launch vehicle design. The additional weight that these components contribute further increases the fuel and structural mass necessary to initially accelerate the reusable stage. The impact of reusability on the mass and cost of the vehicle is minimised when the stage is larger, and when the velocity at the initiation of the return trajectory is decreased. Because of this mass increase on any stage which is to be designed to be reusable, most current reusable launch vehicle designs include only reusable first stages, with later stages being expendable.

The structural mass fraction of a rocket stage increases as the gross mass decreases. This means that the additional mass necessary for reusability will have a larger effect on a small launch system. Due to this, many of the current developments in small satellite launch systems are focussed on expendable rockets.

2.2.1 Small Satellite Launchers

What point do I want to make in this section?-tie in to other launchers and reusability-point out gaps in technology ie reusable small satellite launchers

Too commercial - reframe in a more scientific way ie advancing human knowledge. cover alternate approaches.-i think focus on reusability-compare capability to similarly sized launchers

The vast improvements in computational technologies in recent years have allowed satellites to decrease in size and cost to a large degree. These factors have lowered the barrier of entry into small satellite manufacturing significantly, driving a surge in the demand for small satellite launches. Many

CHAPTER 2. LITERATURE REVIEW

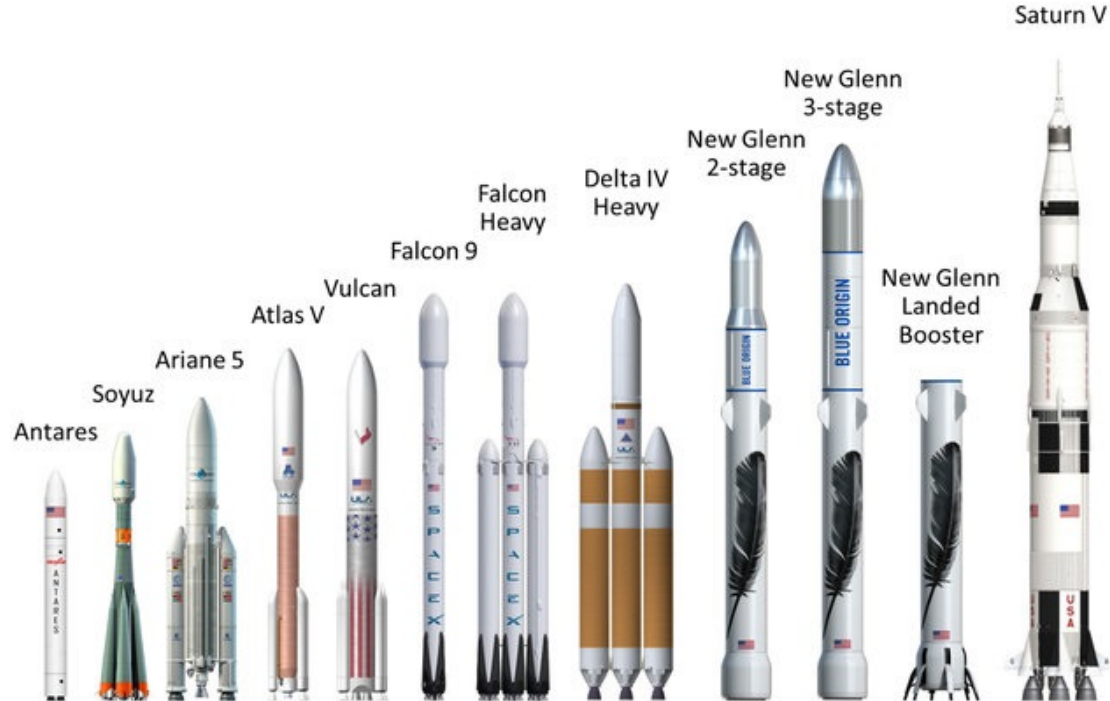


Figure 2.3: cite blue origin

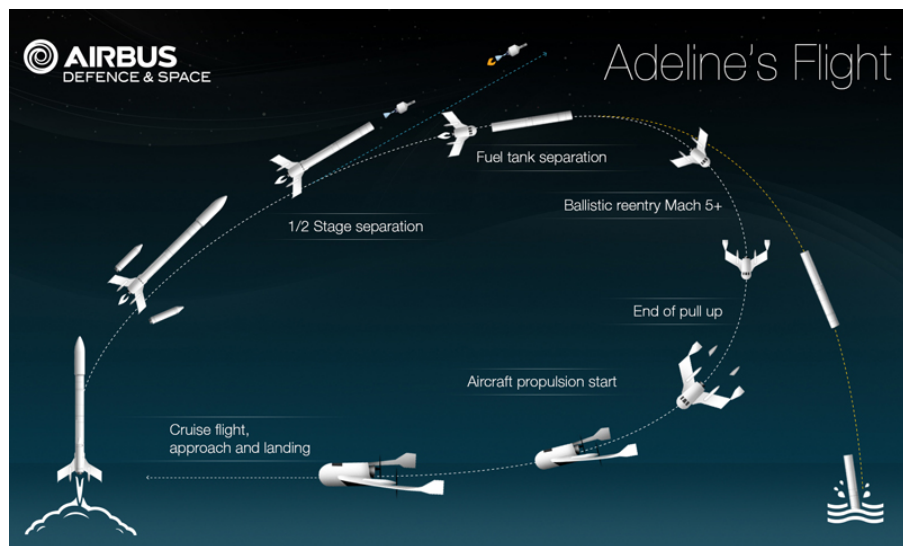


Figure 2.4

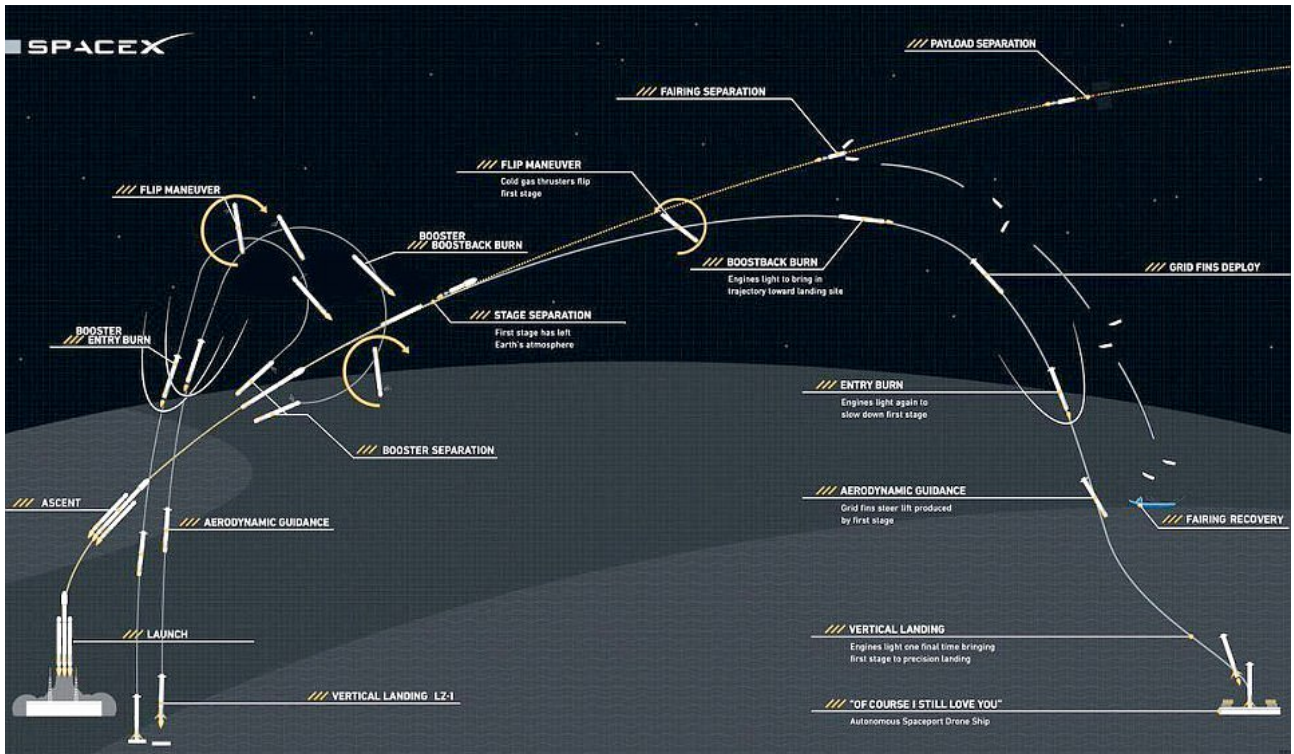


Figure 2.5: <http://www.dailymail.co.uk/sciencetech/article-5361789/Ride-Elon-Musks-Starman-travels-space.html>

private and public companies are currently developing small satellite launchers to tap into this new market. These organisations are currently developing launchers to offer bespoke launches with low costs and relatively rapid turn around times. A summary of the small satellite launchers currently in active development is shown in Table ?? . Many of these launchers are projected to be available within the next few years, and will offer cost-per-kg comparable to piggybacking on larger launches.

The majority of the small satellite launchers in development are non-reusable. Non-reusable small satellite launch systems aim to reduce costs by creating a launch system which is as cost-efficient as possible to produce and launch. This generally entails making use of conventional, well-tested designs, combined with state of the art manufacturing techniques, such as 3-D printing. This method allows for rapid development, although it has an intrinsic cost limit due to the requirement of manufacturing a new launch system for each launch. Reusable small satellite launchers have far higher initial development costs, but also have the potential for large advantages in the long term. Reusable small satellite launchers have the potential for lower cost-per-launch than expendable systems, with increased launch flexibility. However, for small satellite systems, novel approaches are required for reusability. It is notable that the launchers with re-use capabilities are entirely within the early stages of development, with no currently projected completion dates.

Much of the market niche fulfilled by each launch system is determined by the payload to orbit capabilities of the vehicle. Although the launchers shown are all classed as 'small satellite launchers',

organisations seeking a launch service will choose a launcher which is designed to launch payloads of comparable size to their desired payload, for maximum cost efficiency. There is a large variation in the payload-to-orbit capabilities of the small satellite launchers in development, ranging between 50kg to 500kg. The rocket-scramjet-rocket system studied in this thesis will target approximately 150kg of payload to orbit, most similar to the Vector-H[71], Haas2CA[3], Bloostar[74] and Electron[51].

The majority of the small satellite launch systems have projected launch costs between \$20000-\$40000USD/kg. The outlier is the Haas2CA[3], developed by ARCA, which has the ambitious target of \$10000USD/kg. The Haas2CA is a single stage to orbit launcher, powered by a hydrogen peroxide/kerosene aerospike engine.

Launcher	Company	Country	Payload Capacity	Cost/Kg (USD)	Availability	Stages & Propulsion	Reusability
Electron [51]	RocketLab	NZ/USA	150Kg to SSO	\$32,600	Available	Rocket-rocket	No
Lynx [1]	XCOR	USA	-	-	-	rocket-rocket	First stage
LauncherOne [72]	Virgin Orbit	UK	300kg to SSO	\$33,000	-	Aircraft-rocket-rocket	Aircraft
Bloostar [74]	Zero2Infinity	Spain	100kg to SSO	\$40,000	-	Balloon-rocket-rocket-rocket	No
XS-1 [43]	Boeing	USA	-	-	-	-	First Stage
Eris [21]	Gilmour Space Technologies	Aus/SG	380kg to LEO	\$23,000-38,000	Q4 2020		No
Black Arrow 2 [25]	Horizon	UK	350kg to SSO	-	2019	Rocket-rocket	No
Haas 2CA [3]	ARCA	USA	100Kg to LEO	\$10,000	2018	Rocket	No
Intrepid-1 [52]	Rocket Crafters	USA	376kg to SSO	\$23,936	Q1 2019	Rocket-rocket	No
KZ-1A [31]	CASIC	China	250kg to SSO	-	-	Rocket-rocket	No
500R [42]	Orbital Access	UK	500kg to SSO	-	-	Aircraft-Rocket	Fully Reusable
Vector-H [71]	Vector Space Systems	USA	160kg to LEO	\$21,875	2018	rocket-rocket-(third rocket optional)	No
SMILE [32]	NLR	EU	50kg	<\$50,000	-	-	-

2.2.2 Airbreathing Access to Space Systems

-need to generalise this section and add more

The possibility of using airbreathing stages in access to space systems has been studied in some detail. These systems have been investigated in various forms including; single stage[45, 73, 70], dual stage [68][37] and tri stage [48] designs. The most prominent of the airbreathing access to space systems currently in development is the SKYLON Spaceplane being developed by Reaction Engines Limited [69]. The SKYLON is a spaceplane which utilises SABRE, a combined cycle airbreathing rocket propulsion system potentially reusable for 200 flights, and is being developed to deliver payloads on the order of 2800kg to heliosynchronous orbit [24].



Figure 2.6: The SKYLON spaceplane [70].

A single stage design has the advantage of being fully contained within one vehicle, which is convenient for reusability and return trajectories however it has been suggested by Smart & Tetlow [58] that these designs suffer from severe limitations as they must contain multiple engines which add mass at later stages of the trajectory and decrease the efficiency of the vehicle. Smart & Tetlow suggest that multistage systems offer significant improvements in payload mass fractions, and have the advantage of using airbreathing stages only within their operable range. Dual stage designs have been investigated in some detail using the 'spaceplane' concept by Mehta & Bowles [37] using life cycle cost analysis in order to take flexibility and reusability into account. Mehta & Bowles conclude that a two stage design is the optimal configuration for reusable hypersonic space access systems, however this study is only based on comparison with single stage to orbit systems, and it is more useful to consider their conclusions as an endorsement of multi stage airbreathing designs in general. They find that multi stage vehicles have higher potential for payload than single stage to orbit (SSTO) systems and have less propellant requirements, partly due to a greater atmospheric cruise capability.

make the point that all of the proposed launchers are large, but that scramjets are easily scalable and efficient at small scales, connect with the next section

2.2.3 Small Airbreathing Launchers

Figure 2.7 shows the operating corridor for scramjet engines, indicating the point at which transition to rocket stage would occur, the lower dynamic pressure limit on engine operation and the upper dynamic pressure limit on the aircraft structure.

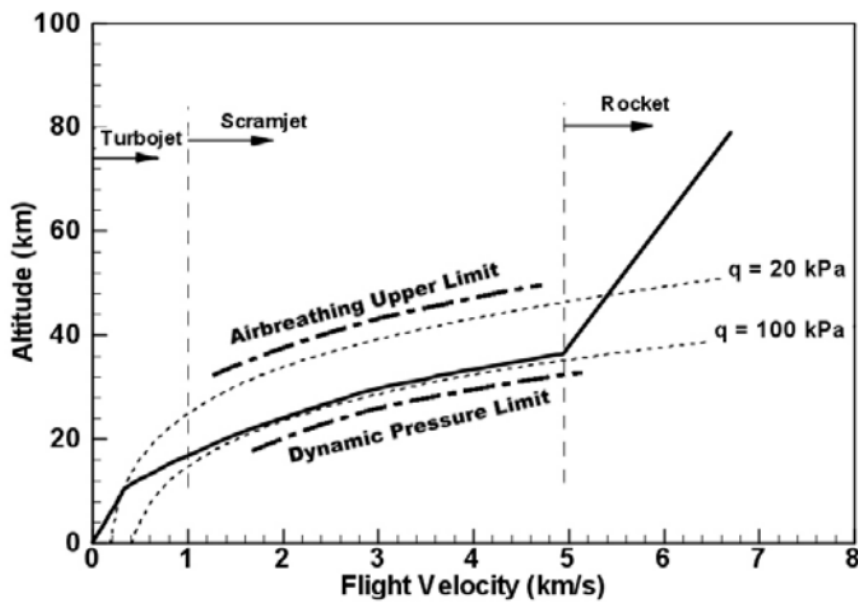


Figure 2.7: The airbreathing vehicle flight corridor [56].

Smart & Tetlow [58] have found that the fuel savings achieved by using a scramjet engine within these limits, coupled with small necessary payload mass, may enable the development of a partially or fully reusable space access system utilising a scramjet powered stage in the near future. Simulations carried out for three stage systems utilising scramjet and rocket engines for small payload delivery show favourable payload mass fractions with a reusable scramjet stage [58]. Scramjet powered vehicles may also offer the ability to put small payloads into orbit with greatly increased flexibility and launch window when compared to similarly sized rocket systems. This has been assessed in a study by Flaherty [18] comparing the United States Air Force's Reusable Military Launch System all-rocket launch vehicle RMLS102 against the Alliant Techsystems rocket/scramjet launch system ATK-RBCC. These vehicles are similarly sized and comparisons were made for payloads launched to rendezvous with satellites in randomly generated orbits. These vehicles were compared using the range of orbital trajectories that each vehicle was able to rendezvous with within one day, determined by launch vehicle range. The rocket/scramjet ATK-RBCC was found to have a large advantage in trajectory flexibility over the rocket only vehicle, in a large part due to the scramjets ability to fly

fuel efficiently over long distances. **put in some quantitative data abot this study** This means in general that a partially scramjet powered accelerator is able to fulfil the specific delivery needs of small payloads over a wider range of orbits within smaller time periods when compared to a fully rocket powered accelerator. This can be advantageous for time critical and orbit dependant payloads which have specific mission requirements to be met.

2.3 The SPARTAN

reorder until after trajectory of 1,2,3 stage vehicles

The three stage, partially reusable, access to space system under development at The University of Queensland utilises the SPARTAN[26] scramjet powered vehicle as the reusable second stage, shown in Figure 2.8. This system is considered in this study as a representative model for three stage, air-breathing access to space system designs. This launch system is designed for small payload deliveries to orbit and will in the future utilise a fly-back rocket booster to accelerate the SPARTAN stage to minimum Mach number required for stable burn, at which point separation occurs and the second stage uses a scramjet engine to accelerate to between approximately Mach 5-9. The first and second stages are to be reusable, the first stage via conversion into a propeller powered drone, and the second stage through either a glide or extra scramjet powered flight to a suitable landing site. **However, the first stage booster considered in this study is a simple disposable design. The ascent profile is of interest to this study, however development of the fly-back trajectory profile requires detailed first stage vehicle design which is outside of the scope of this study. DONT MIX LIT REVIEW AND STUDY**

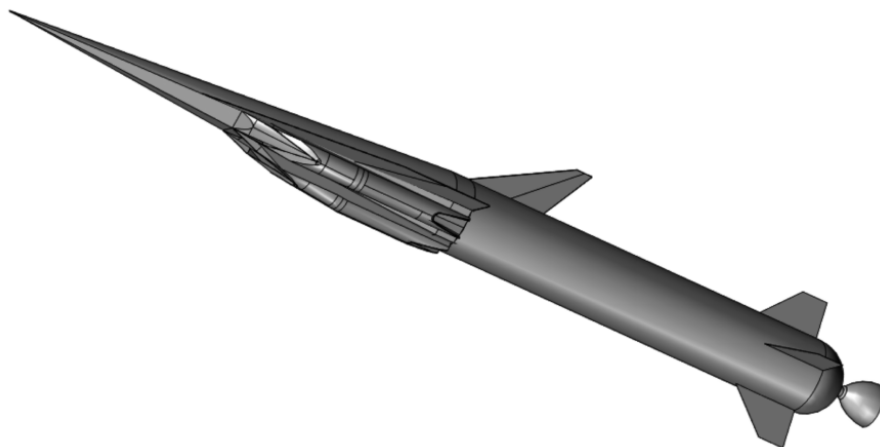


Figure 2.8: An early design of the socket-scramjet-rocket launch system incorporating the SPARTAN [26].

The third stage will be a disposable rocket stage, which will then deliver the payload to orbit, exiting the atmosphere and performing a Hohmann transfer.

This system is in the preliminary design stage, with estimates of payload mass fraction indicating that 1.26% PMF is possible when delivering a 257.4kg payload to low earth orbit [47]. This compares well with existing space systems of similar size, with the advantage of being designed for reusability. The second stage vehicle has been designed to a detailed level, and optimised for payload delivery to heliosynchronous orbit.

The SPARTAN has been studied in some detail, simulated over a constant dynamic pressure trajectory with variation in the aerodynamic surface properties of the vehicle.

2.3.1 Scramjet Engine Model

Much more info, how is off design performance calculated, what model is used.

To deliver a payload to orbit, the SPARTAN uses four Rectangular-to-Elliptical Shape Transition (REST) scramjet engines, with inlets configured to allow installation on a conical forebody. This study uses engines configured to fly between Mach 5 and 10, this type of engine is known as a C-RESTM10 engine[48]. The REST model has been studied experimentally for flight at off design conditions by Smart & Ruf [57]. The REST engine has been used as it has been proven to operate successfully at off-design conditions, an extremely important property for this study as the scramjet stage experiences a range of Mach number flight conditions, and significant variation in dynamic pressure.

A propulsion database of the C-RESTM10 has been provided for this study by Prof. Michael Smart.

2.4 First Stage Rocket Booster

review engine options and modelling/scaling techniques

The SPARTAN scramjet vehicle must be accelerated to its minimum operating speed by a first stage rocket booster. This booster must be capable of efficient operation from launch at sea level until staging. It is envisioned that the SPARTAN system will eventually use a reusable flyback booster[48]. However the flyback of the first stage is outside the scope of this study. Instead, a model of an existing first stage booster will be used, for which the Falcon-1e was chosen.

The SpaceX Falcon-1e launch system was a proposed small satellite launch system which would have entered use after 2010[60], but was discontinued and superseded by the Falcon-9 project. The Falcon-1e was designed to launch payloads between 600-900kg to low Earth orbit, with flexible orbit altitude and inclination. The Falcon-1e was to be the next generation of the Falcon-1[60], a launch tested, modern launch system.

The Falcon-1e was chosen for its appropriate size and the proven flight effectiveness of the Falcon-1. The first stage of the Falcon-1e is powered by a Merlin 1C LOX/Kerosene turbopump engine. The

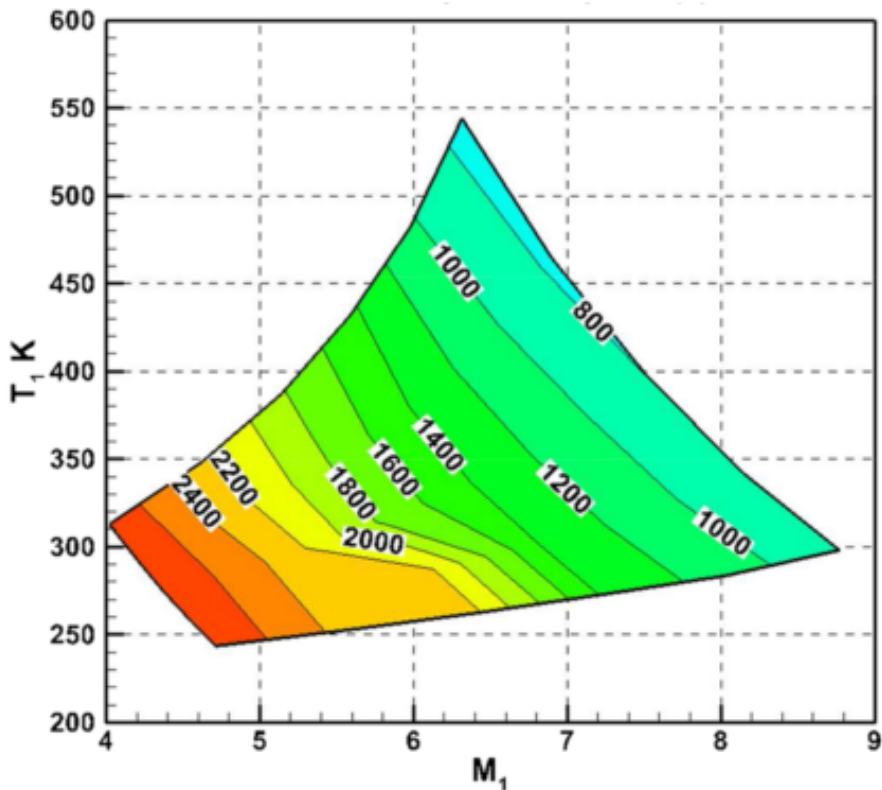


Figure 2.9: The C-RESTM10 propulsion database, specific impulse.

first stage rocket is designed to be a Falcon-1e first stage scaled lengthwise to 50% of its original length. REMOVE THIS - do not describe design in lit review

2.5 Exoatmospheric Rocket Engines

expand this to include control of third stage, identify losses/penalties

After scramjet stage burnout, the upper stage rocket must exit the atmosphere, and accelerate the payload to orbital velocity. This requires a rocket engine with sufficient thrust to accelerate the third stage rocket out of the atmosphere, and a diameter small enough to allow the rocket to fit within the fuselage of the SPARTAN. Table 2.1 shows a comparison study of upper stage rocket engines.

Engine	Fuel Supply	Fuel	Thrust	Isp	Mass	Diameter	Length	Thrust Vector Capability
Aestus	Pressure-fed	MMH/NTO	27.5kN	320s	110kg	1.27m	2.2m	4° & 4° by mechanical adjustment
OMS	Pressure-fed	MMH/NTO	26.7kN	316s	118kg	1.168m	1.956m	8°
Aestus II	Pump-fed	MMH/NTO	46kN	337.5s	148		2.2m	6°
RS-72	Pump-fed	MMH/NTO	55.4kN	338s	154kg		2.286	6°
ATE	Pump-fed	MMH/NTO	20kN	345s	57.9kg	0.38m	1.4m	15°
AJ10-118K	Pressure-fed	A-50/NTO	43.3kN	320.5s	124.5kg	1.53m	2.7m	Fixed
Kestrel	Pressure-fed	LOX/Kerosene	30.7kN	317	52kg	1.1m	1.9m	Yes, Unknown limits
R1-10-3A								

Table 2.1: Comparison of upper stage rocket engines.

2.6 Partially-Airbreathing Launch Vehicle Ascent Trajectories

discuss trim - investigated by Dawid

Current simulations of the SPARTAN vehicle have been carried out with the assumption of a 50kpa dynamic pressure trajectory, a likely design point of the vehicle and scramjet engine. Constant dynamic pressure trajectories have been used for airbreathing vehicle simulation due to the trade-off between structural loading and engine performance for hypersonic vehicles [41]. As dynamic pressure increases so does the structural loading on the vehicle, however scramjet thrust is directly reliant on dynamic pressure ie. an increase in dynamic pressure directly means more air into the engine inlet. A constant dynamic pressure is viewed as being an acceptable compromise between these two factors. This form of trajectory has so far been simulated using proportional integral derivative (PID) feedback control, directly investigated since 1998 by Olds & Budianto [41]. This is a simple and effective form of control for systems being simulated over a constant dynamic pressure path [46]. This form of control utilises minimises an error function as the vehicle moves along its trajectory. This error function causes the controls of the vehicle to be modified by a feedback term which is a function of the error including proportional, integral and derivative terms. The result is a trajectory which is suitably close to the objective design point, with minimal overshoot and steady state error which can cause oscillations around the specified design value. Figure 2.10 shows an example of a constant gain PID controller as applied to the SPARTAN vehicle being simulated to a design point of 50kPa dynamic pressure. Oscillations can be observed around the design point due to overshoot and steady state error, factors which are prevalent in PID control systems.

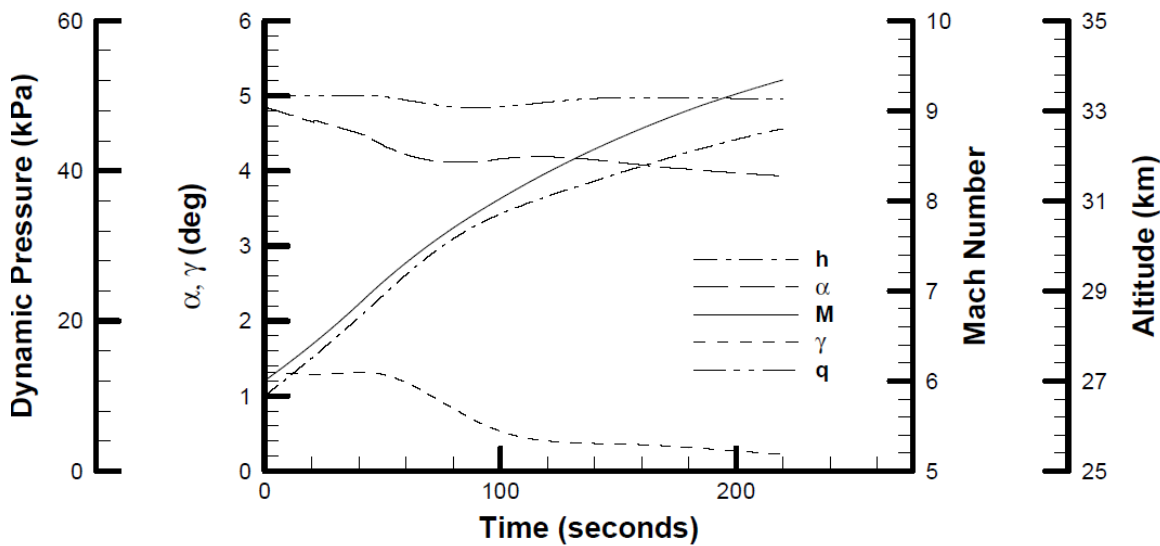


Figure 2.10: An example of a constant gain PID controller, controlling the SPARTAN trajectory around a 50kPa dynamic pressure design point [46].

It is possible that a constant dynamic pressure trajectory may not be the most appropriate trajectory

for the second stage vehicle, as there is a variety of aerodynamic factors that must be considered in designing optimal payload to orbit flight. It may be optimal for the vehicle to fly at less than maximum dynamic pressure at point throughout the trajectory, most likely at the first to second and second to third stage separation points. For a constant dynamic pressure trajectory the second-third stage transition will occur at a very low trajectory angle. This is suboptimal for the third stage rocket, which needs to perform a large pull up manoeuvre at high dynamic pressure. Launching this system at higher angle or altitude may improve third stage fuel usage greatly, at a small cost to the second stage fuel, allowing a greater payload to be delivered to orbit.

2.6.1 Single-Stage Vehicles

Optimal trajectories have previously been developed for launch systems integrating airbreathing and rocket propulsion within single-stage-to-orbit (SSTO) vehicles [45, 34, 67]. These optimal trajectory studies found unanimously that a pull-up manoeuvre before the end of the airbreathing engine cut-off was the optimal flight path for the SSTO airbreathing-rocket vehicles being investigated. A pull-up was found to be optimal for vehicles where the rocket engines are not ignited until circularization altitude [45, 34] as well as vehicles where the rocket engine is ignited immediately after airbreathing engine cut-off [67]. For SSTO vehicles a pull-up manoeuvre is a simple trade-off between the altitude at airbreathing engine cut-off and the velocity achievable at cut-off. Due to the entire vehicle being lifted into orbit, this becomes a relatively simple problem of engine efficiency. The airbreathing engine is used for its high efficiency, until the dynamic pressure drops below the operable limit of the airbreathing engine, or until the thrust provided by the airbreathing engine is significantly counteracted by the effects of drag and gravity.

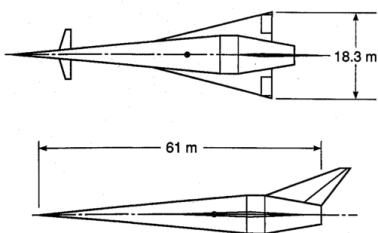


Figure 2.11

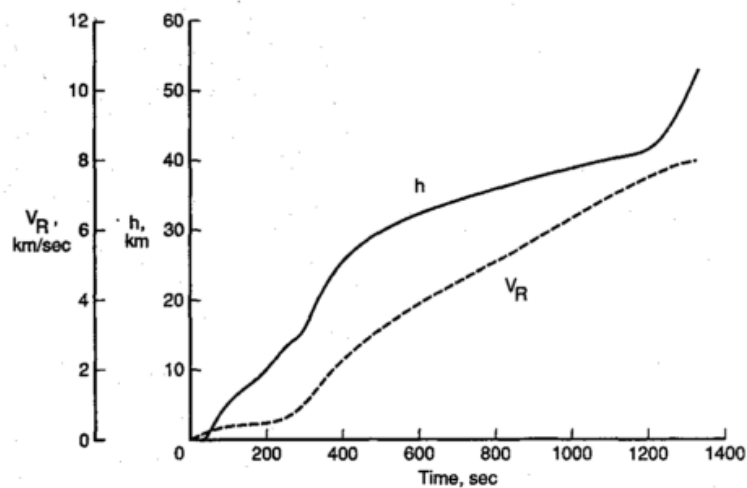


Figure 2.12: Powell

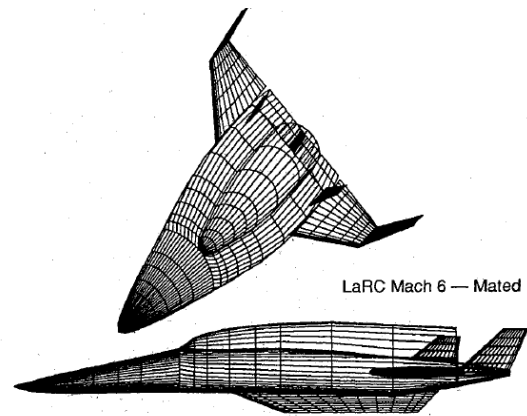


Figure 2.13

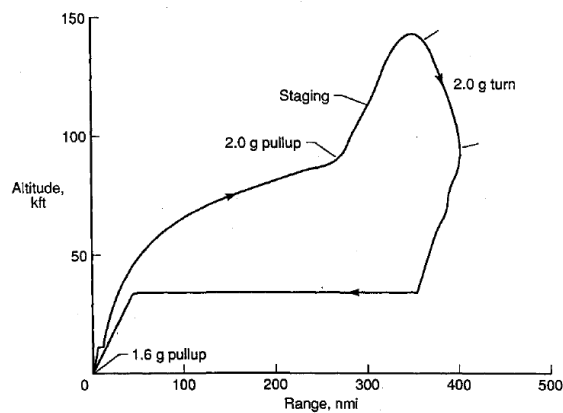


Figure 2.14: Wilhite

2.6.2 Multi-Stage Vehicles

For a multi-stage to orbit vehicle, calculating the optimal trajectory for maximum payload flight is significantly more difficult. A multi-stage vehicle has one or more stage transition points, where the vehicle separates a component which is discarded or reused later, and does not continue to orbit. At a stage transition point there is a large change in the mass and aerodynamics of the launch system. This change in flight dynamics makes finding the optimal stage transition point more complicated. To find the optimal separation point there is a trade-off between: I. The high efficiency of the scramjet engines, II. The thrust produced by the scramjet engines, III. The potential thrust of the rocket engines, IV. The energy necessary to increase the altitude of the scramjet stage, V. The aerodynamic efficiency when performing the required direction change. All of these factors must be considered in order to generate an optimal trajectory.

There has been a number of studies which have identified a pull-up manoeuvre as being advantageous for a multi-stage system [68, 73, 37]. However, in these studies a pull-up manoeuvre has been specified in order to decrease the dynamic pressure of the vehicle at airbreathing-rocket stage separation.

In the studies by Tsuchiya et al.[68] and Wilhite et al.[73], decreased dynamic pressure is necessary for the successful operation of the orbital rocket stages, of the systems under investigation. In these studies the airbreathing stages pull-up to the maximum allowable dynamic pressure for the rocket-powered orbital stages. When the orbital stages are able to operate, stage separation occurs. These pull-up manoeuvres demonstrate the advantages of a pull-up for the operation of the orbital stages, allowing the aerodynamic and thermal loading on the vehicle to be reduced. However these pull-up manoeuvres are not performed as part of optimal trajectories, instead they are designed to ensure that the performance constraints of the systems are met.

Mehta & Bowles [37] prescribe a 2g pull-up at flight conditions of Mach 10, 95000 ft for an airbreathing stage in order to "lower dynamic pressures and to achieve the optimal launching flight

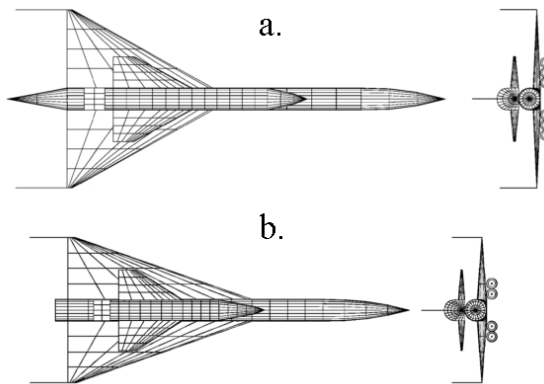


Figure 2.15: a) Airbreathing b) Airbreath- Rocket

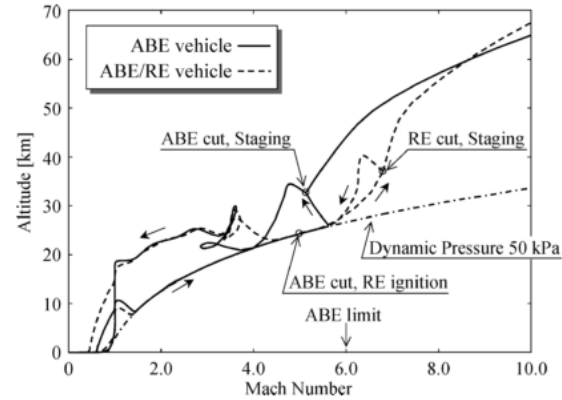


Figure 2.16: The trajectory of the launch system developed by Tsuchiya and Mori [68]



Figure 2.17

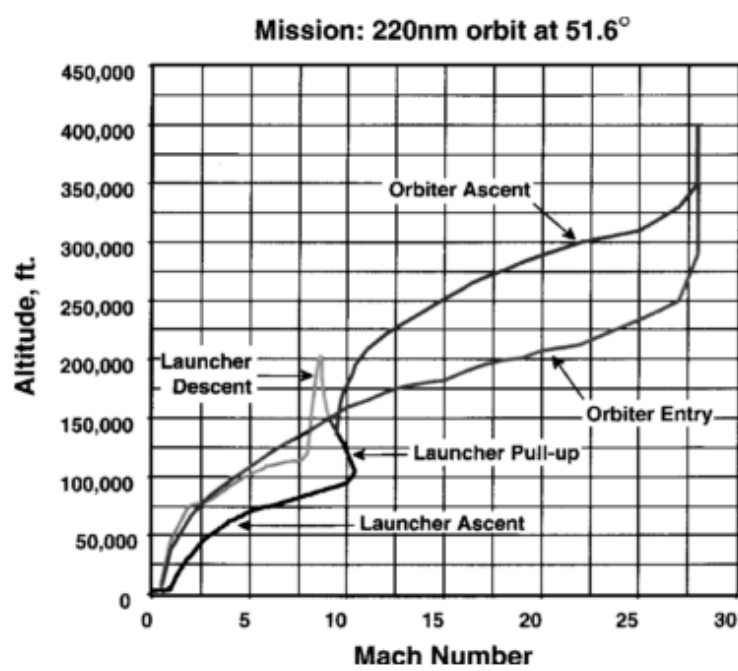


Figure 2.18: The trajectory of the launch system developed by Mehta and Bowles [37].

path angle for the orbiter vehicle”. This indicates that a pull-up manoeuvre before airbreathing-rocket transition is considered the optimal trajectory, however this study does not optimise the shape or magnitude of the pull-up manoeuvre, only considering the increased performance of the rocket vehicle.

2.7 Hypersonic Vehicle Flyback Trajectories

Past studies of the SPARTAN vehicle have assumed that a fly-back to launch site is possible after third stage separation[48]. However, this fly-back has not yet been simulated. A simulation of the fly-back of the SPARTAN is necessary in order to assess the viability of the SPARTAN concept. The fly-back of the SPARTAN is a crucial component to the viability of the rocket-scramjet-rocket launch system. The SPARTAN must return to the initial launch site to enable refurbishment to begin immediately, and so that there is no significant transportation of the SPARTAN required between launches. Due to the second-third stage staging velocity, it is complicated for the SPARTAN to cover the necessary fly-back distance. To maximise fuel efficiency, it is desirable for the SPARTAN to perform a minimum-fuel fly-back to the initial launch site, with the best-case scenario being for the fly-back to use no fuel at all.

There are three main methods that have been studied for potential hypersonic vehicle return; glide-back, cruise-back and boost-back. Glide-back involves the hypersonic vehicle returning to base and landing entirely using its aerodynamics. This requires sufficient lift to sustain the hypersonic vehicle over the entire return range, as well as the controllability to land the hypersonic vehicle in level flight. For a hypersonic trajectory a fully glide-back return flight is most likely unobtainable. This is due to the large downrange distance flown, and the large initial velocity at the beginning of the fly-back trajectory, when the vehicle is oriented away from the landing site. Multiple studies have investigated the maximum staging velocity allowable for the glide-back flight of a booster. In these studies, the maximum separation velocity for glide-back to be feasible has been found to be between Mach 3-4 at 30km-120km downrange distance, with higher initial velocities or longer downrange distances requiring fly-back under power[23, 65].

Cruise-back involves the inclusion of subsonic engines, which are used to power the fly-back of the hypersonic vehicle until landing similar to a conventional aircraft. These engines may be included solely for the fly-back[23], or used in the acceleration phase for low velocity acceleration[37, 65, 73]. The addition of subsonic engines powering a constant velocity cruise-back phase allows the accelerator to return to base with a similar trajectory to that of traditional aircraft, allowing the velocity and altitude of the accelerator to be precisely controlled. However, the addition of subsonic engines necessary for cruise-back increases the mass of the vehicle significantly, leading to decreased mass efficiency and increased design complexity[23].

A preferable mode of powered fly-back is to use the existing hypersonic airbreathing engines dur-

ing the return trajectory in a boost-back trajectory. Using the existing airbreathing engines allows for range to be added to the return trajectory, without the inclusion of additional engines. The hypersonic airbreathing engines can be operated at appropriate times during the fly-back, when they will be most impactful on the return trajectory range. However, the hypersonic airbreathing engines may only be used within their operating region, and vary in thrust and efficiency dependent on flight conditions. Hypersonic airbreathing engines have maximum efficiency at low Mach numbers[48], with the thrust produced depending on the dynamic pressure and inlet conditions, which vary with the trajectory path and angle of attack of the vehicle. This added complexity requires the use of trajectory optimisation methods to find the most efficient flight path for return to the launch site, and to ensure that the return of the vehicle under its own power is viable.

2.7.1 Examples of Optimised Fly-Back Trajectories

Tetlow et al. [65] compare powered cruise-back to glide-back flight for the return of the first stage booster of a rocket powered two-stage launch vehicle. The powered flyback vehicle uses airbreathing engines to cruise back to the launch site at relatively low speeds. The powered flyback and the glide-back cases are analysed separately to determine the difference in the optimal staging velocities. Figure 2 shows the optimised deceleration phase for the cruise-back vehicle, terminating at cruise-back conditions. This trajectory shows three distinct skips, with the minimum trajectory angle progressively decreasing between each. Tetlow et al. conclude that the 'skips' are due to the rate of density increase being greater than the deceleration rate 'causing increased lift and levelling out of the altitude profile'[65]. This trajectory was optimised for minimum cruise-back fuel mass, indicating that the 'skips' are the optimal trajectory shape to maximise range in high initial velocity fly-back. The powered cruise-back vehicle is able to stage at 3000m/s due to the ability to cover a large distance during cruise-back. The glide-back vehicle was optimised to find the maximum possible staging velocity at which a turn and glide-back is still possible. This was found to be at 1200m/. Figure 3 shows the corresponding optimal deceleration trajectory, terminating at sustainable glide conditions. This trajectory again shows multiple skips. The low allowable separation velocity of 1200m/s for the glide-back booster potentially suggests that the SPARTAN will require powered flyback. Tetlow et al. assume an admittedly optimistic L/D of 7 at Mach 0.9, and maximum angle of attack of 40 deg. However, the mass of the vehicle in this study is up to 1182 tons. A lower L/D may be acceptable for a lighter vehicle.

A maximum staging velocity at which glide-back is possible is also investigated by Hellman [23]. Hellman uses a suboptimal, scheduled trajectory simulation to investigate the flyback capabilities of a reusable rocket booster. Hellman finds that Mach 3 is the upper staging limit for a glide-back booster. This agrees with Tetlow et al. that high staging velocities are not possible for glide-back boosters, suggesting that the SPARTAN will require powered return flight.

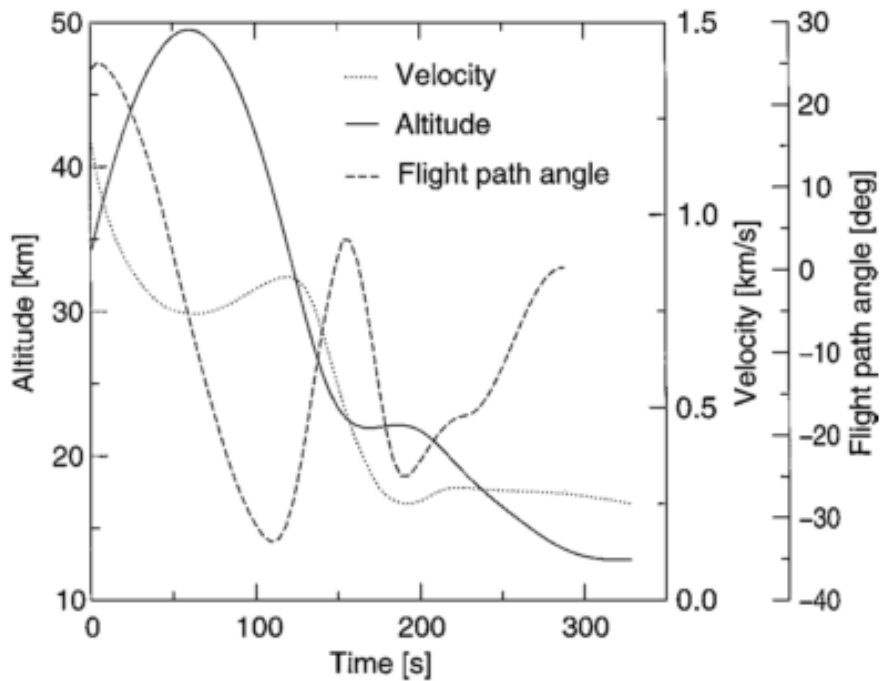


Figure 2.19: The flight path of a glide-back booster, developed by Tetlow et al. CITEXX.

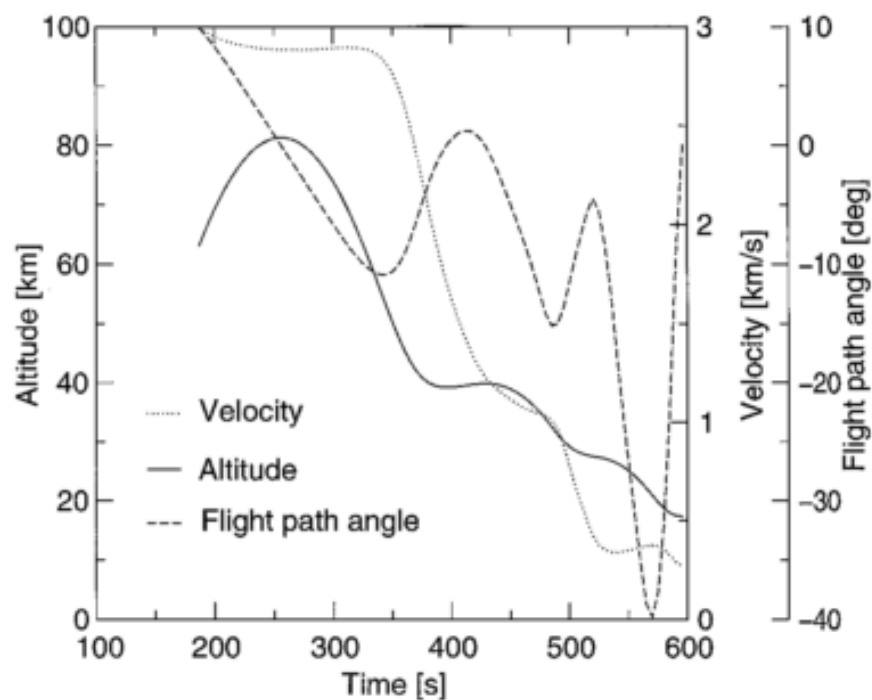


Figure 2.20: The flight path of a powered fly-back booster, developed by Tetlow et al. CITEXX.

The possibility of an airbreathing vehicle reigniting high speed airbreathing engines for short periods has been investigated by Tsuchiya and Mori [68]. Tsuchiya and Mori investigate two conceptual launch vehicles; a vehicle powered solely by airbreathing propulsion returning after separation of an orbital stage at Mach 5.1, and an airbreathing/rocket vehicle returning after a separation at Mach 6.8[68]. For the purposes of fly-back these vehicles are very similar, both using the high speed airbreathing engines during return flight. The optimal launch and return trajectories for these vehicles are shown in Figure 2.16. The separation for the airbreathing vehicle occurs at Mach 5.1, and the separation for the airbreathing/rocket vehicle at Mach 6.8. Both optimised return trajectories follow a relatively similar path. A long skip is performed, with both vehicles hitting the dynamic pressure limit. Both vehicles ignite the airbreathing engines at around Mach 3.5 for several tens of seconds to extend the range of the fly-back manoeuvres. After this, the vehicles descend and land at the launch site. The velocity at the landing point is not constrained, causing the airbreathing vehicle to land at slightly under Mach 1, and the airbreathing-rocket vehicle to land at approximately Mach 0.5. The latter is comparable with the landing velocity of the space shuttle [53]. These boosters fly to a downrange distance of 600-625km from the launch site, and separate from the orbital accelerator at a dynamic pressure of 15kPa[68]. At the start of their respective return trajectories, both boosters turn with a bank angle of 130-145°. Both the fully-airbreathing and partially-airbreathing vehicles ignite their airbreathing engines for 'several tens of seconds' at approximately Mach 3.5, in order to extend the flight range of the vehicles and return to the initial launch site[68]. Less than 5% of the vehicles initial propellant was required to return the vehicles to the initial launch sites[68].

These optimised return trajectories show three distinct sections; a turn manoeuvre, a skipping phase, and a high L/D descent. The skipping phase is similar to the boost-skip trajectory of the space shuttle CITEXX, which uses repeated entries into the atmosphere, and skips out, to extend the range of an atmospheric entry. A skipping trajectory has been shown to be range optimal for hypersonic vehicles able to skip out of the atmosphere [39], as well as vehicles flying entirely within the atmosphere[39, 12]. A skipping trajectory has also been shown to be optimal for an air-breathing hypersonic vehicle thrusting throughout the trajectory[9]. The range optimal operation of the air breathing engine is shown to be repeated ignitions at the trough of each skip. The scramjets are ignited as the vehicle climbs after the through, as the Mach number decreases to the minimum operable conditions of the scramjet engines. Minimising the Mach number during operation in this way maximises the efficiency of the scramjet engines.

When compared to the vehicles investigated by Tsuchiya and Mori[68], the SPARTAN separates from its third stage rocket at a considerably higher Mach number of Mach 9.1, as well as at a considerably higher dynamic pressure of 33.9kPa. The SPARTAN must also cover a longer fly-back range of 878km. In addition, the C-REST scramjet engines are limited to operating at hypersonic speeds of Mach 5.1 or higher. These design differences create substantially more challenging conditions than those studied by Tsuchiya and Mori. Consequently, it is necessary to investigate the ability of the

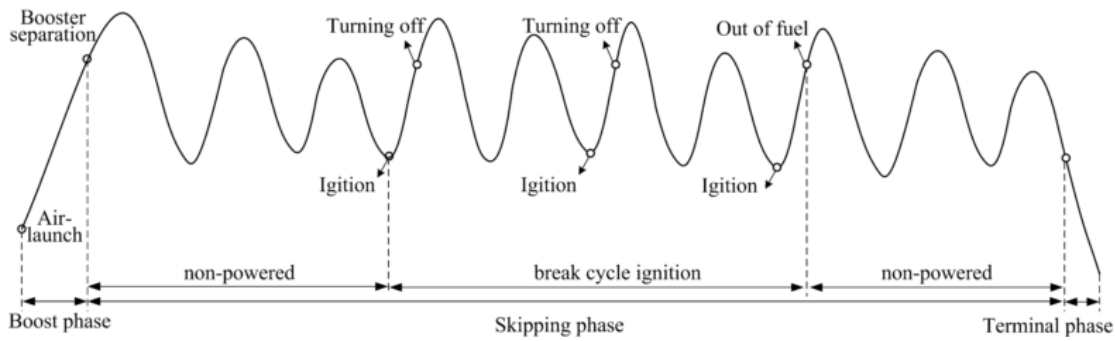


Figure 2.21

SPARTAN to return to the launch site following separation. From comparisons of the studies within this section it is evident that an optimisation of the return flight of the SPARTAN is required, and that a simply defined trajectory is not appropriate. TALKIGN ABOUT MY WORK

2.8 Optimal Control

KEEP THIS SECTION AN BROAD AS POSSIBLE - describe all alternatives

be more generic here To this point analysis of the SPARTAN trajectory has been performed using PID feedback control, assuming a constant dynamic pressure trajectory [46]. PID feedback control simulates the vehicle flight and manoeuvres the vehicle so that the trajectory conforms to a defined design point. Currently the trajectory of the SPARTAN has been simulated to align as closely as possible with 50kPa flight, a problem for which PID control is well suited.

more concise This study aims to find the optimal trajectory path for the SPARTAN that will produce maximum payload to orbit capability for the three stage system. Feedback control is infeasible for finding an optimal trajectory shape as there is no single design point at each stage of the simulated trajectory to calibrate towards. A control method is required that can take into account all aerodynamic factors at every timestep in order to find an optimal trajectory. Defining the trajectory simulation as an optimisation problem allows the trajectory to be solved at every point simultaneously, producing an optimal trajectory over the entire simulation space. Optimal control theory is widely used in situations where an optimal trajectory path must be found, and has been used widely in aerospace applications. However a trajectory optimisation has not been attempted on a three stage airbreathing system, and is usually reserved for simpler systems as there can be issues with convergence and long computation times [13]. This does not rule out using an optimisation method on a complex aerodynamic system however it does reinforce that choosing the correct optimisation procedure and defining the problem in the correct way is integral to developing an accurate solution method. This study aims to find a method of optimisation that is applicable to a complex aerodynamic trajectory and to apply this to the SPARTAN vehicle to produce an optimal trajectory shape for

maximum payload delivery to heliocentric orbit.

For an optimisation of a complex trajectory there are a variety of optimal control methods that are useful for specific problem types. These are separated into two categories: direct and indirect solution methods. Indirect methods are based on the calculus of variations or minimum principle model, and generally result in high accuracy solutions to optimisation problems [8]. However indirect models suffer from the drawbacks of small radii of convergence and the fact that the equations to be solved often exhibit strong nonlinearity and discontinuities. This means that indirect methods will not be solvable unless the problem is very well defined with a minimum of nonlinearity, making indirect methods unsuitable for many complex optimisation problems, such as aerospace vehicle simulations which can exhibit strong nonlinear behaviour and have a wide solution space.

Direct methods transform an optimisation problem into a nonlinear programming (NLP) problem which can be solved computationally [61]. NLP solvers solve the optimisation problem defined as [4]:

$$\text{Minimise} \quad f(x) \quad (2.1)$$

$$\text{Subject to} \quad g_i(x) \leq 0 \quad \text{for } i = 1, \dots, m \quad (2.2)$$

$$\text{and} \quad h_j(x) = 0 \quad \text{for } j = 1, \dots, n \quad (2.3)$$

An optimisation problem that has been discretised in this form can thus be solved using any of a variety of NLP solvers. One of the most effective methods of solving twice differentiable NLP problems is sequential quadratic programming (SQP) [7] for which there is a variety of commercial solvers available such as NPSOL, SNOPT and packages within MATLAB.

more concise In order for these packages to be able to solve an optimisation problem it must be presented in discretised form, and as such must be transformed using approximation techniques. The task of approximating a continuous optimisation problem in discrete NLP solvable form is not simple. SQP solvers can very easily run into convergence issues when provided with an optimisation problem which has not been well defined over a logical solution space. Also, any approximation must be carried out with care that the accuracy of the solution is not compromised. There are multiple ways to approximate a continuous optimisation problem directly as an NLP problem, the most common of which are shooting and collocation methods. The differences in the behaviour of each method are related to the interaction between the SQP solver and the discretisation method by which the problem is defined, and can affect the stability and accuracy of the solution as well as the solution time of the problem. For this study of in atmosphere trajectory optimisation with complex atmospheric and vehicle properties it was desired that a method be found with maximum stability and accuracy for a relatively large solution space, while solution time is a secondary priority.

2.8.1 The Single Shooting Method

The oldest and simplest method of approximating continuous optimisation problems as NLP problems is the direct single shooting method. Direct single shooting discretises the control function over the solution space, and solves this directly as an NLP by integrating the vehicle dynamics, or state variables, along the trajectory at each trajectory guess. Single shooting is simple to apply and has been used since the 1970s for rocket trajectory optimisation [27]. Single shooting methods suffer from nonlinearity problems, ie. an optimisation problem solved using the single shooting method will potentially struggle to solve if the problem exhibits even small nonlinearities, due to being unable to converge to an optimal solution. This makes the single shooting method unsuitable for complex problems such as a scramjet model, as there are many nonlinear factors inherent in atmosphere and airbreathing engine modelling.

2.8.2 The Multiple Shooting Method

Direct multiple shooting is a popular solution to trajectory optimisation problems. This method solves some of the instabilities of the single shooting method by splitting the trajectory into multiple shooting arcs, and collocating these at specific time points. This creates a system of discontinuities, illustrated in Figure 2.22, which are gradually removed by the solver algorithm until the trajectory is continuous. These discontinuities allow greater flexibility for the solver than is afforded by the single shooting method. The multiple shooting problem is solved as an NLP through discretisation of the state and control variables at each time node and integration for the state variables x over each shooting arc t_k [62]:

$$\dot{x} = v = f[x(t), u(t)] \quad (2.4)$$

With the state variables subject to the boundary conditions:

$$r[x(t_0), x(t_f)] = 0 \quad (2.5)$$

And solving for the unknown values s_i :

$$x(t_i) = s_i, \quad i = 1, 2 \dots N \quad (2.6)$$

The control variables at the nodes are guessed and the state variables are integrated along the trajectory, with each node segment being considered separately. A matching condition is introduced that must be met between each segment; ie. the trajectory must be continuous. [38]

$$\mathbf{X}(\mathbf{s}) = \begin{Bmatrix} x(t_1; s_0, v_0) - s_1 \\ x(t_2; s_1, v_1) - s_2 \\ \vdots \\ x(t_N; s_{N-1}, v_{N-1}) - s_N \\ r[x(s_0), x(s_N)] \end{Bmatrix} = \mathbf{0} \quad (2.7)$$

This is now in the form of an NLP problem which may be solved in a standard NLP solver. ie. minimise:

$$\min J(s, v) = \sum_{i=0}^{N-1} J_i(s_i, v_i) \quad (2.8)$$

subject to:

$$x[t_{i+1}, s_i, v_i] - s_{i+1} = 0 \quad (2.9)$$

$$r[x(s_0), x(s_N)] = 0 \quad (2.10)$$

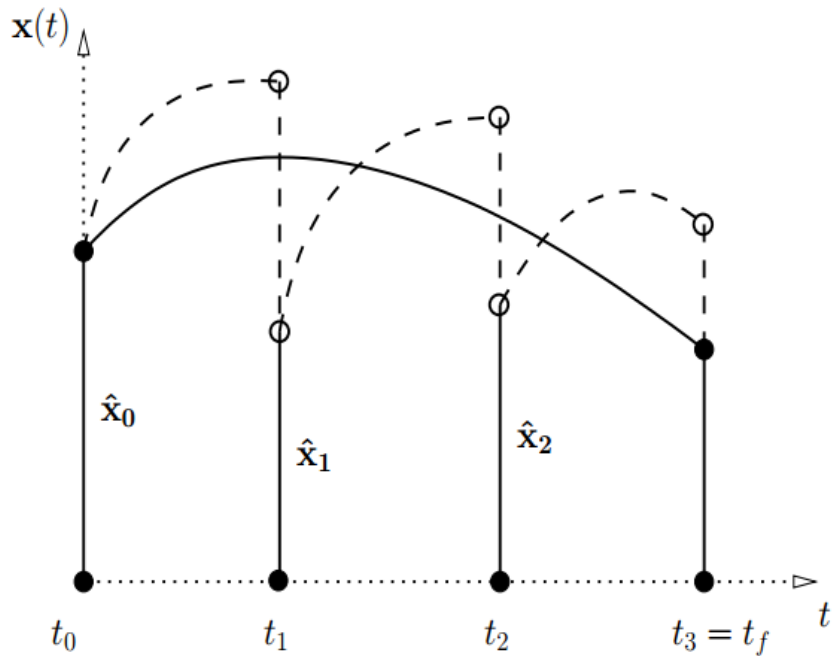


Figure 2.22: An illustration of the subdivision associated with multiple shooting [38]. Dashed lines illustrate the initial trajectory guess and the solid line indicates the final trajectory once the joining conditions are met.

The multiple shooting method has greatly improved convergence compared to the single shooting method, removing much of the susceptibility to instabilities resulting from nonlinear effects. How-

ever, the multiple shooting approach still suffers from a relatively small radius of convergence and slow computation times. Radius of convergence is extremely important to this study as the optimal solution cannot be approximated to a great degree of accuracy, and as such multiple shooting was deemed inappropriate for this study. It was desired to find a method with a global radius of convergence to apply to the optimisation problem being considered.

2.8.3 The Pseudospectral Method

check some of my claims about the pseudospectral method and cite GPOPS papers

GPOPS USES HP-ADAPTIVE GAUSS, WHICH HAS BEEN SHOWN TO improve(?) GAUSS
I should show the hp-adaptive gaussian method

Direct Trajectory Optimization and Costate Estimation via an Orthogonal Collocation Method - benson is quite a good paper (the first?) explaining gaussian ps method

also look at gpops 1 manual

The most promising method found to address the issue of radius of convergence is the direct collocation approach, which provides global radius of convergence with the additional advantage of smaller computational time [17]. Direct collocation methods discretise the control and state equations of the optimal control problem, and use these as constraints in an NLP problem similarly to the multiple shooting approach. However the state functions in collocation methods are approximated by polynomial functions over the solution space, inherently being continuous at each collocation node rather than the state functions being integrated over each timestep. The derivative of the state functions then become a constraint within the NLP, being equated to the polynomial approximation functions by the solver algorithm. The method used to discretise the derivative functions is very important to the accuracy of the collocation method, with trapezoidal, Hermite-Simpson and pseudospectral methods being popular choices.

The most accurate form of collocation method is the pseudospectral, or orthogonal collocation method[14], which uses some elements of spectral method approximation to accurately approximate derivative terms. The pseudospectral method was first introduced in 1972 by Kreiss & Oliger [30] as an efficient way to compute meteorology and oceanography problems. The pseudospectral method is now garnering a large amount of attention for its ability to rapidly and accurately solve a wide variety of optimal control problems. The pseudospectral method employs the use of orthogonal polynomials such as Legendre or Chebychev polynomials to approximate the state and control functions at a specific set of collocation points[Huntington2007, 14]. The pseudospectral method has the property that when evaluated at the specific collocation points, the functions approximating approximate state and control are exactly equal to the continuous function being approximated at that point.

A large usability advantage of the pseudospectral method is the ability to generate Hamiltonian and costate values easily[22, 15]. The Hamiltonian and costate values allow a solution to easily and

quickly be checked to determine if some of the necessary conditions for optimality are being met. This is useful to determine initially if the optimal solution calculated by the pseudospectral solver is valid.

The pseudospectral method discretises the optimisation problem for application of an NLP solver. The initial form of the optimisation problem is that of a generic Bolza optimisation problem, described by a continuous Bolza cost function:

$$J(\mathbf{u}, \mathbf{x}, \tau_f) = M[\mathbf{x}(\tau_f), \tau_f] + \int_{\tau_0}^{\tau_f} L[\mathbf{x}(\tau), \mathbf{u}(\tau)] d\tau \quad (2.11)$$

Subject to a set of state dynamics, which describe the behaviour of the system over the solution space:

$$\dot{\mathbf{x}}(\tau) = f[\mathbf{x}(\tau), \mathbf{u}(\tau)] \quad (2.12)$$

These are constrained by boundary conditions of the system at the initial and final time points:

$$\psi_0[\mathbf{x}(\tau_0), \tau_0] = \mathbf{0} \quad (2.13)$$

$$\psi_f[\mathbf{x}(\tau_f), \tau_f] = \mathbf{0} \quad (2.14)$$

Three primary pseudospectral methods are described in this chapter. All of these methods make use of Lagrange interpolating polynomials. These methods use different collocation points.

The Legendre Pseudospectral Method

The Legendre polynomial method[16] uses Legendre-Gauss-Lobatto points for collocation. These create efficient and simple relationships for the evaluation of time-continuous optimisation problems [14]. The Legendre pseudospectral method uses the Legendre polynomial, defined as L_N :

$$L_N = \frac{1}{2^N N!} \frac{d^N}{dt^N} (t^2 - 1)^N \quad (2.15)$$

The Legendre-Gauss-Lobatto points, $t_l, l = 0, \dots, N$, are given by:

$$t_0 = 0$$

$$t_N = 1$$

and $t_l, l = 1 \leq l \leq N - 1$ are the zeros of \dot{L}_N .

The Legendre pseudospectral method transforms the problem to lie on the interval $t \in [-1, 1]$, so that the cost function (Equation 2.11) is discretised as follows:

$$J[\mathbf{x}(t_k), \mathbf{u}(t_k)] = \frac{\tau_f - \tau_0}{2} \sum_{k=0}^N L[\mathbf{x}(t_k), \mathbf{u}(t_k)] w_k + M(\mathbf{x}(t_N), \tau_f) \quad (2.16)$$

where w_k is a weighting function defined as:

$$w_k = \frac{2}{N(N+1)} \frac{1}{[L_N(t_k)]^2} \quad (2.17)$$

The state equations (Equation 2.12, in this case the system dynamics) are described at each LGL point by:

$$\frac{(\tau_f - \tau_0)}{2} \mathbf{f}[\mathbf{x}(t_k), \mathbf{u}(t_k)] - \sum_{l=0}^N D_{kl} \mathbf{x}(t_l) = \mathbf{0} \quad (2.18)$$

Where D is the differentiation matrix, defined at each entry k, l by:

reduce the spacing between equations...

$$k \neq l \quad D_{kl} = \frac{L_N(t_k)}{L_N(t_l)} \frac{1}{t_k - t_l} \quad (2.19)$$

$$k = l = 0 \quad D_{kl} = -\frac{N(N+1)}{4} \quad (2.20)$$

$$k = l = N \quad D_{kl} = \frac{N(N+1)}{4} \quad (2.21)$$

$$otherwise \quad D_{kl} = 0 \quad (2.22)$$

The boundary conditions are expressed analogously to the continuous problem:

$$\psi_0[\mathbf{x}(t_0), \tau_0] = \mathbf{0} \quad (2.23)$$

$$\psi_f[\mathbf{x}(t_N), \tau_f] = \mathbf{0} \quad (2.24)$$

The Chebychev Pseudospectral Method

CGI collocation points [22] $t_k = \cos(\pi(N - k)/N), k = 0, \dots, N$

The Gauss Pseudospectral Method

A large advantage of the pseudospectral method is the ability to generate Hamiltonian and costate values easily, detailed by Gong et al. [22] and Fahro & Ross [15]. The Hamiltonian and costate values allow a solution to easily and quickly be checked for accuracy. The Hamiltonian equalling zero is a necessary (but not sufficient) condition for optimality. In order to make a preliminary test for an optimal solution, the Hamiltonian must be observed to be close to zero along the entire trajectory.

expand on this, and optimality conditions

2.8.4 Pseudospectral Examples

this section needs to be linked with the hypersonic vehicle trajectories that use the pseudospectral method

need a six dof example, and a multiple state example

In order to assess the applicability of the pseudospectral method to an in atmosphere trajectory optimisation problem, the range of existing solutions utilising the pseudospectral method has been investigated. The pseudospectral method has been proven to be extremely effective for simulations in aerospace applications and has been proven in flight applications such as the zero propellant manoeuvre of the International Space Station in 2007, where the ISS was rotated 180 degrees without any propellant used following a pseudospectral method solution [5]. The pseudospectral method has been used successfully in a multitude of studies for the trajectory optimisation of hypersonic vehicles[33, 28, 75, 66, 12, 9, 50, 39].

The pseudospectral method has been used for the guidance of re-entry vehicles including in-atmosphere dynamics, to keep a vehicle on a desired three degree of freedom path in real-time in a study by Tian & Zong [66]. The pseudospectral method was found to generate an accurate trajectory around the desired reference trajectory, satisfying all necessary constraints in real-time for six state variables with minimal error. Nonlinear effects are an intrinsic part of simulating a complex aerodynamic system, and this study indicates that the pseudospectral method will be able to simulate the SPARTAN vehicle and is appropriate for use in this study.

Chai et al.[9] investigate the range optimal trajectory of a scramjet-powered hypersonic missile. Chai et. al successfully compute an optimal trajectory for an airbreathing hypersonic vehicle in three degrees of freedom[9]. The hp-adaptive pseudospectral method is compared to the Gauss pseudospectral method and the direct shooting method. Both pseudospectral methods show greater precision and robustness than the direct shooting method, and are reported to be much more computationally efficient.

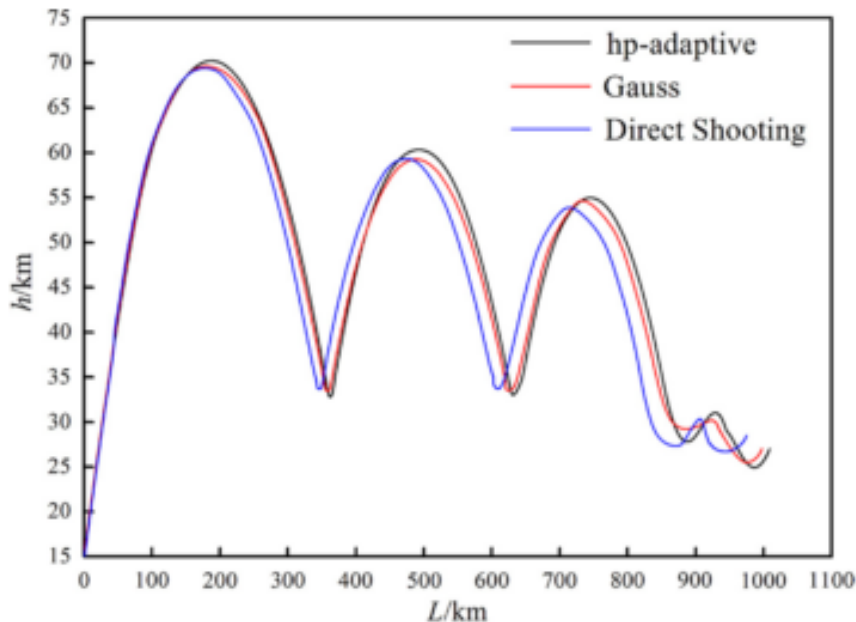


Figure 2.23

ally efficient. The direct shooting method takes 268.2s to complete, whereas the Gauss pseudospectral method completes optimisation in 12.7s, and the hp-adaptive pseudospectral method takes only 5.3s[9]. The pseudospectral methods produce similar results. The hp-adaptive pseudospectral method shows a slight range increase over the Gauss pseudospectral method due to its ability to redistribute the collocation points adaptively, which improves robustness.

These results indicate that the pseudospectral method does not exhibit instabilities with nonlinear effects such as atmospheric density varying the dynamics of the system being optimised, and that the pseudospectral method can be used for systems with at least up to six state variables.

Based on the proven track record of the pseudospectral method in simulation situations, it was decided that using the pseudospectral method for the optimisation of the rocket-scramjet-rocket system was a sound and feasible decision. It has been necessary to investigate the range of solvers available that will utilise a pseudospectral method to solve an optimisation problem with the desired capabilities and usability.

2.8.5 Available Solvers

change this section to reflect more current perspectives. expand on what each program actually does.
Add programs like POST/POST2 (direct shooting?), OTIS, TRANSWHORP, ASTOS

The pseudospectral method has a number of solvers available commercially, the foremost of which are DIDO, produced by Elissar Global [54], GPOPS II [49] and PROPT, a module integrated with TOMLAB [55]. These solvers utilise nonlinear programming techniques to solve optimal control

problems in discretised form and are all similar in their operation. These have been investigated for a variety of considerations with details available in Section ??.

There are a number of existing programs that can complete optimisation problems using the pseudospectral method and as such creating an optimiser from scratch was considered to be overly time consuming and not a useful contribution. A number of programs were found, which are detailed in Table 2.2. An effort was made to find an open source program that could complete the desired op-

Software	Platform	Cost	Notes
DIDO	MATLAB	\$50 (Student)	Simple and automated with free trial available. Documentation readily available. Can perform required problem. Provides costates and Hamiltonian values.
GPOPS II	MATLAB	\$100	Free trial available, but was unable to obtain. Some documentation available. Can perform required problem.
ROC-HJ Solver	C++	Free	A basic solver for some specific optimal control problems. Does not perform collocation.
PROPT (IPOPT)	MATLAB	\$500	No free trial. Documentation available. Can perform required problem.
Imperial College OCS	MATLAB	Free	Documentation and download unavailable
PSOPT	C++	Free	Open source and can perform required problem. Not updated, many modules out of date.

Table 2.2: Summary of programs capable of pseudospectral optimisation.

timisation however it was found that all open source programs studied were out of date or not well supported. Out of the premium packages available GPOPS II and DIDO were considered the best options, both being proven in aerospace applications, with available free trials and affordable price points. Free trials were requested from both, however the free trial for GPOPS II was not received while the free trial for DIDO was received with good customer service provided. On reception of the DIDO trial it was found that DIDO provides the required optimiser package in an easy to use form, with sufficient documentation and examples provided to streamline the simulation process. DIDO also provides costate and Hamiltonian values, used for verifying that the optimised solution is accurate and physically sound, as well as the lowest price point and benefit of being proven in both real space applications and in-atmosphere simulations. After weighing these considerations DIDO was selected as the best program to use for the pseudospectral optimisation and simulation.

2.9 Aerodynamic Analysis

- preliminary design requires fast and easy aerodynamics

Simulating the trajectory of access to space vehicles requires the aerodynamics of the launch vehicle to be characterised accurately. This entails the creation of large aerodynamic coefficient databases, which cover the operable region of the vehicle, and include the effect of control surface deflections. The liability of the vehicle design to change during the preliminary design phases renders highly accurate CFD or experimental studies expensive and inefficient CITATION. Instead, solutions are found which are able to approximate the aerodynamic characteristics to an appropriate accuracy, while providing fast set-up speeds as well as computation times.

2.9.1 HYPAERO

need to expand to be a general review of solvers available (unbiased). include brief discussion on turbulence. discuss viscous effects

Hypaero is an aerodynamic calculation tool developed for the preliminary design of hypersonic vehicles. HYPAERO uses strip theory, dividing the surface of the vehicle into panels to calculate aerodynamic properties along the aircraft as illustrated in Figure 2.24. In strip theory two dimensional sections are created running the length of the vehicle, defining streamlines along the vehicle faces. Pressure, Mach number and skin friction are calculated along these streamlines to compute the aerodynamic coefficients of the vehicle. The Aerodynamic analysis of the SPARTAN has been performed using HYPAERO by Jazra et al. [26]. The aerodynamic coefficients of the SPARTAN vehicle have been provided for this study by Dawid Preller.

NEED TO CHANGE THIS to clarify where I'm using this

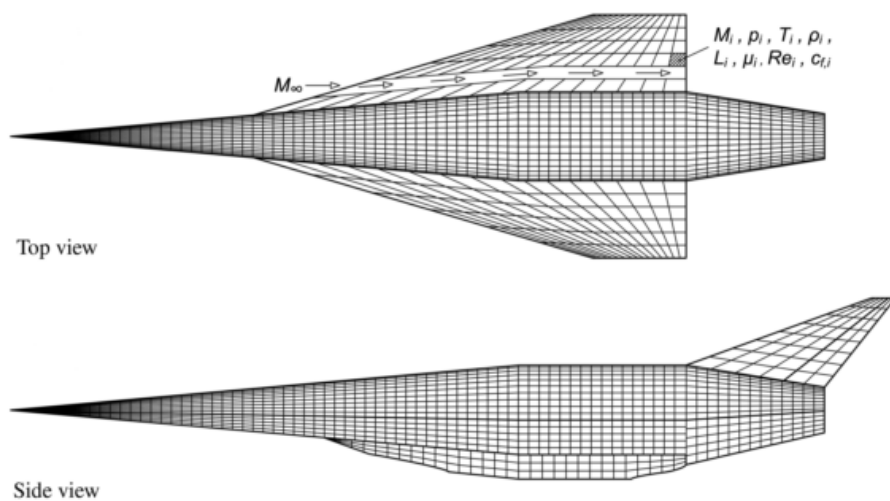


Figure 2.24: HYPAERO analysis surface grid [26].

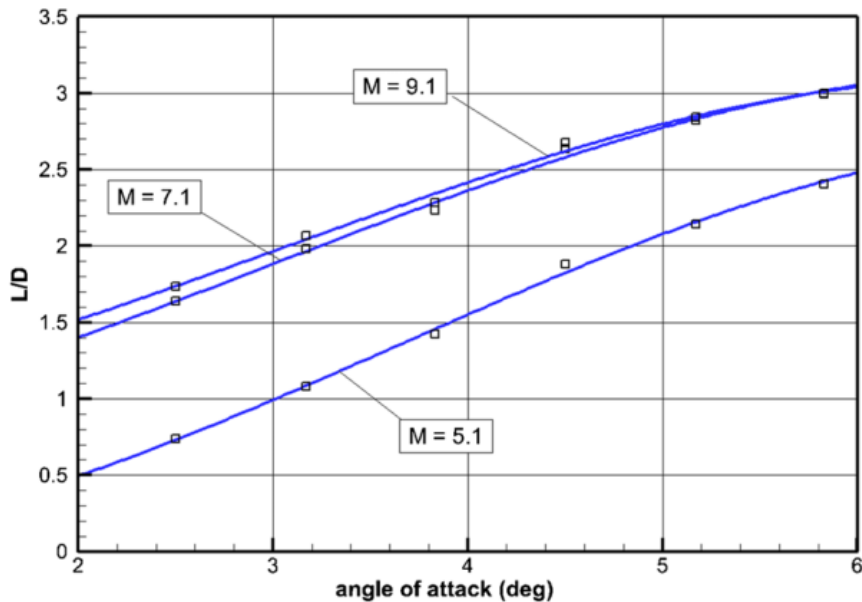


Figure 2.25: SPARTAN aerodynamics, developed using HYPAERO [48].

2.9.2 CART3D

Insert an example of a validation of CART3D

CART3D is an inviscid CFD package, designed for use during preliminary vehicle design and analysis CITATION. CART3D requires only a surface triangulation of the vehicle being analysed. CART3D features adjoint mesh adaption, and uses cartesian 'cut-cells' which intersect the surface, allowing complex geometries to be analysed. The mesh automatically refines as the simulation progresses, reducing error. The absence of a requirement for a user generated mesh allows CART3D to be easily applied to complex launch vehicle designs, as well as allowing for simple modification of control surface deflections and flight conditions. CART3D has been used extensively for aerodynamic simulations in preliminary design, including analysis of the Skylon spaceplane[36], HIFiRE-5[29], and in low sonic boom shape optimisations[2]. Mehta et al. used CART3D to analyse the Skylon spaceplane, in a study which investigated the aerodynamics of the vehicle as well as the plumes produced by the Reaction Engines LTD SABRE engines[36]. The Skylon was analysed at a range of mach numbers from 2.625 to 16.969, at altitudes from 15.326km to 75.771km. These results indicate the applicability of CART3D over a wide range of Mach numbers, which is of particular use to this study. During a study by Aftosmis & Nemec where CART3D was applied to low sonic boom shape optimisation, CART3D was shown to have good agreement with experimental results in tests at Mach 1.6.

The wide Mach number range of CART3D, along with its ease of use and demonstrated accuracy, makes CART3D a useful tool for this study.

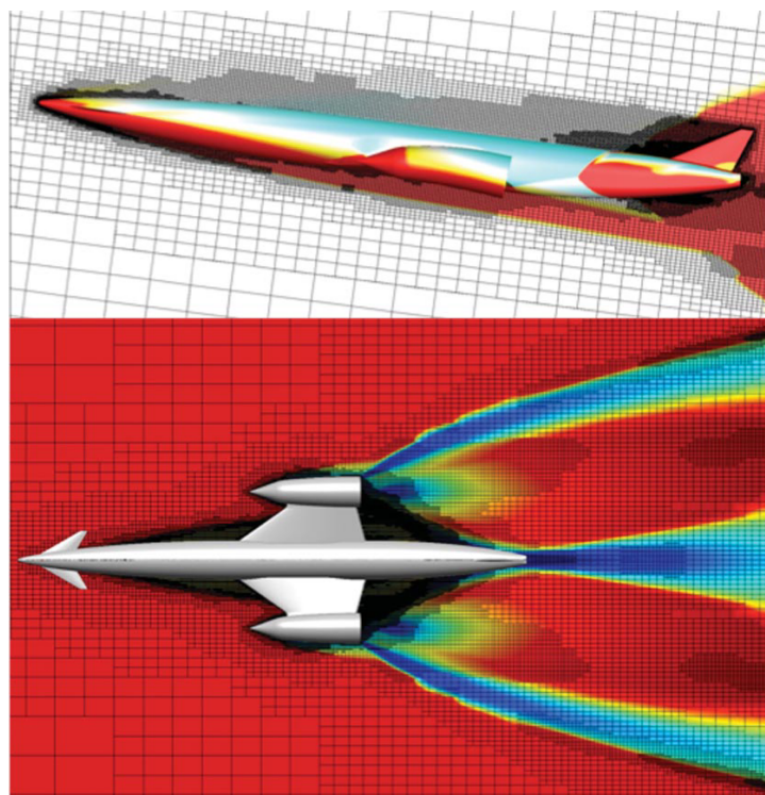


Figure 2.26: The Skylon spaceplane, simulated using CART3D at Mach 12.189, $\alpha = 7.512^\circ$ [36]. Cell distribution produced by mesh adaption is shown.

2.9.3 Missile DATCOM

Missile DATCOM is a widely used, semi-empirical, aerodynamic prediction tool for missile configurations. Missile DATCOM is capable of calculating the aerodynamic forces, stability derivatives and moments over a range of angle of attack and Mach number values, allowing an aerodynamic database to be generated simply and rapidly. Missile DATCOM has been shown to produce close agreement with experimental wind tunnel data for normal force and pitching moment coefficients, and reasonable agreement for axial force coefficients [59].

2.10 Summary

This chapter has reviewed literature relevant to this thesis. Add more details.

CHAPTER 3

LAUNCH VEHICLE DESIGN AND SIMULATION

In order to be competitive in the emerging small satellite market, a small satellite launcher must be cost-effective, reliable, and capable of launching on a flexible schedule. The inclusion of airbreathing engines within a small satellite launch system has the potential for improving cost effectiveness compared to disposable rocket-powered launchers, by allowing partial reusability of a launch system. The airbreathing engine most appropriate for small satellite launch systems are scramjet engines, which operate efficiently within the hypersonic regime, with the capability to operate over a relatively large Mach number range compared to turbojet or ramjet engines. A launch system incorporating scramjets must necessarily include two rocket-powered flight stages; a first stage rocket to accelerate the system from launch to the minimum operational Mach number of the ramjet or scramjet engines; and a third stage rocket to accelerate the payload at exoatmospheric conditions and place it into the correct orbit. This chapter presents the design and modelling of a rocket-scramjet-rocket launch system in which the scramjet stage is reusable for multiple launches. For this launch system to be economically viable, the scramjet stage must be capable of accelerating to a high Mach number, and then returning to its initial launch site for re-use. Returning to the initial launch site removes the need for costly and time-consuming transportation, and allows the refurbishment and refuelling of the scramjet stage to begin immediately. This rocket-scramjet-rocket launch system is designed to launch satellites on the order of 200kg to a 567km altitude sun-synchronous orbit. A sun synchronous orbit is targeted as it is a potentially desirable orbit for small satellite missions, being advantageous for imaging purposes due to its low altitude and consistently timed overpasses. This orbit is consistent with previous studies which have investigated rocket-scramjet-rocket small satellite launch systems, allowing the missions developed in this study to be compared and contrasted to unoptimised mission profiles. The rocket-scramjet-rocket launch system described in this chapter is used as a representative model for an airbreathing, partially-reusable, multi-stage small satellite launcher.

The rocket-scramjet-rocket launch system used in this study has been designed based on the

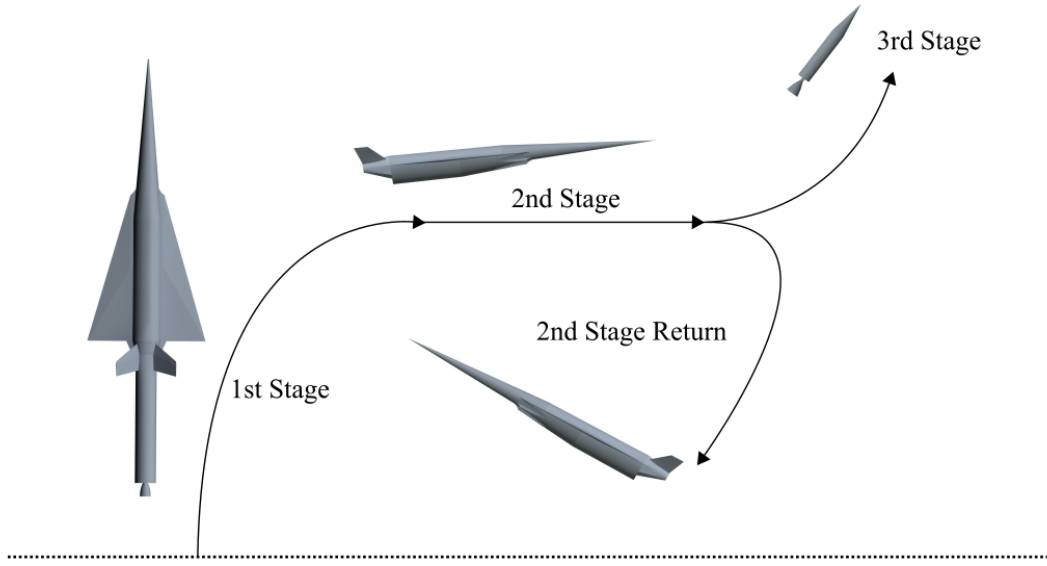


Figure 3.1: The launch process of the rocket-scramjet-rocket launch system, presented in simplified form.

SPARTAN scramjet accelerator developed by Preller & Smart [CITATIONXX]. The SPARTAN is a scramjet-powered accelerator being developed by The University of Queensland and Hypersonix. The SPARTAN has been designed for small satellite launches, as part of a rocket-scramjet-rocket launch system. The SPARTAN has been used as the basis for design of the launch system, as it is the most complex stage of the system, and its unique trajectory requirements drive the design of the other stages. The trajectory of a launch system involving scramjet propulsion is significantly different to that of a fully rocket-powered launch system. Figure 3.1 shows a simplified representation of the launch trajectory for the vehicle simulated in this study. The operation of the scramjet engine requires in-atmosphere flight, at high dynamic pressure conditions for long periods of time. The launch system must be designed to withstand the high structural loading and heating generated by flight at these conditions. The SPARTAN vehicle is mounted to the front of the first stage rocket. The launch system is launched vertically under rocket power, from a traditional small rocket launch facility. This configuration allows the SPARTAN to take the brunt of the aerodynamic forces and heating, as well as allowing the use of the control surfaces of the SPARTAN. During first stage rocket operation, the launch system pitches rapidly, reaching close to horizontal flight to allow the SPARTAN to stay at high dynamic pressure conditions. The SPARTAN is accelerated to its minimum operating velocity of approximately Mach 5, at which point separation occurs. The SPARTAN's four scramjet engines are ignited, and The SPARTAN is accelerated through the atmosphere, reaching approximately Mach 9. At this point, the specific impulse of the scramjet engines, and thus the efficiency of the SPAR-

TAN, have decreased, and the third stage rocket is separated. The third stage rocket accelerates and performs a pull-up, before cutting its engine and coasting out of the atmosphere. Once the rocket is exoatmospheric, the engine is reignited, performing first a circularisation burn, and then a Hohmann transfer to the intended orbit. Meanwhile, the SPARTAN banks and executes a fly-back manoeuvre to return to its initial launch site. The SPARTAN extends landing gear, and lands on a traditional runway in the style of a conventional aircraft. The SPARTAN is able to be rapidly refurbished and remounted for further launches. To fulfil the requirements of this trajectory, The SPARTAN must be able to fly and manoeuvre at all Mach numbers from 0 to 9, as well as being able to withstand high structural and heating loads without significant deterioration.

The three stage launch system incorporating the SPARTAN is shown in Figures 3.2 & 3.3. The size and external design of the SPARTAN scramjet accelerator are used exactly as defined for the Baseline SPARTAN vehicle defined by Preller & Smart. The internal layout has been designed for the SPARTAN to carry a large fuel volume while allowing the third stage to fit within the fuselage. The first and third stages have been designed for this study. The third stage rocket replaces the third stage used in previous SPARTAN studies, which was powered by a Pratt & Whitney RL-10-3A engine, with a rocket stage powered by a SpaceX Kestrel engine. The SPARTAN design is presented first, as the design of the SPARTAN drives the design of the first and third stage rockets.

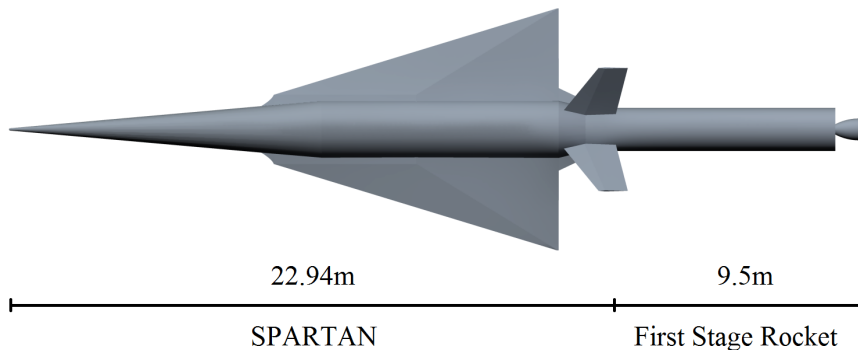


Figure 3.2: The rocket-scramjet-rocket launch system, top view, showing the SPARTAN and first stage.



Figure 3.3: The rocket-scramjet-rocket launch system, side view, showing the SPARTAN and fuel tanks, along with the third and first stages.

3.1 Second Stage Scramjet

3.1.1 The SPARTAN Accelerator

The SPARTAN vehicle in this study is designed based on the work by Preller & Smart CITATION. The SPARTAN is 22.94m long, with a frontal cone half angle of 5° [CITEXX DAWIDS THESIS]. A mass breakdown of the SPARTAN is shown in Table 3.1, adapted from [CITAXX Dawids thesis]. The fuel tank sizes and total fuel mass are sized to accommodate for the Kestrel-powered third stage, described in Section 3.3. This study assumes that the third stage is stored within the fuselage of the

Part	Fuselage	Wings	Tanks	Systems	Landing Gear	Scramjets	Fuel
Mass (kg)	2861.6	350.7	179.4	707.5	188.9	669.0	1562.0

Table 3.1: Mass breakdown of the modified SPARTAN vehicle.

SPARTAN for simplicity. It is assumed that the release mechanism for the third stage is able to be situated within the available space surrounding the third stage, however the release mechanism is not considered further in this study.

The fuel tanks are sized to fit around the kestrel-powered third stage. There are three fuel tanks; two cylindrical tanks situated underneath the third stage; and a truncated conical tank in the nose. The conical fuel tank is designed to fit immediately forward of the third stage. This fuel tank is 8m long, leaving 1.47m^3 of space in the nose for cooling systems, frontal landing gear and any additional systems or sensors which are necessary in the nose cone. The cylindrical tanks are positioned underneath and slightly to either side of the third stage, leaving space underneath for vehicle systems. The cylindrical fuel tanks are designed to be 8.5m long, with diameters of 0.87m, sized to give a nominal total tank volume of 22m^3 . The fuel tanks hold a total of 1562kg of LH2 fuel. This assumes an LH2 density of 71kg/m^3 , slightly denser than LH2 at phase transition point at 1 atm. The mass of the fuel tanks is scaled from Dawid Preller's Baseline vehicle model of the SPARTAN, giving a total fuel tank mass of 179.4kg.

3.1.2 Propulsion

The SPARTAN is powered by four underslung scramjet engines, fuelled by liquid hydrogen. These engines are Rectangular To Elliptical Shape Transition (REST) engines, configured to allow for a conical forebody (C-REST). REST engines have a rectangular to elliptical shape transition inlet, and an elliptical combustor, offering simplicity in design as well as reduced thermal loading and viscous drag compared to scramjets with planar geometries [63]. REST engines are also specifically designed to operate over a wide range of Mach numbers, and at off design conditions, making them particularly applicable to use on scramjet accelerator vehicles.

Propulsion Modelling

The properties of the C-REST scramjet engines must be modelled at every flight condition which the SPARTAN may experience during its flight. The thrust generated by the C-REST engines determines how rapidly the SPARTAN accelerates, and the efficiency of the engines determines the total flight time, and influences the separation point of the third stage rocket. The C-REST engines are simulated separately to the aerodynamic simulations of the SPARTAN, using quasi-1D simulation for simplicity. The engine model takes the conditions at the inlet, and calculates the exit conditions and propulsive properties of the engine. The engine exit conditions are added into the aerodynamic simulations and the propulsive properties are used in the simulated vehicle model.

Before the flow enters the engine, it is affected by the conical shock generated by the forebody of the SPARTAN. Figure 3.4 shows the locations of the flow properties which are necessary to calculate engine performance. The ambient atmospheric conditions are calculated by interpolation using the 1976 NASA Atmospheric properties[40]. The flow properties at the inlet of the engines is calculated using the Taylor-Maccoll analysis method for conical shocks[CitationXX]. This calculation is performed in the cone_shoot program provided for this study by Prof. Michael Smart[CitationXX?]. The flow conditions following the conical shock are shown in Figure 3.5.

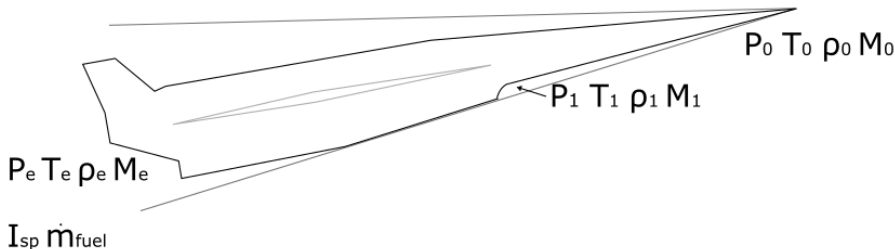


Figure 3.4: The locations of conditions relevant to C-REST engine simulation.

The engine model used is a CRESTM10 database[48], analysed using quasi-1D simulation and provided for this study by Prof. Michael Smart. This database provides data points of engine performance over inlet conditions within the operational range, at 50kPa dynamic pressure equivalent conditions. The specific impulse data set is shown in Figure 3.6. This data is interpolated using bivariate splines for the given inlet conditions, to calculate specific impulse produced by the engine. During flight the C-REST inlet conditions will stay within the region bounded by the available data. However, for the purposes of the trajectory optimisation, it is necessary for the vehicle model to be able to extrapolate for ISP and equivalence ratio data. This extrapolation is linear, and is used to drive the optimisation, but does not directly affect the final solution. For operation at high Mach numbers, the fuel mass flow rate is assumed to be stoichiometric, so that $m_f = 0.0291\dot{m}$. This ensures that the scramjet engines are performing at high efficiency throughout the acceleration of the scramjet stage. However, the C-REST engine is a fixed geometry engine, primarily designed for operability at high

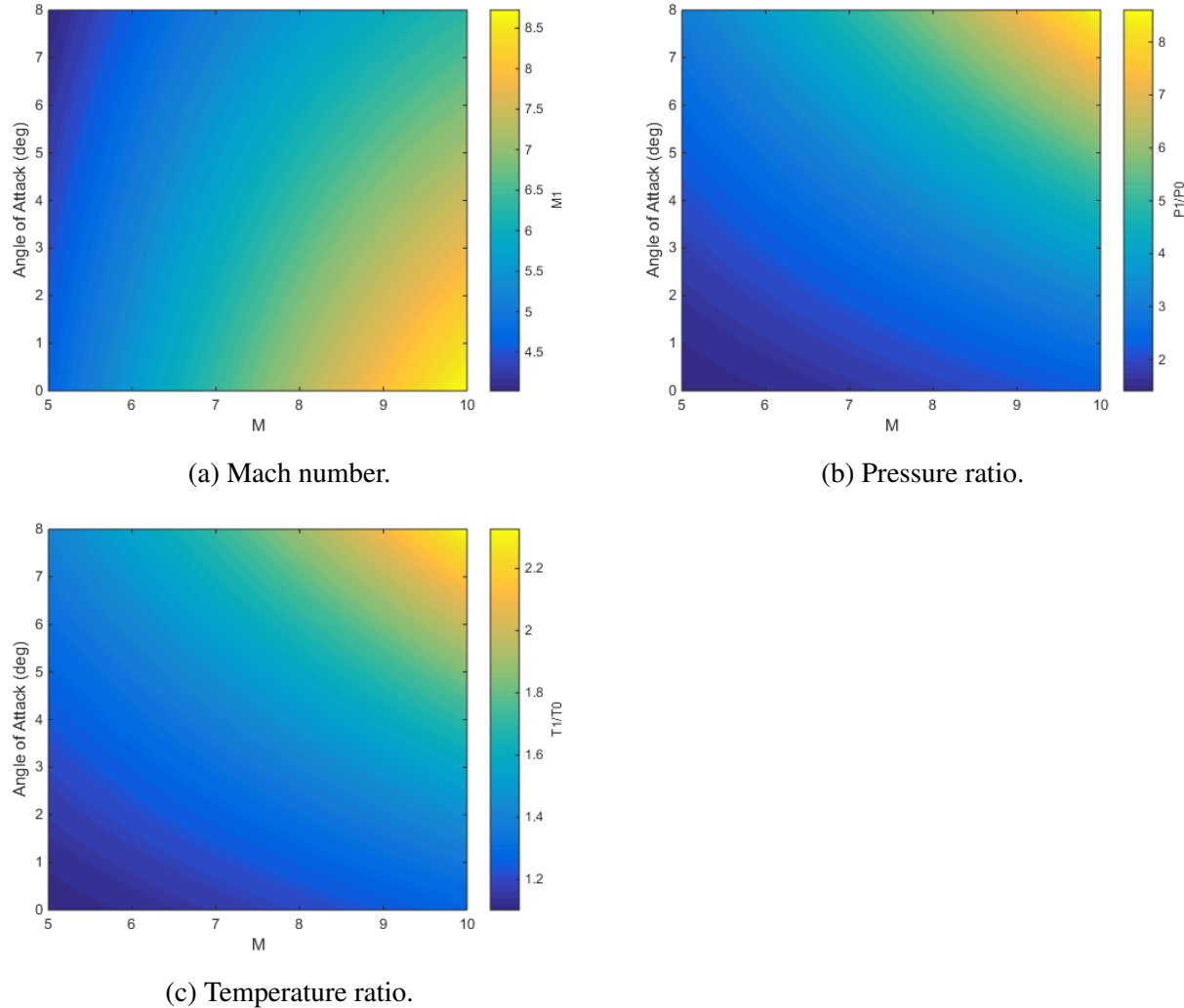


Figure 3.5: Flow conditions after the conical shock generated by the vehicle nose cone. Figure a) shows the Mach number, b) shows the pressure ratio, and c) shows the temperature ratio following the conical shock.

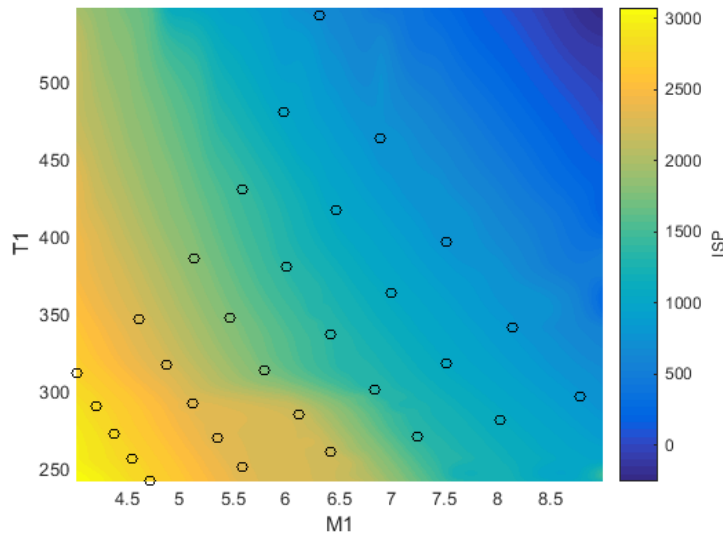


Figure 3.6: Specific impulse of the CRESTM10 engines with input temperature and Mach number. Available data points are indicated.

Mach numbers[48]. At lower Mach numbers, the addition of excessive fuel may cause the engine to choke and unstart, resulting in total loss of thrust[48]. To avoid unstart, an equivalence ratio (ϕ) of less than 1 is set at low Mach numbers. The equivalence ratio interpolation is linear, as the number of data points available for interpolation is low. The equivalence ratio over the range of SPARTAN operation is shown in Figure 3.7. The fuel mass flow rate is determined by approximating the flow into the inlet as an ideal gas;

$$\dot{m} = 0.9 m_c A_{cap} P_0 M_0 \sqrt{\frac{\gamma_0}{R_{air} T_0}},$$

$$\dot{m}_{fuel} = \left(\frac{m_{fuel}}{m_{ox}} \right)_{st} \phi \dot{m}$$

Explain details of C-REST calculator here, including mass capture rate and capture area modifiers.

Need details from Michael. Citation for this?

The multiplier of 0.9 is an approximate term included to account for losses due to asymmetry within the engine. The thrust for each engine, T , is obtained by inclusion of the interpolated specific impulse, ie.

$$T = g_0 \dot{m} I_{sp}.$$

3.1.3 The Aerodynamics of the SPARTAN

In order for the trajectory of the SPARTAN to be successfully simulated and optimised, the aerodynamics of the SPARTAN must be calculated for the large range of flight conditions experienced during the acceleration and return flights. The aerodynamics of the SPARTAN are calculated at set flight conditions covering the breadth of necessary conditions, and the results are tabulated in databases. During

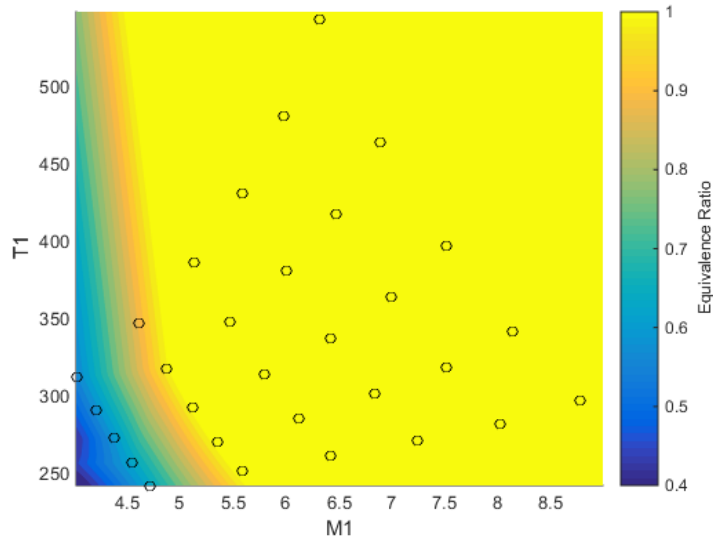


Figure 3.7: Operable equivalence ratio of the CRESTM10 engines with input temperature and Mach number. Available data points are indicated.

simulation, the aerodynamics of the SPARTAN are determined by interpolation over the aerodynamic databases using bivariate splines.

The aerodynamics are calculated for Mach numbers between 0-10, angles of attack between 0° and 10° , and for altitudes between 0-40km. Separate aerodynamic simulations are performed for engine-on and engine-off conditions, as the operation of the scramjet engines changes the aerodynamic characteristics of the SPARTAN significantly. When the engines are powered on, the engines are generating thrust on the internal nozzle, as well as on the boat-tail and base. When the scramjet engines are not operational air flows through the flowpath without fuel injection, generating a large amount of drag. The drag, lift and moment coefficients are determined by interpolating for Mach number, angle of attack, altitude, and centre of gravity as it shifts during flight. The drag and lift produced by each stage of the vehicle are calculated using the standard definition of the aerodynamic coefficients:

$$F_d = \frac{1}{2} \rho c_d v^2 A, \quad (3.1)$$

$$F_L = \frac{1}{2} \rho c_L v^2 A. \quad (3.2)$$

The aerodynamics of the SPARTAN have been calculated using CART3D, an inviscid CFD package used in the preliminary design of aerospace vehicles. Cart3D utilises adjoint mesh adaption with a Cartesian cut-cells approach to produce an iteratively refined mesh to fit a flow solution. CART3D is been used to generate the aerodynamic database of the SPARTAN vehicle due to its applicability in both the subsonic and supersonic regimes, and its robustness across multiple flow solutions [16].

CART3D has previously been used to analyse hypersonic vehicles, and has shown fair agreement with experimental data across multiple studies CITATIONXX.

Trim Analysis

The SPARTAN is trimmed during flight using control surfaces on the wings. The trim is incorporated into the aerodynamic databases prior to trajectory simulation, assuming that the SPARTAN is trimmed at all conditions during flight. The SPARTAN is trimmed using control surfaces on the wings, shown

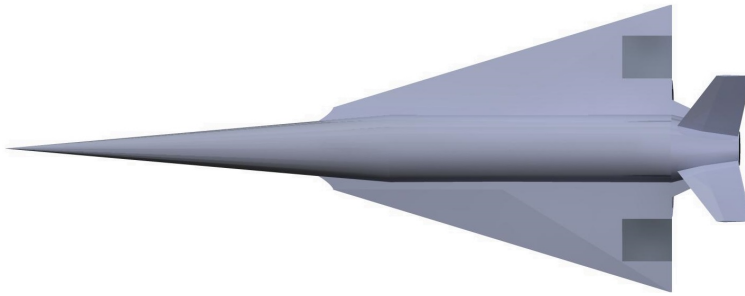


Figure 3.8: SPARTAN model showing control surfaces. Dimensions to be included.

in figure 3.8. Trim is determined by calculating the aerodynamic moment coefficient with zero flap deflection, then calculating the flap deflection necessary to balance the aerodynamic moments to zero. The moment generated by the body and wings of the SPARTAN is balanced by the moment generated by the ailerons, as well as the thrust moments on the engines and boat tail, when the C-REST engines are powered on. The force balance on the SPARTAN is shown in Figure 3.9. This trim balancing is calculated prior to trajectory optimisation for computational efficiency.

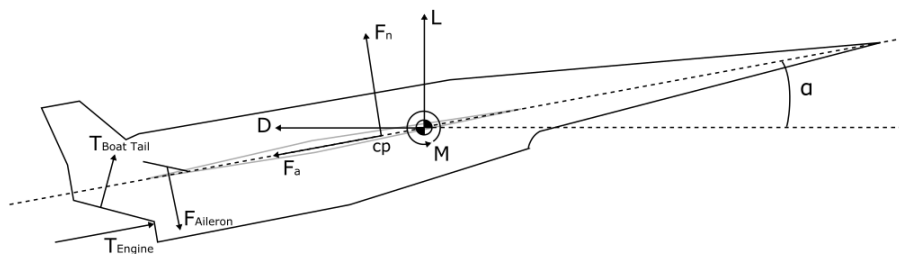


Figure 3.9: The forces on the SPARTAN during flight.

The centre of gravity of the SPARTAN is calculated using CREO. The centre of gravity varies during flight due to fuel consumption and third stage release, changing the necessary flap deflections for trim. Consequently, aerodynamic databases are created for centre of gravity conditions of;

- full fuel including third stage,

- empty of fuel including third stage,
- empty of fuel after third stage release.

At each of these conditions, aerodynamic coefficients and flap deflections necessary for trim are calculated. For simplicity, it is assumed that structural, systems and landing gear masses are homogeneously distributed throughout the centre fuselage of the SPARTAN. The calculated centre of gravity for the SPARTAN without the third stage rocket is 14.52m along the body length. The centre of gravity of the SPARTAN is varied as fuel is depleted throughout the acceleration phase, as well as when the third stage rocket is released. A point mass model is used in conjunction with the aerodynamic database, and atmospheric properties obtained from the U.S Standard Atmosphere 1976[26]. The SPARTAN is assumed to be trimmed at all conditions during flight. The trimmed aerodynamics of the SPARTAN are determined by modelling the flaps at deflected states of -20° , -10° , 10° , and 20° . Each of these deflected states were modelled in CREO and a surface mesh was created in Pointwise. The aerodynamics at each flap deflection were calculated at 0° angle of attack for Mach numbers between 0.2 and 10. For each aerodynamic data point of Mach numbers between 0.2 and 10, and angle of attacks from 0° to 10° , the necessary flap deflection are calculated, and the additional lift and drag produced by the flaps are added. The addition of trimmed aerodynamics is calculated for scramjet engines on, and engines off conditions. Due to centre of gravity variation, the trim analysis is calculated three times; at the beginning of SPARTAN acceleration; at the end of SPARTAN acceleration, when fuel has been depleted; and after the third stage has been released. The trimmed aerodynamic databases at the beginning and end of acceleration are interpolated between as the centre of gravity varies due to fuel depletion. After the third stage is released, the centre of gravity is kept constant, and a single trimmed aerodynamic database is used.

Figure 3.10 shows the necessary flap deflections to trim the SPARTAN. An Engine-on case is shown at a centre of gravity of XXm corresponding to full-fuel with third stage, and an Engine-off case is shown for a centre of gravity of XXm, corresponding to a fuel-empty state after third stage release. Additional figures illustrating the variation in moment coefficients are shown in Appendix XX. The flap deflections are designated as negative up. Negative flap deflection necessary for trim indicates that the centre of pressure is aft of the centre of gravity, and that the vehicle has positive static margin, and is generally likely to be stable.

Comment on stability here when final aerodynamics are calculated. Comment on the effect of each trim map, how it impacts lift etc.

Database Generation

The trimmed aerodynamic databases of the SPARTAN are generated in full prior to trajectory simulation to improve the computational efficiency of the simulation. The aerodynamic coefficients of lift, drag and moment are tabulated, and these tables are interpolated between during simulation. The

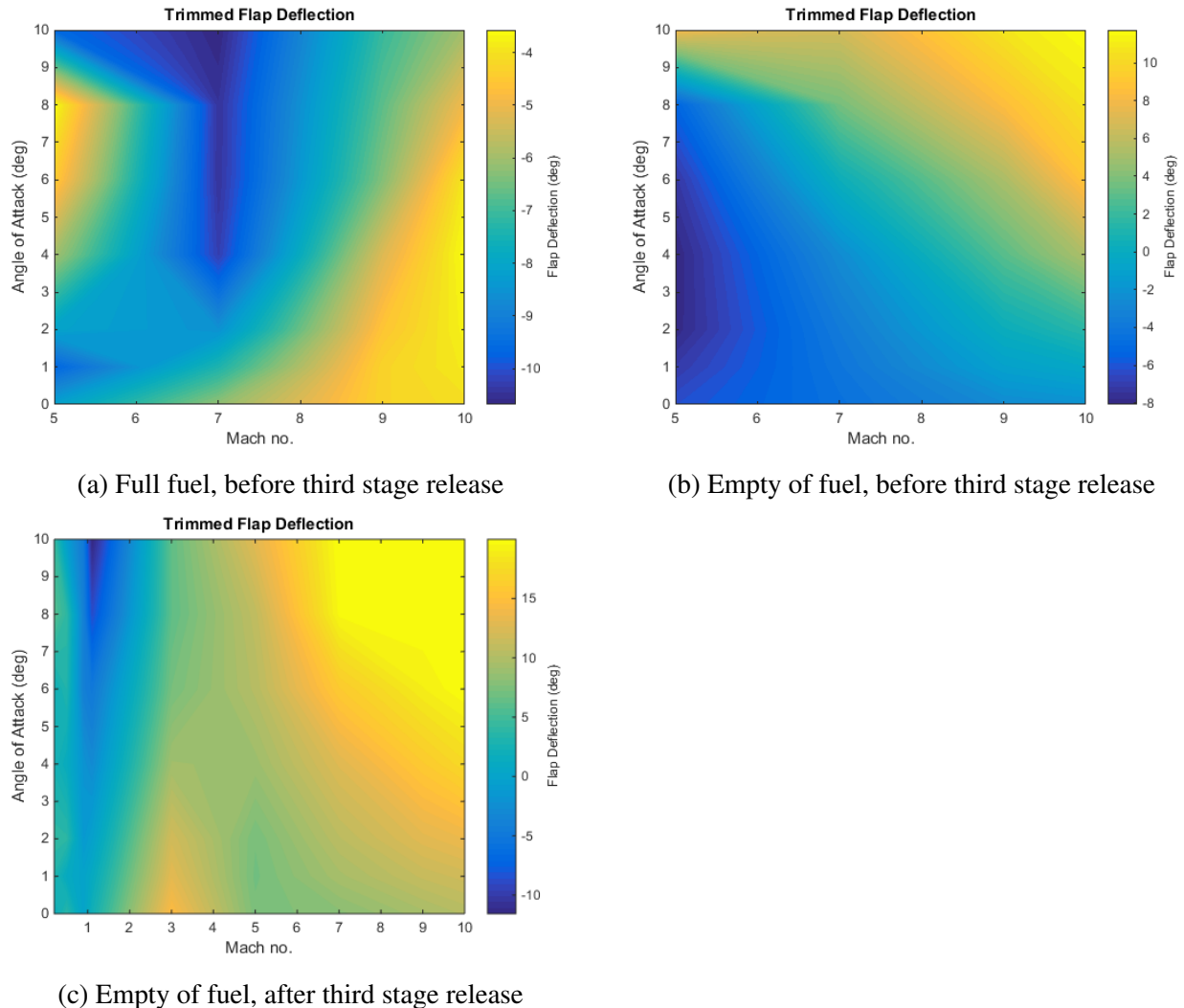


Figure 3.10: Flap deflection required for trim of the SPARTAN. Negative up. **Change colourmap to have same range**

process for generating the aerodynamic databases is shown in Figure 3.11. An initial surface trian-

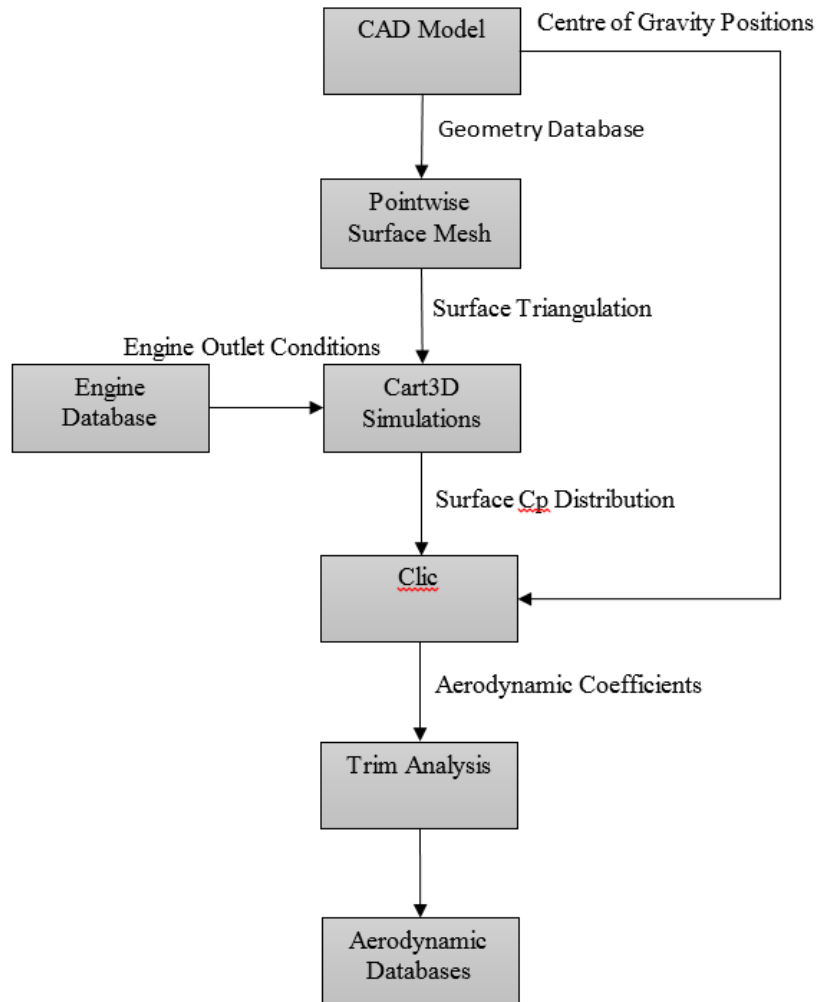


Figure 3.11: Process for generating aerodynamic databases.

gulation of the SPARTAN is created in Pointwise, shown in Figure 3.12. This is then imported into CART3D as a watertight surface. The CART3D Meshes are initiated with an outer boundary distance of 40 times the vehicle length. This boundary distance was observed to produce suitable free stream conditions and good mesh convergence. Nine mesh adaption levels are used. Nine levels have been observed to generally produce good convergence, with moderate computation times of 1-3 hours per simulation. The convergence of the residuals and forces are investigated to ascertain if a solution has converged. Figure XX shows an example solution validation for Mach 7, 2° angle of attack, engine-on conditions. Good convergence can be observed in the force functionals, with a corresponding decrease in the residual values indicating solution convergence.

CART3D validation image here, showing decreasing residuals and converging functionals.

Following simulation in CART3D over the required flight conditions, the aerodynamic databases

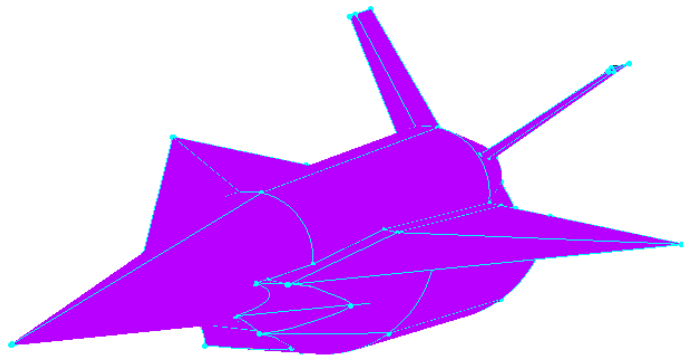


Figure 3.12: Surface triangulation of the Baseline SPARTAN. Need to recolour this image.

were generated. The simulation files were processed using Clic, a subprogram of CART3D used to calculate aerodynamic forces and moments, given surface pressure distributions. The solutions were processed for the necessary centre of gravity positions. At each flight conditions data point, and for each centre of gravity position, the necessary flap deflection for trim are calculated. The additional lift and drag generated by the flap are added to the untrimmed aerodynamics to create a trimmed database.

Engine-On Aerodynamics

The engine-on aerodynamics of the SPARTAN are used during the simulation of the acceleration phase, when the C-REST engines are operational at all times, as well as during the fly-back phase, when the engines are operational for a short time to aid the SPARTAN in returning to its initial launch site. The plumes of the SPARTAN are simulated using CART3D, using SurfBC boundary conditions which produce inflow and outflow conditions at the inlet and exit of the scramjet engines[Pandy2004]. The exit conditions calculated by the CRESTM10 database, as defined in Section 3.1.2, are set as the outflow conditions for the CART3D surface. The scaled engine modelled in the CRESTM10 propulsion analysis has an exit area of 0.5586m^2 , smaller than the nozzle exit area on the SPARTAN, of 0.9719m^2 . To accommodate for this, the outflow surfaces are scaled to the exit area of the C-Rest engines simulated by quasi 1-D analysis, to ensure that the outflow conditions match the required nozzle position. The outflow surfaces are positioned inside the nozzle on the SPARTAN model, so that the area of the outflow surface is 0.5586m^2 . The surface triangulation of the SPARTAN with outflow surfaces is shown in Figure 3.13. CART3D performs simulations nondimensionally, and requires the outflow conditions of a boundary to be normalised. The outflow conditions of P_e , ρ_e and M_e given by the CRESTM10 propulsion model are normalised to CART3D nondimensionalised variables as follows CITATIONXX;

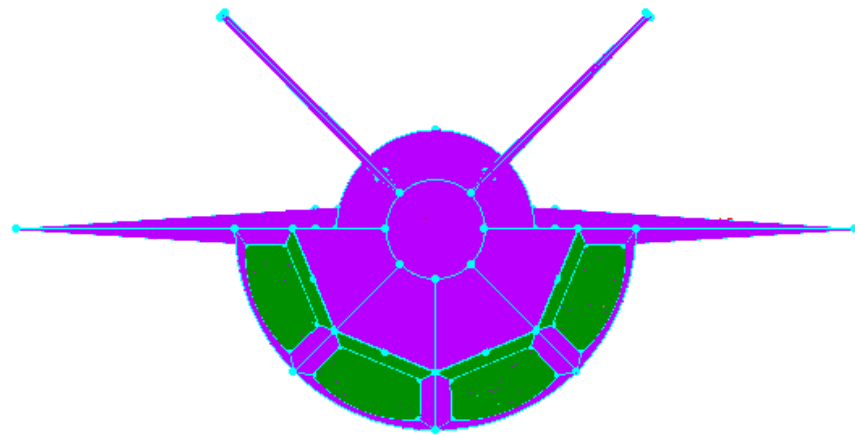


Figure 3.13: Pointwise view of the SPARTAN showing engine outlet boundaries.

$$P_e^* = P_e / (\gamma_0 P_0), \quad (3.3)$$

$$\rho_e^* = \rho_e / \rho_0, \quad (3.4)$$

$$M_e^* = \sqrt{\gamma_e / \gamma_0 (M_e \sqrt{P_e^* / \rho_e^*})^2}. \quad (3.5)$$

Where * indicates the nondimensionalised input to CART3D. This nondimensionalisation includes a correction on the Mach number to account for γ_e variation, which is not possible to include directly in CART3D[36]. Engine-on aerodynamic calculations are performed for Mach numbers 5,7,9 and 10, and at altitudes from 20km to 40km. The plumes of the scramjet engines exit the nozzle of the SPARTAN, and are further expanded onto the boat tail on the rear of the SPARTAN fuselage, shown in Figure 3.14. This expansion causes significant force on the boat tail of the SPARTAN, generating additional lift, thrust and moment forces. The trimmed aerodynamics of the SPARTAN with C-REST engines on are shown in Figure 3.15.

Engine-Off Aerodynamics

During the majority of the return flight, the scramjet engines are not operational, and the SPARTAN is gliding without power. The return phase takes the SPARTAN from third stage separation, at approximately Mach 9, to landing approach at low subsonic speeds. While the engines are not powered on air flows through the flowpath without fuel injection, generating a large amount of drag. The aerodynamics of the SPARTAN are calculated using CART3D for Mach numbers from 0.2 to 10, and angle of attack values from 0° to 10° to cover the range of flight conditions experienced during the

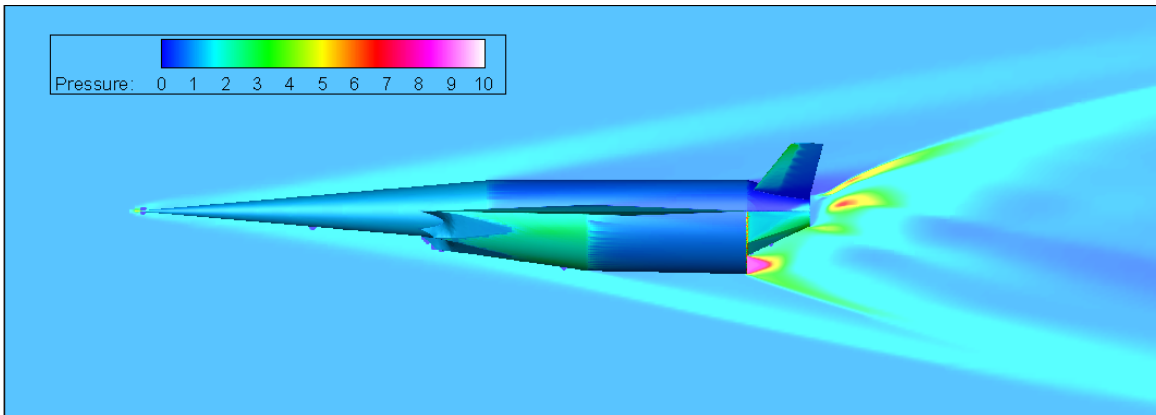


Figure 3.14: Engine-on CART3D simulation at Mach 7, 6° angle of attack, and 24km altitude. **improve the quality of images - max quality when exporting from tecplot**

fly-back of the SPARTAN. An example CART3D solution is shown for a Mach 7 engine off condition in Figure 3.16. Figure 3.17 shows the engine off aerodynamic characteristics of the SPARTAN vehicle over the range of Mach numbers and angle of attack values analysed. These results show a distinct maximum region in the L/D of the SPARTAN at high Mach numbers, within the hypersonic regime. Below Mach 5, the L/D of the SPARTAN decreases sharply. This is caused by the scramjet engines unstarting, generating significant drag. The unstalled scramjet engines are shown in Figure 3.18. **I have not confirmed that this is the sole cause yet. I will add some more info here when I have run some more simulations.**

3.2 First Stage Rocket

The first stage rocket is required to deliver the second stage to near horizontal flight at Mach 5.1 flight conditions, after which it is discarded. To achieve this, the first stage rocket is modelled as a Falcon-1e first stage scaled down lengthwise to 9.5m, keeping the original diameter of 1.67m[CITATIONXX]. The Falcon-1e has been chosen due to its appropriate scale, and the proven flightworthiness of the Falcon-1. The first stage is attached to the rear of the scramjet second stage and is powered by a single LOX-kerosene Merlin 1-C engine. A connecting cowl has been modelled between the first stage rocket and the SPARTAN to improve the aerodynamic profile. The first stage has a structural mass of 1356kg, determined by scaling of the structural mass of the Falcon-1e. The engine mass of the Merlin 1-C is kept constant during scaling at 630kg[CITATIONXX]. The mass of the fuel in the first stage is scaled as part of the optimisation routine, as the dynamics of the vehicle, and its ability to reach a given separation point, are very closely coupled to the available fuel mass.

The thrust and specific impulse of the Merlin 1-C are determined by interpolation between the sea level and vacuum specific impulse of the Merlin 1-C, shown in Table 3.2, with pressure. Thrust scaling is determined by linear pressure scaling using nozzle exit area, $T = T_{SL} + (p_e - p_{SL})A_e$. The

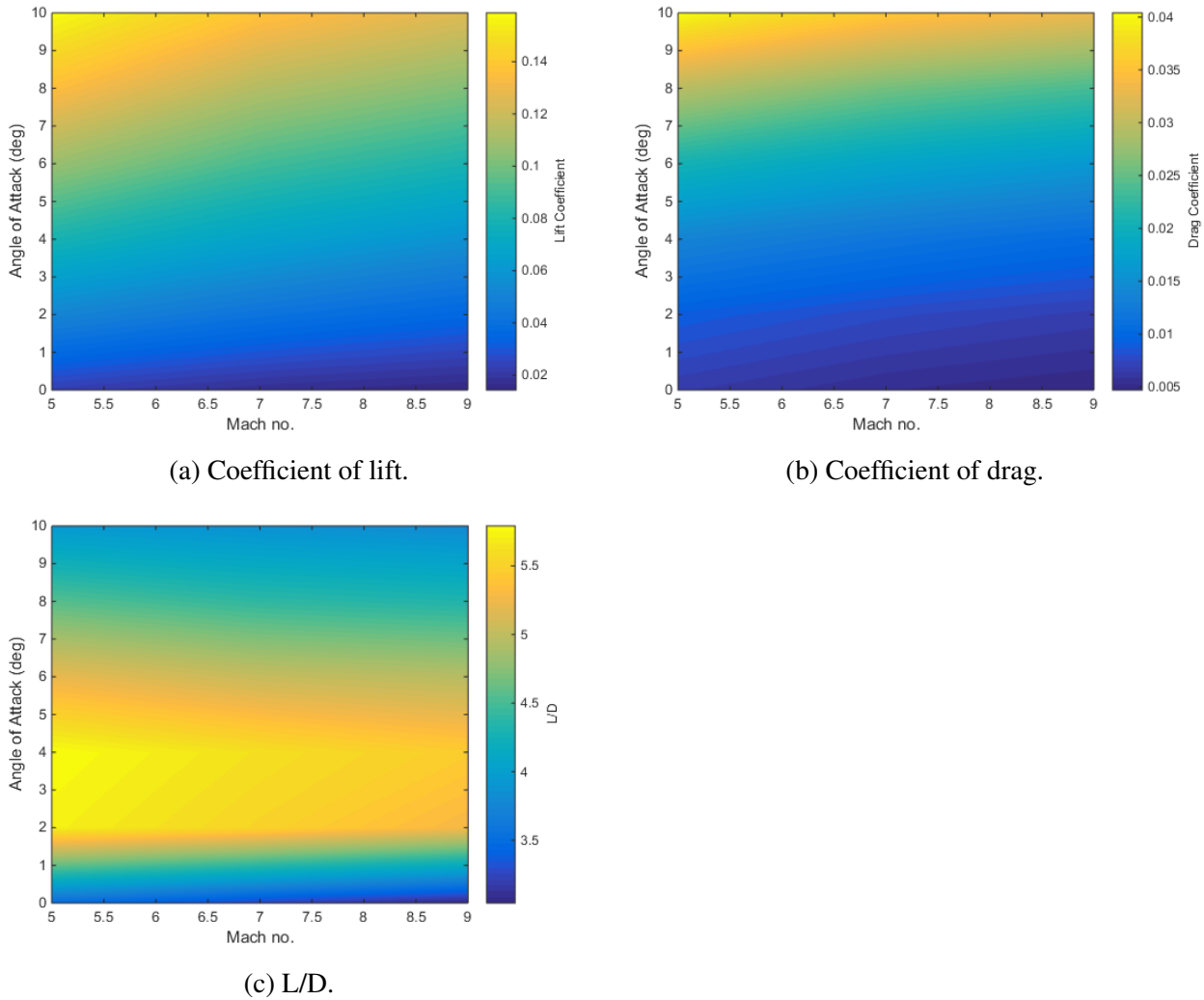


Figure 3.15: Trimmed aerodynamic coefficients with the C-REST engines powered on. Coefficients correspond to a reference area of 62.77m^2 . **NOTE: I need to run a new clic case for these plots without nozzle or boat tail**

Merlin 1-C is throttled down to a constant 85% to allow the first stage to pitch over more easily.

3.2.1 Aerodynamics Including First Stage

The aerodynamics of the launch system during first stage flight are calculated in a similar manner to those of the SPARTAN without the first stage rocket, as detailed in Section 3.1.3. The aerodynamics of the SPARTAN and first stage rocket are calculated using CART3D. The first stage aerodynamics are modelled between angles of attack of 0° to -5° , as the first stage will be flying at negative angle of attack to induce faster pitch-over. Mach numbers from 0.2 to 5.1 (second stage separation velocity) are simulated. Figure 3.19 shows an example CART3D simulation case, at Mach 2, -1° angle of attack. The coefficient of lift, drag and aerodynamic moment are tabulated for each simulation. Figure 3.20

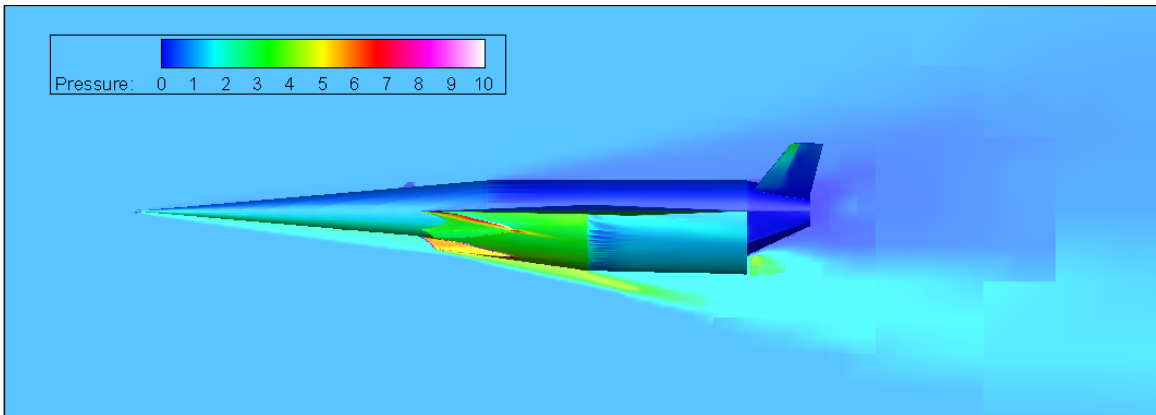


Figure 3.16: CART3D flow result for the SPARTAN, at Mach 7, 6° angle of attack.

$I_{SP_{SL}}$	275s
$I_{SP_{vac}}$	304s
T_{SL}	555.9kN
A_e	$0.552m^2$

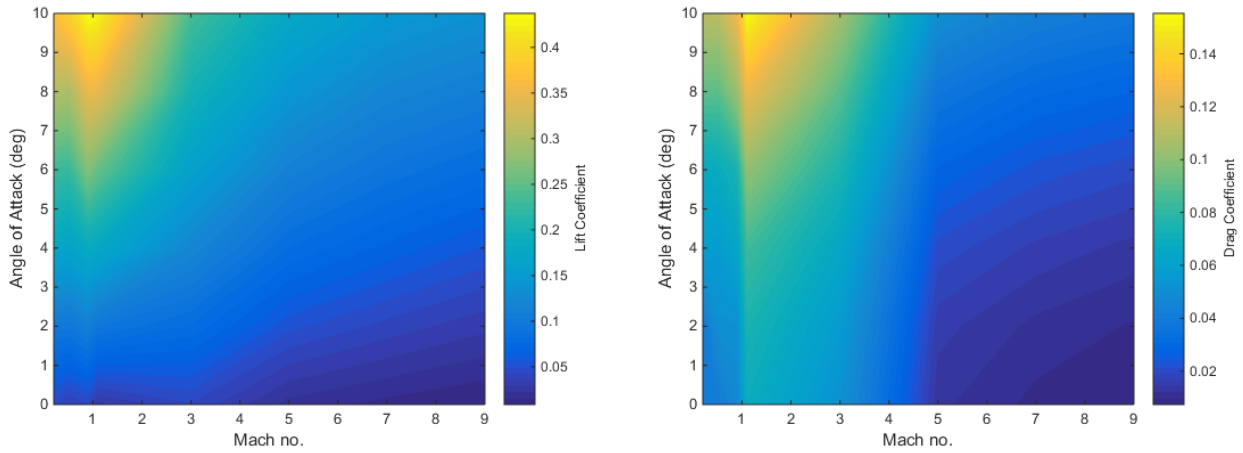
Table 3.2: First Stage Engine Properties [CITATIONXX].

shows the lift and drag coefficients of the first stage, as well as the lift-over-drag, across the simulated Mach Numbers and angles of attack. Before the trajectory is simulated, the launch vehicle is trimmed using the ailerons of the SPARTAN. The simulations of the SPARTAN with flap deflections between -20° and 20° are used to calculate the deflection necessary to trim the vehicle, as described in Section 3.1.3, and the additional lift and drag generated by the ailerons is added to the aerodynamic database of the first stage launch vehicle.

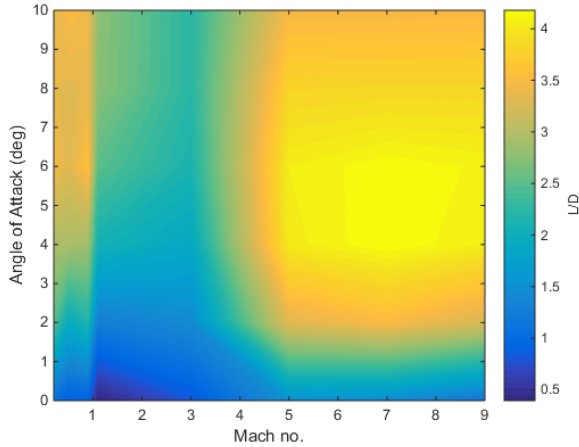
3.3 Third Stage Rocket - Baseline

The third stage has a total length of 9m, with a 3m long nose, 4.5m long centrebody and 1.5m long engine. In this study the third stage rocket has been designed to accommodate a SpaceX Kestrel engine. In previous studies, the third stage has been designed to be powered by a Pratt & Whitney RL-10-3A pump-fed engine. The Kestrel has been used over the RL-10-3A for its cost effectiveness. As a pressure-fed engine, the Kestrel trades off specific impulse for weight and cost savings when compared to the RL-10-3A. As the only expendable portion of the system; the cost of the third stage is one of the main drivers of overall system cost. Reducing the cost of the third stage allows the cost of launch to be directly reduced.

The third stage rocket is released at the end of the scramjet accelerator burn, and lifts the payload out of the atmosphere and into the desired orbit. The third stage weighs a total of 3300kg. This has been chosen as a nominal design weight, to satisfy the fuel necessary to achieve orbit with an



(a) Coefficients of lift of the SPARTAN, calculated using CART3D. (b) Coefficients of drag of the SPARTAN, calculated using CART3D.



(c) L/D of the SPARTAN.

Figure 3.17: Trimmed aerodynamic Characteristics of the SPARTAN with C-REST engine powered off. Coefficients correspond to a reference area of 62.77m^2 .

acceptable payload, while also allowing for ample payload volume. The internal layout of the third stage rocket is shown in Figure 3.21. The third stage has a structural mass fraction of 0.09, similar to the Falcon 1 second stage [60]. This gives a total structural mass (without heat shield) of 285.7kg.

The kestrel engine used in the third stage is modified to have 50% increased propellant mass flow rate, giving a mass flow rate of 14.8kg/s. The nozzle exit of the Kestrel engine has been kept constant at 1.1m diameter. An increase in mass flow necessitates a corresponding increase in throat area. This increase in throat area decreases the area ratio of the nozzle. The initial area ratio is 60, measured from schematics in the Falcon-1 Users Guide. A 50% mass flow increase corresponds to a 50% throat area increase, which causes the area ratio to decrease to 40. This decrease in area ratio results in a 2% loss of efficiency from the nozzle, measured from the thrust coefficient relationships shown in Figure 3.22[64]. The coefficient of thrust is calculated for a specific heat ratio of 1.20, as this is close to the

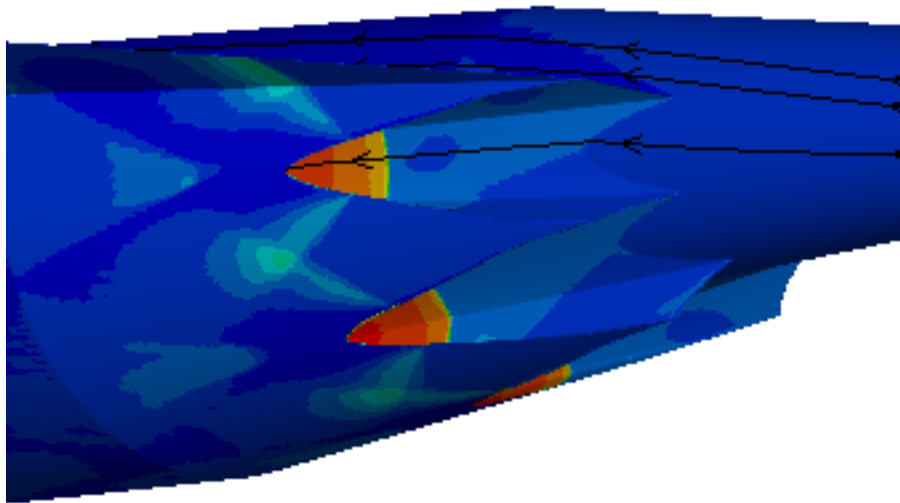


Figure 3.18: Unstarted scramjet engines. Placeholder Image, this will be improved.

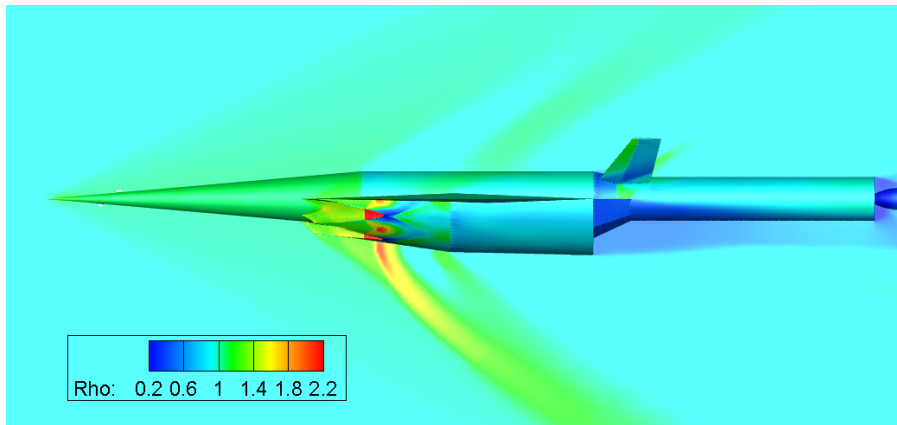


Figure 3.19: CART3D result for the SPARTAN and first stage vehicles at Mach 2, -1° angle of attack.

specific heat ratio of oxygen and RP-1 of 1.24[64]. The modified specific impulse of the engine is 310.7s.

3.3.1 Heat Shield Sizing

Note: need to present more of the logic which led to this heat shield design. Need to get this from Michael S.

The third stage rocket is separated from the SPARTAN at a high dynamic pressure, after which it spends a considerable amount of time accelerating in-atmosphere before reaching exoatmospheric conditions. This release into a high dynamic pressure environment creates a large amount of heating, which must be mitigated by heat shielding. The third stage is protected while in-atmosphere by a heat shield, weighing 125.6kg. This heat shield is constructed from a phenolic cork cylinder, a reinforced

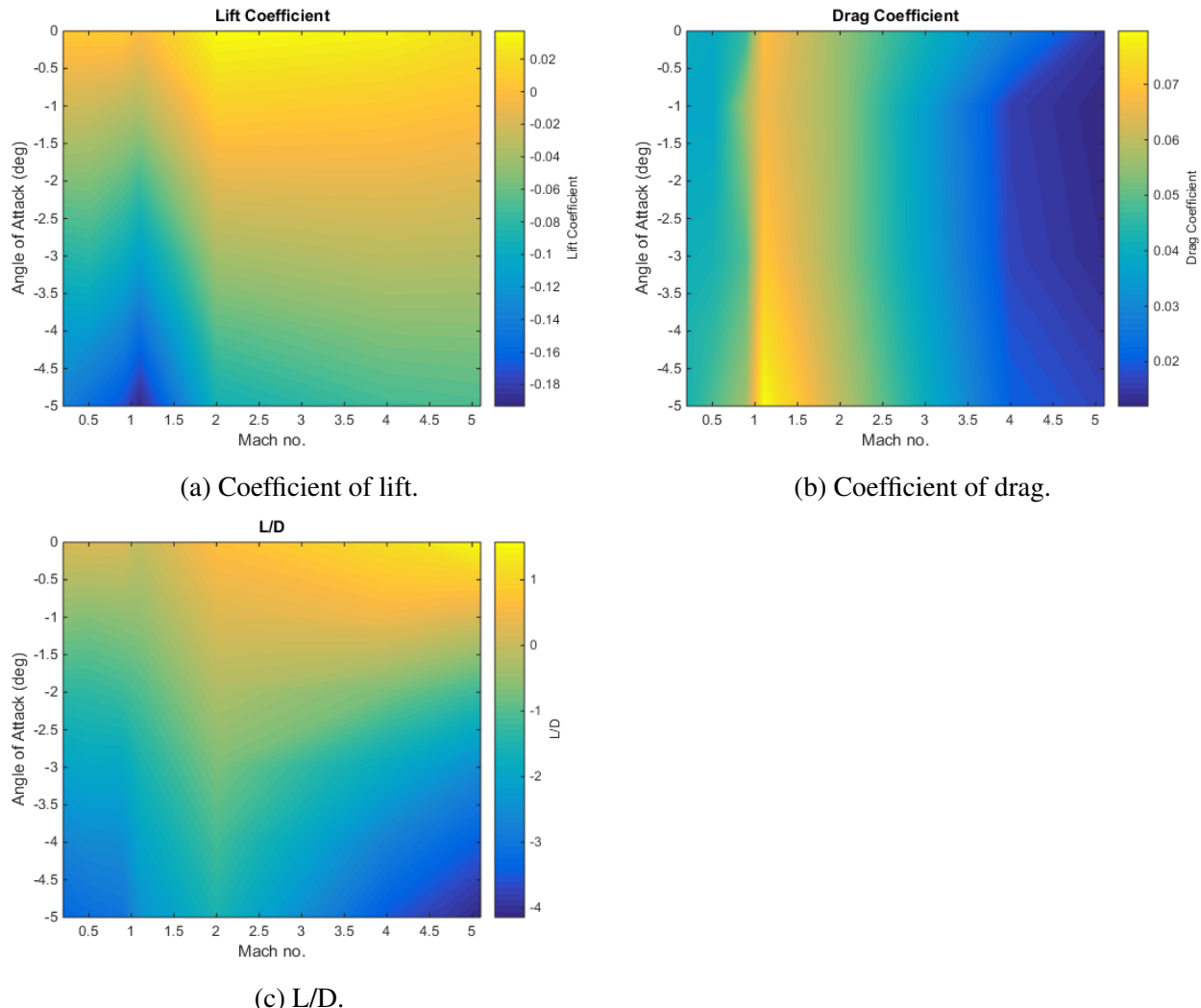


Figure 3.20: Aerodynamic characteristics of the SPARTAN including the first stage rocket.



Figure 3.21: The third stage rocket, showing major internal features. *note:labels to be added*

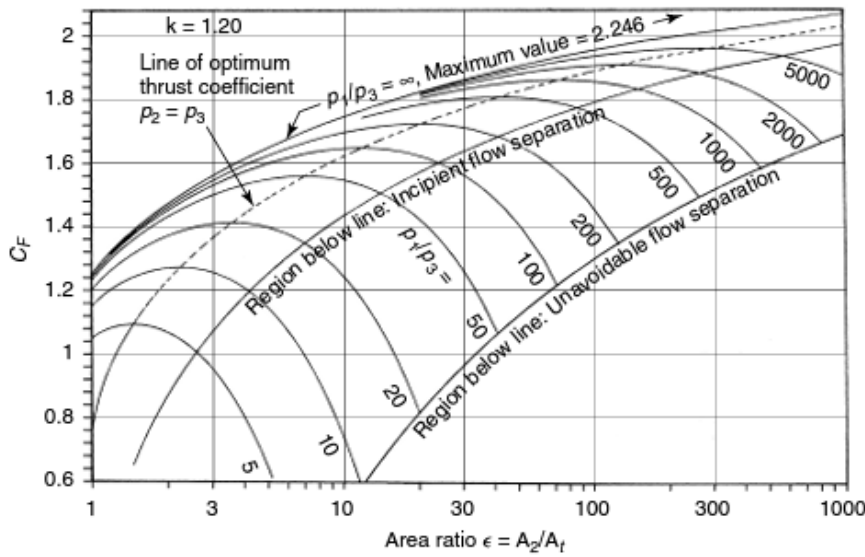


Figure 3.22: Variation in coefficient of thrust with area ratio [64].

carbon-carbon nose cone, and a tungsten nose tip.

Part	Density	Geometry	mass
Tungsten Nose	$\rho_{Tungsten} = 19.25 \text{ g/cm}^3$	50mm diameter cylinder, spherical tip	12.6kg
C-C Cone	$\rho_{CC} = 1800 \text{ kg/m}^3$	10mm thick, conical	89.3kg
Phenolic Cork Cylinder	$\rho_{PhenolicCork} = 320 \text{ kg/m}^3$	5mm thick, cylindrical	23.7kg

Table 3.3: Third stage heat shield breakdown.

3.3.2 Fuel Tank Sizing

The internal design of the third stage is allowed to be slightly variable as the trajectory is optimised. The third stage mass is fixed at 3300kg, and the calculated payload-to-orbit varies by exchanging leftover fuel mass for effective payload mass. To calculate the dynamics of the third stage, the fuel tanks have been approximately sized, assuming 160kg of payload-to-orbit. Realistically the exchange between fuel and payload mass would cause the fuel tanks to be resized slightly. For the purposes of this study the fuel tanks are assumed to be of constant size for simplicity. Currently this is a reasonable assumption as the internals of the rocket are very simplified. The structural mass is held constant at 9%. The third stage carries a total propellant mass of 2736.7kg. Table 3.4 breaks shows the component break-down of the LOX oxidiser and RP1 fuel.

	LOX	RP1
Ratio	2.56	1
Density	1141kg/m ³	813kg/m ³ [35]
Volume	1.7248m ³	0.9455m ³
Mass	1968.0 kg	768.7 kg

Table 3.4: Third stage fuel distribution.

3.3.3 The Aerodynamics of the Third Stage Rocket

The third stage aerodynamics have been calculated using Missile DATCOM [REFXX], a preliminary design tool for estimating the aerodynamic characteristics of missile and rocket vehicles. Missile DATCOM utilises empirical methods, along with various estimation techniques, to compute the aerodynamics of missile-like vehicles across the subsonic, supersonic and hypersonic regimes. The aerodynamics of the third stage rocket are shown in Figure 3.23. The code used to compute the aerodynamics of the third stage rocket is detailed in Appendix XX.

Thrust Vectoring

The third stage rocket is controlled via thrust vectoring. The centre of pressure is calculated using missile DATCOM. The thrust vector is set so that the moment generated by the engine matches the lift force acting at the centre of pressure, shown in Figure 3.24. The maximum thrust vector limit has been set to 8°. As no data on the maximum thrust vectoring capabilities of the kestrel engine was able to be found, this was set to the maximum gimbal range of the Aestus pressure-fed engine and OMS, similar pressure fed engines CITATIONXX.

The centre of gravity is determined using CREO, and is at XXm from the nose. It is assumed that the mass of the structure of the rocket (excluding fuel tanks, heat shielding, engine and payload) is distributed homogeneously for simplicity. The third stage rocket is statically unstable. Flying this rocket at an angle of attack will require an advanced automatic controller, as the only control available is produced by thrust vectoring. This study assumes that the third stage rocket is able to be controlled over any required trajectory, as long as the thrust vector limits of the vehicle are not exceeded.

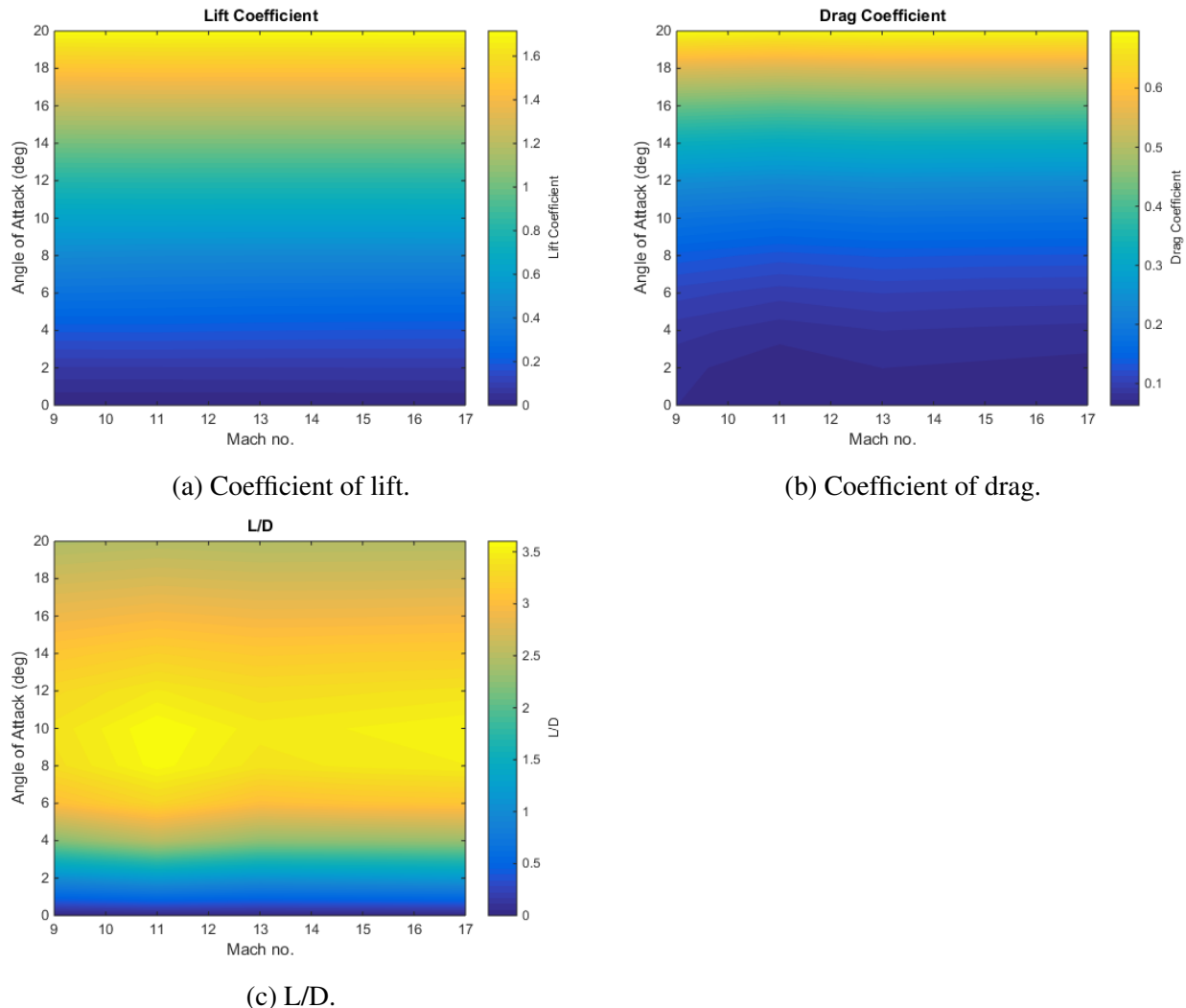


Figure 3.23: Aerodynamic characteristics of the baseline third stage rocket, for a reference area of 0.95m^2 .

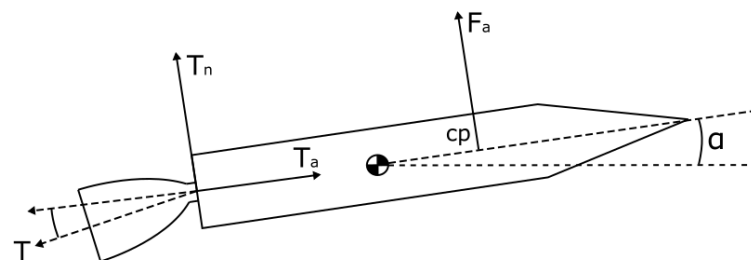


Figure 3.24: Thrust vector force balance.

CHAPTER 4

LODESTAR

This chapter covers the optimal control program LODESTAR, which has been used to simulate the optimal trajectories of the rocket-scramjet-rocket system. The basics of optimal control and the optimal control methods used are presented, as well as the specific problem formulation used by LODESTAR.

The program LODESTAR (Launch Optimisation and Data Evaluation for Scramjet Trajectory Analysis Research) has been developed to aid with the simulation and trajectory optimisation of space launch systems. LODESTAR is a MATLAB based trajectory optimiser which utilises GPOPS-2, a proprietary pseudospectral method optimisation package as well as MATLAB's inbuilt SQP solver. LODESTAR optimises a trajectory towards a user-defined objective function, such as constant dynamic pressure or maximum payload-to-orbit. LODESTAR accurately models both rocket-powered and scramjet-powered vehicles in 5 degrees of freedom. LODESTAR contains multiple modules configured for the SPARTAN launch system, which are able to optimise trajectories for;

1. The ascent of the first stage rocket.
2. The ascent of the second stage scramjet-powered accelerator.
3. The flyback of the second stage scramjet-powered accelerator.
4. The ascent of the third stage rocket.

LODESTAR performs optimisation using four classes of variables, primals, controls, constraints and costs, which define the optimisation problem being solved. Primals are the variables which define the physical trajectory and are dependent on other primals and the control variable. The control variables are independent in the solution space and can be modified freely by the solver algorithm within the prescribed limits. Constraints bound the primal and control variables to a well defined solution space and events confine the primal and control values to a specified value at a specific point

in time. The cost variables define the target of the optimisation problem. A solution is found when the cost is minimised to a suitable accuracy.

GPOPS-II and DIDO require these variables to be precisely described. LODESTAR contains multiple modules that calculate the vehicle aerodynamic properties and run external simulations which then feed data back to the pseudospectral solver for evaluation. Modules calculate the vehicle aerodynamic and engine output at each point along the trajectory. The vehicle model module takes this data and calculates the mass of the vehicle as well as the 6 degree of freedom motion derivatives of the vehicle along the trajectory. As this is an iterative process, the calculated motion derivatives do not match the motion approximation exactly until convergence is achieved (This is a fundamental property of the pseudospectral method, see Section 2.8.3).

-XX define the iterative process here, include evaluation of the optimisation variables, and sequential quadratic programming

The cost is calculated using the primal variables. The trajectory is evaluated to produce the final cost of the trajectory. The final step of each iteration is updating the primal derivatives, which is performed by the dynamics file. The primal derivatives and cost are evaluated by DIDO to determine if the trajectory has produced a suitable result.

4.1 Optimal Control

The pseudospectral method and direct single shooting techniques used by LODESTAR are described in detail in sections XX. Practically, the implementation of these techniques involves the specification of the set of constraints and objectives which govern the optimisation problem. These constraints inform the optimiser of the bounds of the optimisation, and perform the functions of limiting the search space to the physically possible (eg. constraining altitude to be greater than ground level) as well as constraining the vehicle within its performance limits (eg. limiting the angle of attack). These constraints also come in the form of initial or terminal constraints, which define the initial conditions of the trajectory as well as any conditions which the trajectory must meet at termination.

The pseudospectral method requires the specification of a set of 'primal variables'. These primal variables describe the physical dynamics of the system. In the pseudospectral method, the dynamics of the system are used as constraints on the optimal control problem;

$$\dot{\mathbf{x}}(\tau) = f[\mathbf{x}(\tau), \mathbf{u}(\tau)]. \quad (4.1)$$

Implementing the dynamics as constraints allows the optimiser to explore each primal variable independently, greatly increasing the robustness of the optimal control problem. However, the constraints may be violated by the optimiser in the process of searching for an optimal solution. A violation of the physical dynamics constraints means that the dynamics of the system may not hold throughout the

Primal Variables	x Position y Position Velocity
Control Variables	Angle of Descent
Initial Constraints	Velocity x Position y Position
Terminal Constraints	x Position y Position
Path Constraints	None
Target Cost	Minimum Time

solution process, causing potential complications for the computational model of the vehicle. Much of the design of the vehicle simulation in this study is driven by the need for smooth, continuous interpolation schemes, and viable extrapolation regions ie. even if the solution is well within the range of all input data sets, the solver must be able to explore all regions within the set bounds.

4.1.1 GPOPS-2 Example - Brachistochrone Problem

This section describes a short example optimal control problem solved in GPOPS-II. The purpose of this example is to demonstrate the effectiveness of the pseudospectral method and GPOPS-II, and to provide a simple example case to establish the terminology of an optimal control problem.

The brachistochrone (from the Greek for 'shortest time') problem is a simple optimal control problem, which describes a ball rolling in two dimensions under gravity. The objective is to find the curve of descent which will minimise the time from point *a*, where the ball is at rest, to point *b*. It is assumed that gravity is constant and that there is no forces other than gravity acting on the ball.

The analytical solution of this problem can be computed using the Euler-Lagrange equation as the equations describing a cycloid:

$$x = A(\theta - \sin \theta),$$

$$y = A(1 - \cos \theta)$$

This problem has been solved using GPOPS-2. Table XX describes the set-up of the optimal control problem in GPOPS-2. The dynamic equations for the Brachistochrone problem are:

$$\dot{x} = v * \cos(u),$$

$$\dot{y} = v * \sin(u),$$

$$\dot{v} = -g * \sin(u).$$

The GPOPS-2 solution to the Brachistochrone problem is shown in Figure XX. This is overlaid with a plot of the optimal solution.

- xx put optimal solution in here **compare to analytical solution (dont include, just have plot)**

The dynamics of the basic Brachistochrone problem are very simple. As the dynamic become

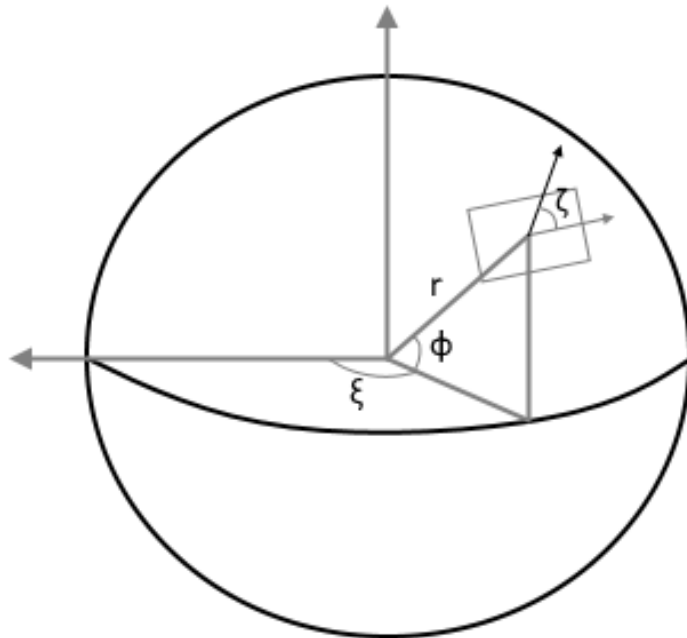


Figure 4.1

more complex, it is no longer possible to obtain an analytical solution.

4.2 The Trajectory Optimal Control Problems

4.2.1 Dynamic Model

The dynamics of the vehicle are calculated in six degrees of freedom, with pitch constrained to zero. The dynamics of all stages are calculated using an geodetic rotational reference frame, written in terms of the angle of attack α , bank angle η , radius from centre of Earth r , longitude ξ , latitude ϕ , flight path angle γ , velocity v and heading angle ζ . The equations of motion are [28]:

$$\dot{r} = v \sin \gamma \quad (4.2)$$

$$\dot{\xi} = \frac{v \cos \gamma \cos \zeta}{r \cos \phi} \quad (4.3)$$

$$\dot{\phi} = \frac{v \cos \gamma \sin \zeta}{r} \quad (4.4)$$

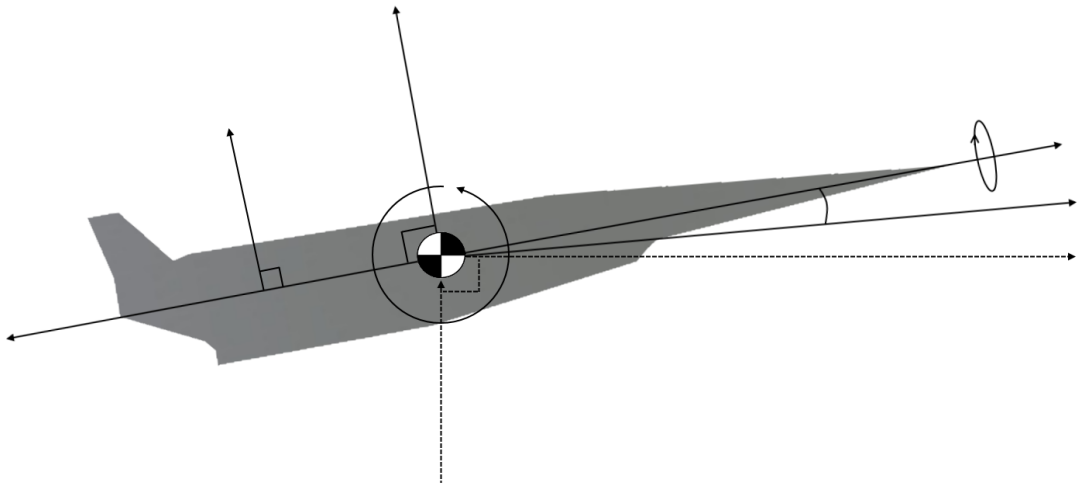


Figure 4.2

$$\dot{\gamma} = \frac{T \sin \alpha \cos \eta}{mv} + \left(\frac{v}{r} - \frac{\mu_E}{r^2 v} \right) \cos \gamma + \frac{L}{mv} + \cos \phi [2\omega_E \cos \zeta + \frac{\omega_E^2 r}{v} (\cos \phi \cos \gamma + \sin \phi \sin \gamma \sin \zeta)] \quad (4.5)$$

$$\dot{v} = \frac{T \cos \alpha}{m} - \frac{\mu_E}{r^2} \sin \gamma - \frac{D}{m} + \omega_E^2 r \cos \phi (\cos \phi \sin \gamma - \sin \phi \cos \gamma \sin \zeta) \quad (4.6)$$

$$\dot{\zeta} = \frac{T \sin \alpha \sin \eta}{mv} - \frac{v}{r} \tan \phi \cos \gamma \cos \zeta + 2\omega_E \cos \phi \tan \gamma \sin \zeta - \frac{\omega_E^2 r}{v \cos \gamma} \sin \phi \cos \phi \cos \zeta - 2\omega_E \sin \phi \quad (4.7)$$

Flow chart of modules details of simulation (5DOF geodetic rotational) details of limits

verification methods -hamiltonian/costates -complementary conditions -forward sim (for sanity checking, will need to detail deficiencies in this) -forward integration -logic check (ie solver is still a heuristic process, run multiple times with varying guess. Is solution logical?)

- outline the pseudospectral method, as implemented in GPOPS? ie with stage definitions

4.2.2 Trajectory Connection Points

The optimisation of a large, nonlinear system is a complex and time-consuming task. The optimisation of the trajectory of the rocket-scramjet-rocket launch system considered in this study is an extremely complex problem, if simulated in its entirety. It is a potentially unmanageable task to produce an optimised trajectory by considering the entire launch trajectory as a single nonlinear programming problem. To mitigate the complexity of the simulation, the trajectory of the rocket-scramjet-rocket launch system has been broken down into subsections, shown in Figure 4.3. These contiguous subsections are then able to be analysed and optimised independently. The subsections of the trajectory are connected through the use of initial and end constraints on the independent optimisation problems. These constraints are described in Table ??.

Section	Initial Constraint	End Constraint
1 st Stage Vertical Ascent (I-II)	Constrained to start at a velocity of 0m/s.	Constrained to fly to 90m altitude and 30m/s velocity.
1 st Stage Pitching Ascent (II-III)	Constrained to start at 90m altitude and 30m/s velocity	Constrained entirely to 2 nd stage initial conditions
2 nd Stage Ascent (III-IV)	Constrained to 1520m/s velocity.	Constrained to 102.0° heading angle, the approximate angle which allows the third stage to reach sun synchronous orbit.
2 nd Stage Return (IV-VI)	Constrained entirely to 2 nd stage ascent end conditions.	Constrained to conditions approaching landing at the initial launch site.
3 rd Stage Ascent (IV-V)	Constrained entirely to 2 nd stage ascent end conditions.	Flight parallel with Earth's surface.
3 rd Stage Hohmann Transfer (V)	Constrained entirely to 3 rd stage ascent end conditions.	Constrained to sun synchronoud orbit.

Table 4.1

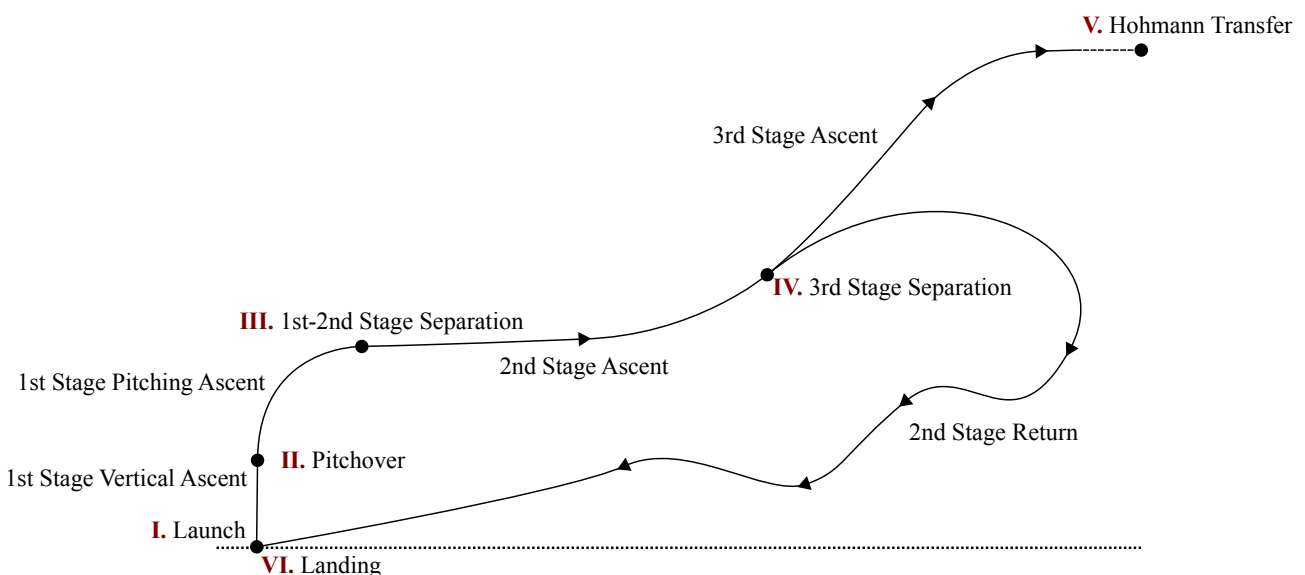


Figure 4.3

4.2.3 First Stage Trajectory

LODESTAR is able to optimise the first stage of a launch vehicle, for an angle of attack controlled trajectory, from launch to a pre-defined end point. LODESTAR is able to optimise for either a maximum velocity or minimum mass optimisation objective.

A maximum velocity case is desired when a specific first stage vehicle design is being investigated.

A minimum mass objective is applicable when the first stage trajectory has a pre-defined end goal.

This is the case with the SPARTAN vehicle where the SPARTAN scramjet accelerator is to be released at its minimum operating conditions at close to horizontal flight. A variable mass for the first stage launch vehicle is desired as the mass has large effects on the dynamics of the vehicle, effecting the trajectory angle change rate, as well as the acceleration and time of flight of the vehicle. It is useful in the preliminary design stages to be able to optimise the mass of the first stage vehicle, allowing a less trial-and-error approach. In the minimum mass case, the launch altitude is slightly variable, as LODESTAR starts optimisation from a set pitchover altitude and velocity, and the pre-pitchover trajectory is calculated to match the pitchover mass.

Input	Contains
Aerodynamic Database	
Initial Constraints	
Terminal Constraints	
Path Constraints	
Target Cost	

The first stage is launched from an area in northern Queensland.

Control Variables

Primal Variables

4.2.4 Second Stage Trajectory

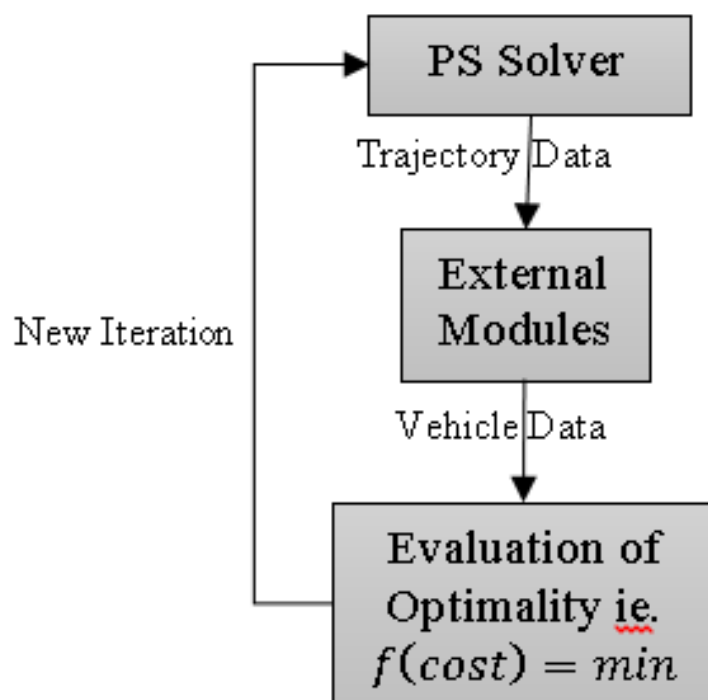


Figure 4.4

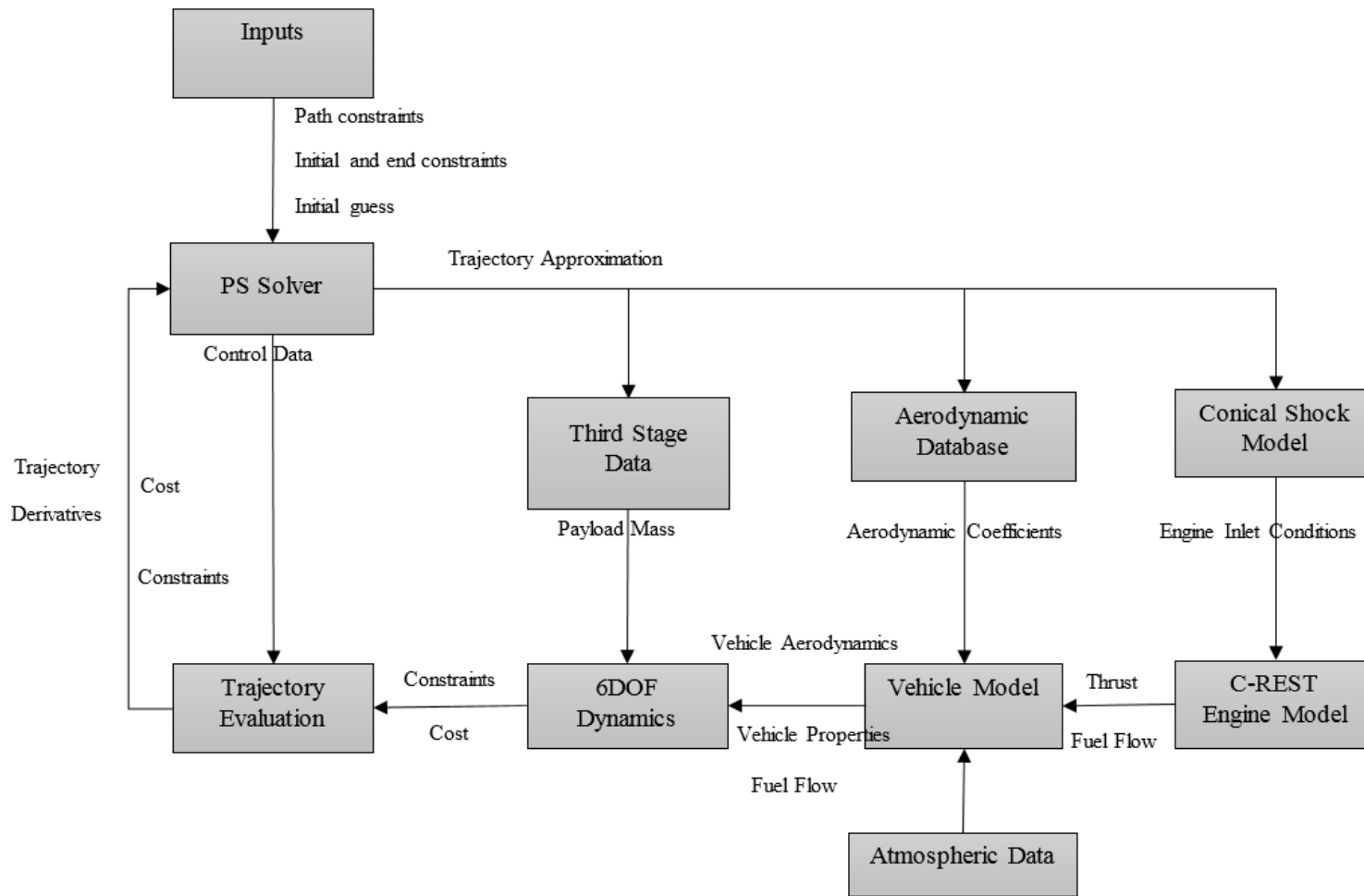


Figure 4.5

LODESTAR is able to optimise the trajectory of airbreathing accelerators in the supersonic or hypersonic regime. LODESTAR is able to optimise for a range of optimisation metrics, including a maximum payload-to-orbit and constant dynamic pressure. The trajectory of the SPARTAN scramjet-powered accelerator has been simulated in LODESTAR.

Initial Constraints	Velocity Fuel Mass Latitude Longitude
Terminal Constraints	Fuel mass Heading Angle
Path Constraints	Dynamic Pressure
Target Cost	Maximum Payload-to-Orbit

Control Variables

Primal Variables

primal variable limits:

4.2.5 Second Stage Return Trajectory

After releasing the third stage rocket, the scramjet-powered second stage must return back to an area close to the initial launch site. During the flyback, the SPARTAN cannot exceed its dynamic pressure limit of 50kPa. The SPARTAN must land on the ground with minimum velocity, within close proximity to the launch area. It is assumed that a landing strip is available at the spot where the SPARTAN lands. The SPARTAN is required to land within a set radius of the launch site. This constraint is;

$$(\phi_{end} - \phi_{launch})^2 + (\xi_{end} - \xi_{launch})^2 - r^2 \leq 0 \quad (4.8)$$

Summary Table

Initial Constraints	Altitude Velocity Flight Path Angle Heading Angle Latitude Longitude
Terminal Constraints	Distance From Launch Site
Path Constraints	Dynamic Pressure
Target Cost	Minimum End Velocity

Control Variables

4.2.6 Third Stage Trajectory

-detail the vehicle dynamics with a free body diagram

Input	Contains
Aerodynamic Database	Mach Number, AoA, CA, CN, CD, CL, cP
Output	Contains

The third stage is required to deliver the payload into heliosynchronous orbit. The heliosynchronous orbit chosen is 566.89km.

Initial Constraints	
Terminal Constraints	
Path Constraints	Angle of Attack
Target Cost	

The third stage trajectory angle is initiated at a heading angle of 102.0° . This is chosen as the heading angle which allows the third stage to closely match the required orbital inclination angle for sun synchronous orbit at 567km, of 97.63° .

-Detail the hohmann transfer

Control Variables

4.2.7 Combined Second Stage Ascent & Return Trajectory

4.2.8 Validation

Optimality Conditions

LODESTAR provides the capacity to partially validate the optimal solution provided by the pseudospectral method solver. This partial validation is used to determine whether the pseudospectral method solver has converged close to an optimal solution of the nonlinear programming problem. It is particularly useful to validate that the optimality and constraint tolerances which have been chosen are sufficiently small, or to check whether the pseudospectral method solver has approached an optimal solution in the case that the defined tolerances are not able to be reached. This partial validation is achieved through the examination of some of the necessary conditions for optimality. The necessary conditions

The control Hamiltonian is investigated to verify that the first order necessary conditions hold. Due to the unconstrained end time of the trajectory problems, $H \equiv 0$ [Pucci2007]. The Hamiltonian is defined as: $H(x(t), u(t), \lambda(t), t) = \lambda^T(t)f(x(t), u(t)) + L(x(t), u(t))$. Make sure this is consistent with format in lit review, link This is calculated using LODESTAR and the Hamiltonian condition

is able to be verified. The Hamiltonian will likely not be exactly equal to zero along the trajectory. This is due to the heuristic nature of the solver, which will approach close to an optimal solution, but never reach it exactly. A sufficiently small Hamiltonian indicates that the end solution approaches an optimal solution, and may be a candidate as an optimised trajectory case.

Costates Complementary conditions

To assess the quality of the optimisation problem solved using the pseudospectral method,

The primal feasibility of the solution is checked through a comparison of the state derivatives, $\dot{x} = f(x, u)$. \dot{x} is first determined through numerical differentiation of the primal variables over the solution time. Then $f(x, u)$ is determined using the dynamics of the system and vehicle model, in the same way that $f(x, u)$ is input to the pseudospectral solver. Examination of the error between the 'expected' state derivatives, and the numerical approximation of the derivatives, $\dot{x} - f(x, u)$, allows the accuracy of the system dynamics to be verified.

GPOPS - output.result.solution.phase.pathmultipliers I believe these should be 0, as they are the mu associated with path constraints (and the function C;0, meaning mu=0)

output.result.solution.phase.costate gives costates, not sure how to use these

include IPOPT infeasibilities infpr and infdu (need to mention GPOPS-2 is based on IPOPT)

Forward Simulations

-both the control check and derivative check

The pseudospectral method considers the dynamics of the system as constraints on the optimal control problem, and solves across the entire trajectory simultaneously. This causes the physical system dynamics to have an associated margin of error, ie. $\dot{x} = f(x)$ will only hold to a certain degree of accuracy. For a well converged solution, this margin of error will be negligibly small, and the dynamics of the system will be consistent with realistic Newtonian dynamics. However, when the problem is not well converged, the dynamics of the system may have a large error. It is possible to make a preliminary check of the system dynamics using the XX (complementary conditions?). However, to be certain that the system is behaving as it should be, a full forward simulation is necessary. This forward simulation starts at the initial conditions prescribed by the pseudospectral method solver, and propagates the dynamics of the system forward in time using numerical approximation. The forward simulation uses only inputs of the control sequence, as solved for by the pseudospectral method.

CHAPTER 5

TRAJECTORIES INVOLVING FLYBACK

5.1 Flyback trajectories

- Details of bounds & guesses, with reasoning.
- Fuel optimised fly-back of the SPARTAN.

5.2 Sensitivity Analysis

- Details of bounds & guesses, with reasoning.
- Variation of L/D & ISP.
- Heat flux analysis

CHAPTER 6

FULL TRAJECTORY OPTIMISATION

add third stage, matrix and trajectory

- Details of bounds & guesses, with reasoning.
- Optimisation of the combined ascent and fly-back trajectories of the SPARTAN.
- Potential Abort Analysis
 - sonic boom estimation?
 - alternate trajectory recommendation?

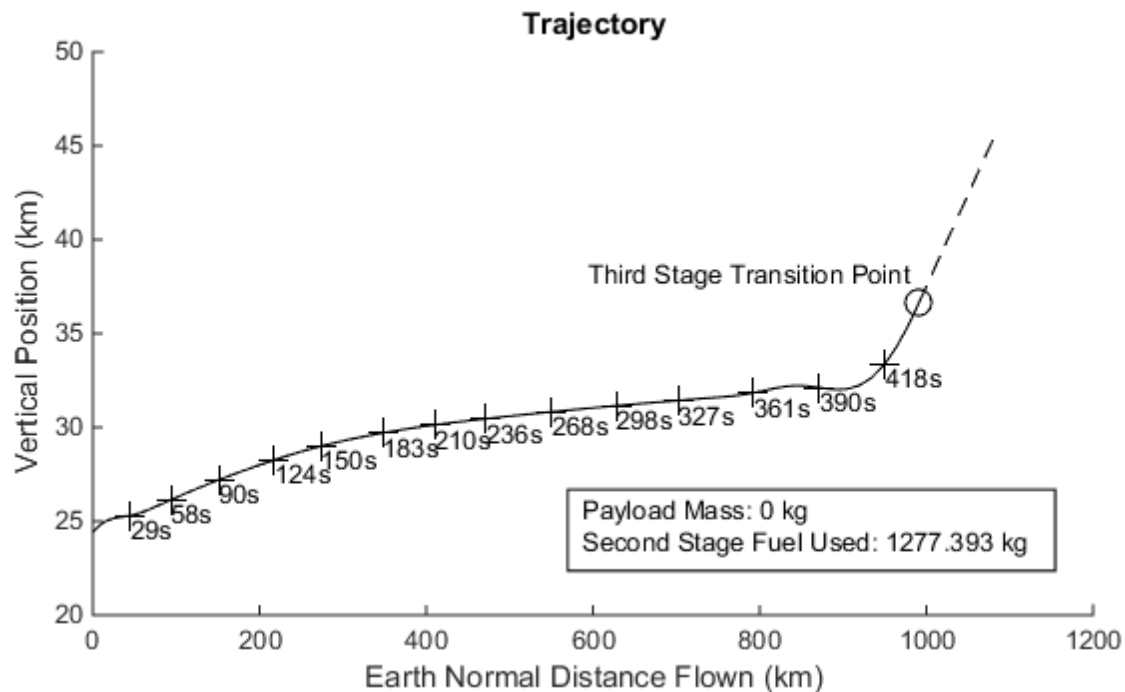


Figure 6.1

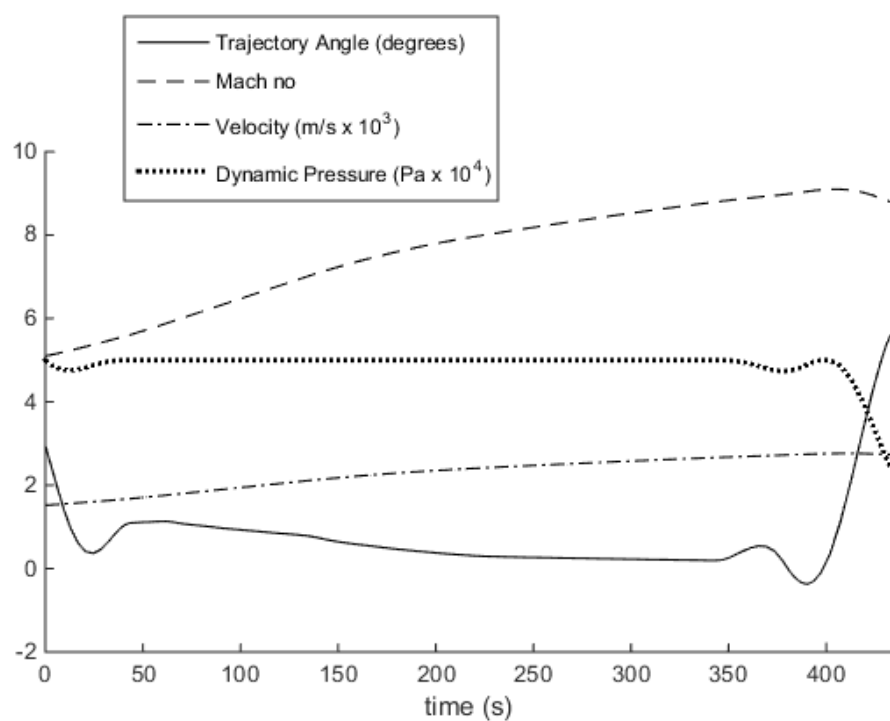


Figure 6.2

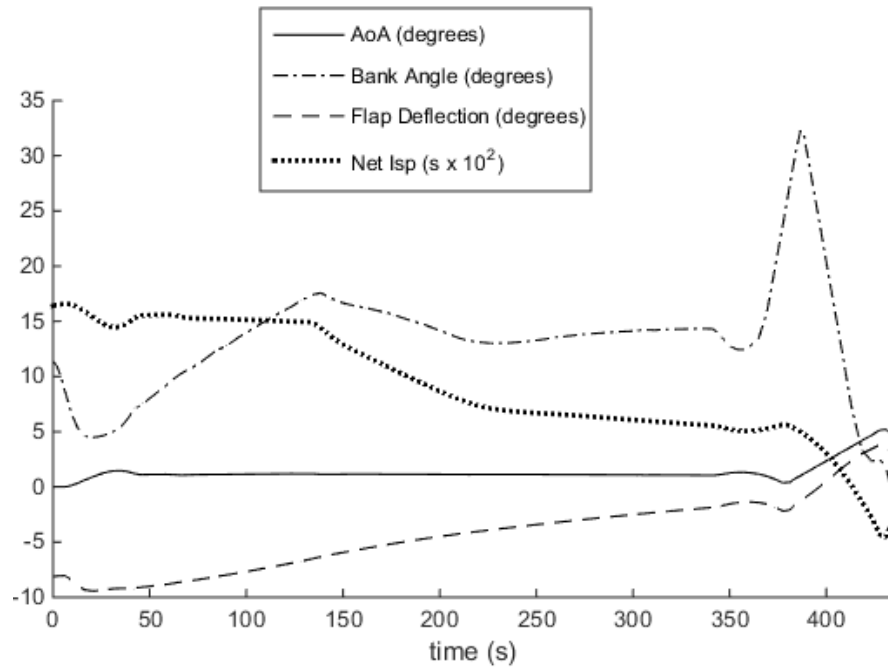


Figure 6.3

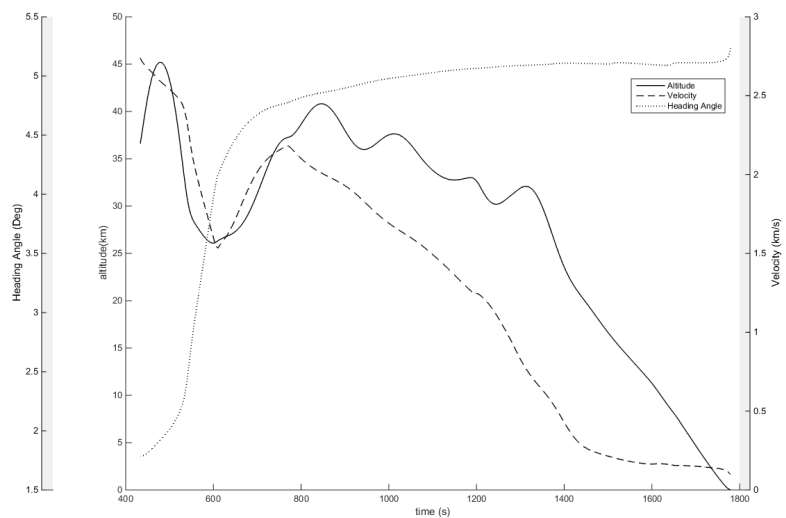


Figure 6.4

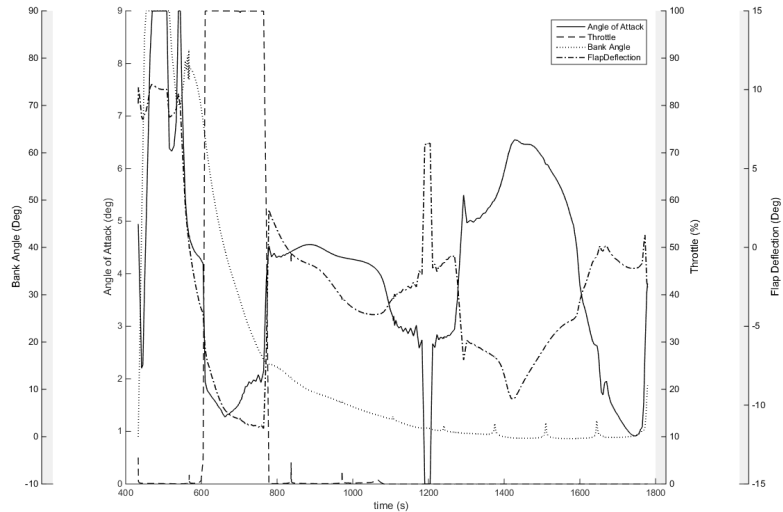


Figure 6.5

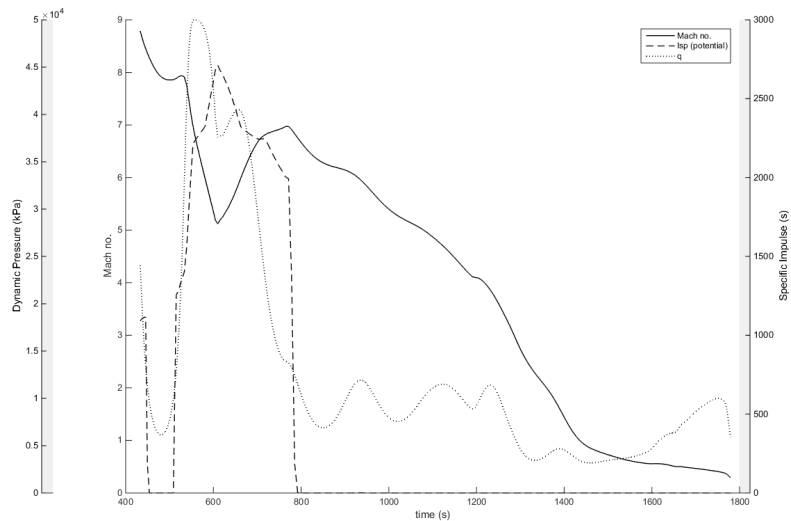


Figure 6.6

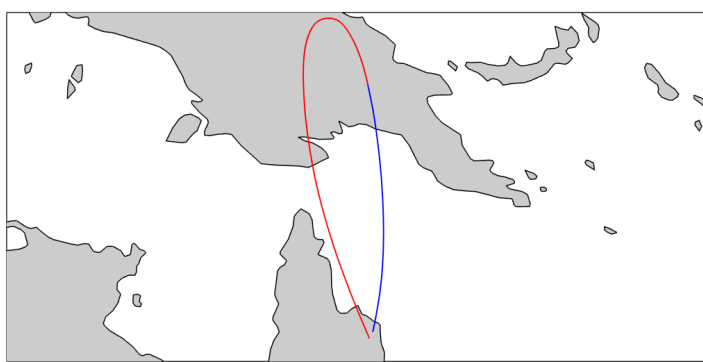


Figure 6.7

CHAPTER 7

THIRD STAGE SIZING STUDY

- I need to frame this well, so that it does not seem to invalidate my previous work
 - Variation of third stage design, changing width, length, thrust, CL and CD of the third stage, and recalculating optimised trajectories.
 - Determine the optimal sizing of the third stage
 - Analyse the variation in the optimal trajectory with variation in third stage design
 - could do a small cost analysis of the third stage using transcost, compare to payload-to-orbit

7.1 Third Stage Sizing

- diameter and length of centrebody changed independently
 - length varied
 - changed mass of cork cylinder
 - changed aerodynamics
 - changed total mass
 - diameter varied
 - changed mass of cork cylinder and C-C cone
 - changed aerodynamics
 - changed total mass
 - changed engine efficiency from nozzle size

CHAPTER 8

CONCLUSIONS

- The optimal ascent trajectory for the rocket-scramjet-rocket three stage launch system involves a pull-up before third stage release.
- The optimal fly-back of the SPARTAN involves several distinct stages, including a boost phase, skip phase and glide phase.
- Description of conclusions from the combined ascent/fly-back trajectory. The combined ascent and fly-back trajectory involves the SPARTAN banking during ascent, to mitigate the distance flown during the ascent trajectory.
- Summary of conclusions from third stage sizing analysis.

8.1 Recommendations for future work

- Design optimisation incorporating trajectory optimisation.
- Sizing of entire system for optimal cost efficiency.

LIBRARY

- [1] Xcor Aerospace. *Lynx Sspacecraft*. 2017. URL: <https://xcor.com/launch/lynx-spacecraft/> (visited on 11/30/2017).
- [2] Michael J. Aftosmis, Marian Nemec, and Susan E. Cliff. “Adjoint-based low-boom design with Cart3D”. In: *29th AIAA Applied Aerodynamics Conference 2011*. June. 2011, pp. 1–17. ISBN: 9781624101458. DOI: [doi:10.2514/6.2011-3500](https://doi.org/10.2514/6.2011-3500). URL: <http://www.scopus.com/inward/record.url?eid=2-s2.0-84872373928&partnerID=tZ0tx3y1>.
- [3] ARCA. *Haas2CA*. 2017. URL: <http://www.arcaspace.com/en/haas2c.htm> (visited on 12/01/2017).
- [4] Mokhtar S. Bazaraa, Hanif D. Sherali, and C. M. Shetty. *Nonlinear Programming: Theory and Algorithms*. John Wiley & Sons, 2013.
- [5] Nazareth Bedrossian, Bastion Technologies, and Louis Nguyen Nasa. “Zero Propellant Maneuvre Flight Results For 180 Degree ISS Rotation”. In: *20th International Symposium on Space Flight Dynamics*. Annapolis, MD, 2007.
- [6] F. S. Billig. “Research on supersonic combustion”. In: *Journal of Propulsion and Power* 9.4 (1993), pp. 499–514. ISSN: 0748-4658. DOI: [10.2514/3.23652](https://doi.org/10.2514/3.23652).
- [7] Pt Boggs and Jw Tolle. “Sequential quadratic programming for large-scale nonlinear optimization”. In: *Journal of Computational and Applied Mathematics* 124.1-2 (2000), pp. 123–137. ISSN: 03770427. DOI: [10.1016/S0377-0427\(00\)00429-5](https://doi.org/10.1016/S0377-0427(00)00429-5). URL: <http://linkinghub.elsevier.com/retrieve/pii/S0377042700004295> \$ \backslash http://www.sciencedirect.com/science/article/pii/S0377042700004295\$.
- [8] R Bulirsch et al. “Combining direct and indirect methods in optimal control: Range maximization of a hang glider”. In: *Optimal Control (Calculus of Variations, Optimal Control Theory and Numerical Methods)* 111 (1993), pp. 273–288.

- [9] Dong Chai et al. “Boost-skipping trajectory optimization for air-breathing hypersonic missile”. In: *Aerospace Science and Technology* 46 (2015), pp. 506–513. ISSN: 12709638. DOI: [10.1016/j.ast.2015.09.004](https://doi.org/10.1016/j.ast.2015.09.004). URL: <http://dx.doi.org/10.1016/j.ast.2015.09.004>.
- [10] Stephen Cook and Uwe Hueter. “NASA’s Integrated Space Transportation Plan 3rd generation reusable launch vehicle technology update”. In: *Acta Astronautica* 53.4-10 (2003), pp. 719–728. ISSN: 00945765. DOI: [10.1016/S0094-5765\(03\)00113-9](https://doi.org/10.1016/S0094-5765(03)00113-9).
- [11] Edward T. Curran. “Scramjet Engines: The First Forty Years”. In: *Journal of Propulsion and Power* 17.6 (2001), pp. 1138–1148. ISSN: 0748-4658. DOI: [10.2514/2.5875](https://doi.org/10.2514/2.5875).
- [12] Christopher L. Darby, William W. Hager, and Anil V. Rao. “Direct Trajectory Optimization Using a Variable Low-Order Adaptive Pseudospectral Method”. In: *Journal of Spacecraft and Rockets* 48.3 (2011), pp. 433–445. ISSN: 0022-4650. DOI: [10.2514/1.52136](https://doi.org/10.2514/1.52136).
- [13] M. Diehl et al. “Fast direct multiple shooting algorithms for optimal robot control”. In: *Lecture Notes in Control and Information Sciences* 340 (2006), pp. 65–93. ISSN: 01708643. DOI: [10.1007/978-3-540-36119-0_4](https://doi.org/10.1007/978-3-540-36119-0_4).
- [14] F. Fahroo and I.M. Ross. “Direct trajectory optimization by a Chebyshev pseudospectral method”. In: *Proceedings of the 2000 American Control Conference*. Vol. 6. Chicago, IL, 2000, pp. 3860–3864. ISBN: 0-7803-5519-9. DOI: [10.1109/ACC.2000.876945](https://doi.org/10.1109/ACC.2000.876945).
- [15] Fariba Fahroo and I. Michael Ross. “Costate Estimation by a Legendre Pseudospectral Method”. In: *Journal of Guidance, Control, and Dynamics* 24.2 (2001), pp. 270–277. ISSN: 0731-5090. DOI: [10.2514/2.4709](https://doi.org/10.2514/2.4709).
- [16] I. Fahroo F. & Ross. “Computational Optimal Control By Spectral Collocation With Differential Inclusion ..” In: *1999 Flight Mechanics Symposium*. May. 1999, pp. 185–200.
- [17] Giorgio Fasano and Janos Pinter. *Modelling and Optimisation in Space Engineering*. New York, NY: Springer, 2013. DOI: [10.1007/978-1-4614-4469-5](https://doi.org/10.1007/978-1-4614-4469-5).
- [18] Kevin W. Flaherty, Katherine M. Andrews, and Glenn W. Liston. “Operability Benefits of Airbreathing Hypersonic Propulsion for Flexible Access to Space”. In: *Journal of Spacecraft and Rockets* 47.2 (2010), pp. 280–287. ISSN: 0022-4650. DOI: [10.2514/1.43750](https://doi.org/10.2514/1.43750). URL: <http://arc.aiaa.org/doi/abs/10.2514/1.43750>.
- [19] Sholto O. Forbes-Spyratos et al. “Trajectory Design of a Rocket-Scramjet-Rocket Multi-Stage Launch System”. In: *Journal of Spacecraft and Rockets - Under Consideration* TBD (2018).
- [20] S.O. Forbes-Spyratos et al. “Trajectory design of a rocket-scramjet-rocket multi-stage launch system”. In: *21st AIAA International Space Planes and Hypersonics Technologies Conference, Hypersonics 2017*. Xiamen, China, 2017. ISBN: 9781624104633.

- [21] Adam Gilmour. *ROCKET STARTUP SHOOTS FOR THE STARS WITH AUD 5 MILLION (USD 3 . 7 MILLION) SERIES A FUNDING*. 2017.
- [22] Qi Gong, I. Michael Ross, and Friba Fahroo. “Costate Computation by a Chebyshev Pseudospectral Method”. In: *Journal of Guidance, Control, and Dynamics* 33.2 (2010), pp. 623–628. ISSN: 0731-5090. DOI: [10.2514/1.45154](https://doi.org/10.2514/1.45154).
- [23] Barry Mark Hellman. *Comparison of Return to Launch Site Options for a Reusable Booster Stage*. Tech. rep. Space Systems Design Lab, Georgia Institute of technology, 2005, pp. 1–18.
- [24] Mark Hempsell. *SKYLON Users Manual*. Reaction Engines Limited, 2014.
- [25] Horizon. *Black Arrow 2*. 2017. URL: <http://www.horizonsas.com/products/> (visited on 12/01/2017).
- [26] Thomas Jazra, Dawid Preller, and Michael K. Smart. “Design of an Airbreathing Second Stage for a Rocket-Scramjet-Rocket Launch Vehicle”. In: *Journal of Spacecraft and Rockets* 50.2 (2013), pp. 411–422. ISSN: 0022-4650. DOI: [10.2514/1.A32381](https://doi.org/10.2514/1.A32381). URL: <http://arc.aiaa.org/doi/abs/10.2514/1.A32381>.
- [27] D. Jezewski. “An Optimal, Analytic Solution to the Linear-Gravity, Constant-Thrust Trajectory Problem”. In: *Journal of Spacecraft and Rockets* July (1971), pp. 793–796.
- [28] Scott Josselyn and I Michael Ross. “Rapid Verification Method for the Trajectory Optimization of Reentry Vehicles”. In: *Notes* 26.3 (2002), pp. 505–508. ISSN: 0731-5090. DOI: [10.2514/2.5074](https://doi.org/10.2514/2.5074).
- [29] Rl Kimmel et al. “HIFiRE-5 flight vehicle design”. In: *AIAA paper* July (2010), pp. 1–17. DOI: [10.2514/6.2010-4985](https://doi.org/10.2514/6.2010-4985). URL: <http://arc.aiaa.org/doi/pdf/10.2514/6.2010-4985>.
- [30] Heinz-Otto Kreiss and Joseph Oliger. “Comparison of accurate methods for the integration of hyperbolic equations”. In: *Tellus A* 1971 (1972). ISSN: 0280-6495. DOI: [10.3402/tellusa.v24i3.10634](https://doi.org/10.3402/tellusa.v24i3.10634).
- [31] *Kuai Zhou (Fast Vessel)*. URL: <https://chinaspacereport.com/launch-vehicles/kuaizhou/> (visited on 12/01/2017).
- [32] Markus Kuhn et al. “Innovative European Launcher Concept SMILE”. In: *21st AIAA International Space Planes and Hypersonics Technologies Conference* March (2017), pp. 1–14. DOI: [10.2514/6.2017-2441](https://doi.org/10.2514/6.2017-2441). URL: <https://arc.aiaa.org/doi/10.2514/6.2017-2441>.
- [33] Huifeng Li et al. “Footprint problem with angle of attack optimization for high lifting reentry vehicle”. In: *Chinese Journal of Aeronautics* 25.2 (2012), pp. 243–251. ISSN: 10009361. DOI: [10.1016/S1000-9361\(11\)60384-1](https://doi.org/10.1016/S1000-9361(11)60384-1). URL: [http://dx.doi.org/10.1016/S1000-9361\(11\)60384-1](http://dx.doi.org/10.1016/S1000-9361(11)60384-1).

- [34] Ping Lu. “Inverse dynamics approach to trajectory optimization for an aerospace plane”. In: *Journal of Guidance, Control, and Dynamics* 16.4 (1993), pp. 726–732. ISSN: 0731-5090. DOI: [10.2514/3.21073](https://doi.org/10.2514/3.21073). URL: <http://arc.aiaa.org/doi/abs/10.2514/3.21073>.
- [35] J W Magee Bruno, T.J., Friend, D. G., Huber, M.L., Laesecke, A., Lemmon, E.W., McLinden, M.O., Perkins, R.A., Baranski, J., Widegren, J.A. *Thermophysical Properties Measurements and Models for Rocket Propellant RP-1: Phase I, NIST- IR 6644*, National Institute of Standards and Technology (U.S.) Tech. rep. 2006.
- [36] Unmeel Mehta et al. “Skylon Aerospace Plane and Its Aerodynamics and Plumes”. In: *Journal of Spacecraft and Rockets* 53.2 (2016), pp. 340–353. ISSN: 0022-4650. DOI: [10.2514/1.A33408](https://doi.org/10.2514/1.A33408). URL: <http://arc.aiaa.org/doi/10.2514/1.A33408>.
- [37] Unmeel B. Mehta and Jeffrey V. Bowles. “Two-Stage-to-Orbit Spaceplane Concept with Growth Potential”. In: *Journal of Propulsion and Power* 17.6 (2001), pp. 1149–1161. ISSN: 0748-4658. DOI: [10.2514/2.5886](https://doi.org/10.2514/2.5886).
- [38] Claas Michalik, Ralf Hannemann, and Wolfgang Marquardt. “Incremental single shooting - A robust method for the estimation of parameters in dynamical systems”. In: *Computers & Chemical Engineering* 33.7 (2009), pp. 1298–1305. ISSN: 00981354. DOI: [10.1016/j.compchemeng.2009.02.002](https://doi.org/10.1016/j.compchemeng.2009.02.002). URL: <http://linkinghub.elsevier.com/retrieve/pii/S0098135409000544>.
- [39] Nathan D. Moshman and Ronald J. Proulx. “Range Improvements in Gliding Reentry Vehicles from Thrust Capability”. In: *Journal of Spacecraft and Rockets* 51.5 (2014), pp. 1681–1694. ISSN: 0022-4650. DOI: [10.2514/1.A32764](https://doi.org/10.2514/1.A32764). URL: <http://arc.aiaa.org/doi/10.2514/1.A32764>.
- [40] NASA. *U.S. Standard Atmosphere, 1976*. U.S. Government Printing Office, Washington, D.C., 1976, pp. 1–243. URL: <http://ntrs.nasa.gov/archive/nasa/casi.ntrs.nasa.gov/19770009539.pdf>.
- [41] J.R. Olds and I.a. Budianto. “Constant Dynamic Pressure Trajectory Simulation with POST”. In: *Aerospace Sciences Meeting & Exhibit*. Reno, NV, 1998, pp. 1–13. DOI: [10.2514/6.1998-302](https://doi.org/10.2514/6.1998-302). URL: <http://citeseerx.ist.psu.edu/viewdoc/download?doi=10.1.1.25.6506&rep=rep1&type=pdf>.
- [42] Orbital Access. *The Orbital 500R*. 2017. URL: <http://www.orbital-access.com/the-orbital-500/> (visited on 12/01/2017).
- [43] DARPA Outreach. *DARPA Picks Design for Next-Generation Spaceplane*. 2017. URL: <https://www.darpa.mil/news-events/2017-05-24> (visited on 11/16/2017).

- [44] A Paull, R.J Stalker, and D Mee. “Thrust Measurements of a Complete Axisymmetric Scramjet in an Impulse Facility”. In: *5TH INTERNATIONAL AEROSPACE PLANES AND HYPERSONICS TECHNOLOGIES CONFERENCE*. 1993.
- [45] Richard W. Powell et al. “Ascent performance of an air-breathing horizontal-takeoff launch vehicle”. In: 14.4 (1991), pp. 834–839. ISSN: 0731-5090. DOI: [10.2514/3.20719](https://doi.org/10.2514/3.20719).
- [46] Dawid Preller and Michael K Smart. “Longitudinal Control Strategy for Hypersonic Accelerating Vehicles”. In: *Journal of Spacecraft and Rockets* 52.3 (2015), pp. 1–6. ISSN: 0022-4650. DOI: [10.2514/1.A32934](https://doi.org/10.2514/1.A32934). URL: <http://dx.doi.org/10.2514/1.A32934>.
- [47] Dawid Preller and Michael K Smart. “Scramjets for Reusable Launch of Small Satellites”. In: *20th AIAA International Space Planes and Hypersonic Systems and Technologies Conference*. July. Glasgow, Scotland, 2015, pp. 1–23. DOI: [10.2514/6.2015-3586](https://doi.org/10.2514/6.2015-3586).
- [48] Dawid Preller and Michael K. Smart. “Scramjets for Reusable Launch of Small Satellites”. In: *Journal of Spacecraft and Rockets Advance On* (2017), pp. 1–13. ISSN: 0022-4650. DOI: [10.2514/6.2015-3586](https://doi.org/10.2514/6.2015-3586). URL: <http://arc.aiaa.org/doi/10.2514/6.2015-3586>.
- [49] Anil V. Rao et al. “Algorithm 902”. In: *ACM Transactions on Mathematical Software* 37.2 (2010), pp. 1–39. ISSN: 00983500. DOI: [10.1145/1731022.1731032](https://doi.org/10.1145/1731022.1731032).
- [50] S. Tauqeer Ul Islam Rizvi, Lin Shu He, and Da Jun Xu. “Optimal trajectory and heat load analysis of different shape lifting reentry vehicles for medium range application”. In: *Defence Technology* 11.4 (2015), pp. 350–361. ISSN: 22149147. DOI: [10.1016/j.dt.2015.06.003](https://doi.org/10.1016/j.dt.2015.06.003). URL: <http://dx.doi.org/10.1016/j.dt.2015.06.003>.
- [51] Rocket Lab. *Electron*. 2016. URL: <https://www.rocketlabusa.com/electron/> (visited on 11/30/2017).
- [52] RocketCrafters. *Intrepid-1*. 2017. URL: <http://rocketcrafters.space/products-services/intrepid-launcher-family/intrepid-1/> (visited on 12/01/2017).
- [53] Paul O Romere, David B Kanipe, and James C Youngt. “Space Shuttle Entry Aerodynamic Comparisons of Flight 1 with Preflight Predictions”. In: *Journal of Spacecraft and Rockets* (1983).
- [54] I M Ross and F Fahroo. “A direct method for solving nonsmooth optimal control problems”. In: *Proceedings of the 2002 {IFAC World Congress}* (2002).
- [55] P E Rutquist and M M Edvall. “PROPT - Matlab Optimal Control Software”. In: *Tomlab Optimization Inc* 260 (2010), pp. –.
- [56] Michael Smart. *Scramjet Inlets*. Tech. rep. 9. The University of Queensland, 2010, pp. 1–24. DOI: [10.2514/5.9781600866609.0447.0511](https://doi.org/10.2514/5.9781600866609.0447.0511).

- [57] Michael K Smart and Edward G Ruf. “Free-jet testing of a {REST} scramjet at off-design conditions”. In: *Collection of Technical Papers - 25th AIAA Aerodynamic Measurement Technology and Ground Testing Conference* AIAA 2006-2955 (2006), pp. 190–201. DOI: [doi : 10.2514/6.2006-2955](https://doi.org/10.2514/6.2006-2955).
- [58] Michael K. Smart and Matthew R. Tetlow. “Orbital Delivery of Small Payloads Using Hypersonic Airbreathing Propulsion”. In: *Journal of Spacecraft and Rockets* 46.1 (2009), pp. 117–125. ISSN: 0022-4650. DOI: [10.2514/1.38784](https://doi.org/10.2514/1.38784). URL: <http://arc.aiaa.org/doi/abs/10.2514/1.38784>.
- [59] Thomas J. Sooy and Rebecca Z. Schmidt. “Aerodynamic Predictions, Comparisons, and Validations Using Missile DATCOM (97) and Aeroprediction 98 (AP98)”. In: *Journal of Spacecraft and Rockets* 42.2 (2005), pp. 257–265. ISSN: 0022-4650. DOI: [10.2514/1.7814](https://doi.org/10.2514/1.7814).
- [60] Space Exploration technologies. *Falcon 1 Launch Vehicle Payload Users Guide*. Tech. rep. Hawthorne, CA: Space Exploration Technologies, 2008, p. 65.
- [61] O. Stryk and R. Bulirsch. “Direct and indirect methods for trajectory optimization”. In: *Annals of Operations Research* 37 (1992), pp. 357–373. ISSN: 0254-5330. DOI: [10.1007 / BF02071065](https://doi.org/10.1007/BF02071065).
- [62] S. Subchan. “A Direct Multiple Shooting for the Optimal Trajectory of Missile Guidance”. In: *Proceedings of the IEEE International Conference on Control Applications* 2.4 (2008), pp. 268–273. ISSN: 1085-1992. DOI: [10.1109/CCA.2008.4629675](https://doi.org/10.1109/CCA.2008.4629675).
- [63] M Suraweera and M K Smart. “Shock Tunnel Experiments with a Mach 12 {REST} Scramjet at Off-Design Conditions”. In: *Journal of Propulsion and Power* 25.3 (2009), pp. 555–564. ISSN: 0748-4658. DOI: [10.2514/1.37946](https://doi.org/10.2514/1.37946).
- [64] George Sutton and Oscar Biblarz. *Rocket propulsion Elements*. 8th. John Wiley & Sons, 2010, p. 67.
- [65] M R Tetlow et al. “Comparison of Glideback and Flyback Boosters”. In: *Journal of Spacecraft and Rockets* 38.5 (1992), pp. 752–758. ISSN: 0022-4650. DOI: [10.2514/2.3742](https://doi.org/10.2514/2.3742). URL: <http://dx.doi.org/10.2514/2.3742>.
- [66] Bailing Tian and Qun Zong. “Optimal guidance for reentry vehicles based on indirect Legendre pseudospectral method”. In: *Acta Astronautica* 68.7-8 (2011), pp. 1176–1184. ISSN: 00945765. DOI: [10.1016/j.actaastro.2010.10.010](https://doi.org/10.1016/j.actaastro.2010.10.010). URL: <http://linkinghub.elsevier.com/retrieve/pii/S0094576510003899>.
- [67] Charles Trefny. “An Air-Breathing Concept Launch Vehicle for Single-Stage-to-Orbit”. In: *35th Joing Propulsion Conference and Exhibit*. May. Los Angeles, CA, 1999.

- [68] Takeshi Tsuchiya and Takashige Mori. “Optimal Design of Two-Stage-To-Orbit Space Planes with Airbreathing Engines”. In: *Journal of Spacecraft and Rockets* 42.1 (2005), pp. 90–97. ISSN: 0022-4650. DOI: [10.2514/1.8012](https://doi.org/10.2514/1.8012).
- [69] Richard Varvill and Alan Bond. “The SKYLON Spaceplane”. In: *Journal of the British Interplanetary Society* 57.October 1995 (2004), pp. 22–32. ISSN: 0007084X.
- [70] Richard Varvill and Alan Bond. “THE SKYLON SPACEPLANE : PROGRESS TO REALISATION”. In: *Journal of the British Interplanetary Society* 61 (2008), pp. 412–418.
- [71] Vector Space. *Vector Launch Vehicle Family*. 2017. URL: <https://vectorspacesystems.com/technology/> (visited on 12/01/2017).
- [72] VirginOrbit. *LauncherOne*. 2017. URL: <https://virginorbit.com/> (visited on 11/30/2017).
- [73] Alan W. Wilhite et al. “Technology and staging effects on two-stage-to-orbit systems”. In: *Journal of Spacecraft and Rockets* 31.1 (1991), pp. 31–39. ISSN: 0022-4650. DOI: [10.2514/3.26399](https://doi.org/10.2514/3.26399).
- [74] Zero2Infinity. *Bloostar*. 2016. URL: <http://www.zero2infinity.space/bloostar/> (visited on 11/30/2017).
- [75] Jiang Zhao and Rui Zhou. “Reentry trajectory optimization for hypersonic vehicle satisfying complex constraints”. In: *Chinese Journal of Aeronautics* 26.6 (2013), pp. 1544–1553. ISSN: 10009361. DOI: [10.1016/j.cja.2013.10.009](https://doi.org/10.1016/j.cja.2013.10.009). URL: <http://dx.doi.org/10.1016/j.cja.2013.10.009>.

APPENDIX A

CART3D RESULTS

A.1 Engine-On Plume Check

-simulate engine-on conditions to check that the plumes do not adversely affect the tail of the vehicle
(justify that I can just remove engines/boattail)

-Mach 5,7,9 at 50kPa

A.2 CART3D Results

-include mesh here

APPENDIX A. CART3D RESULTS

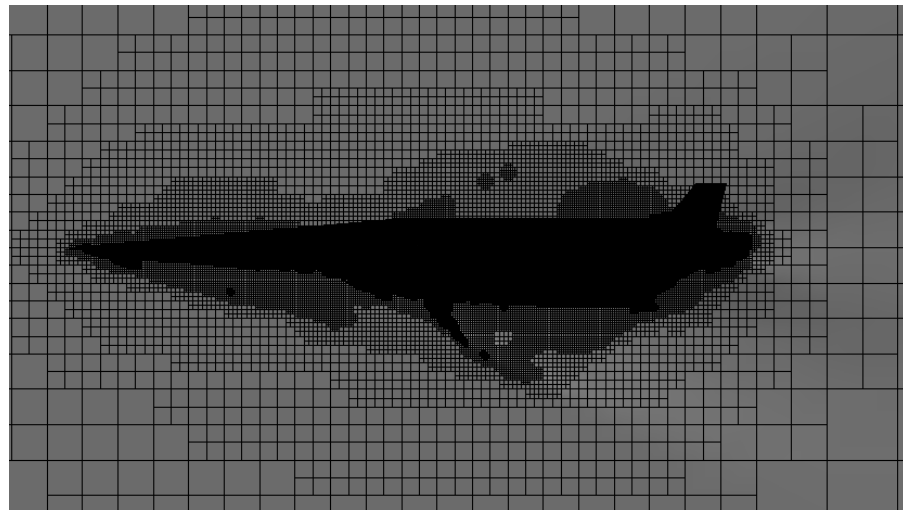


Figure A.1

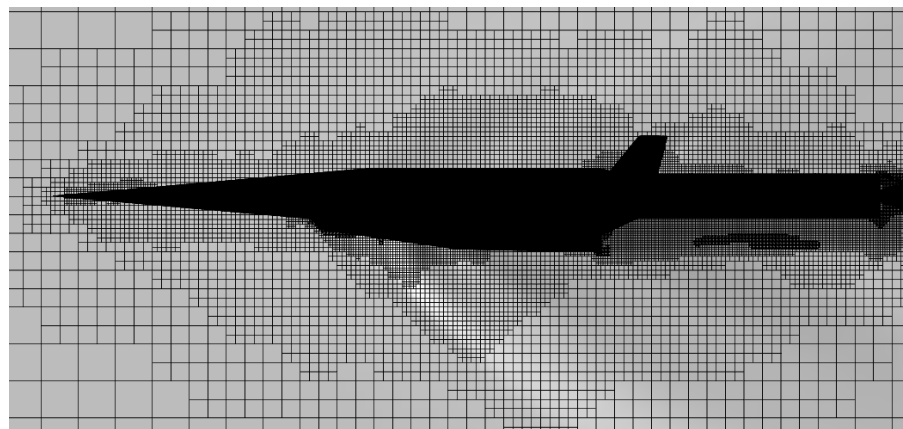


Figure A.2: Mesh generated by CART3D around the SPARTAN and first stage vehicles.

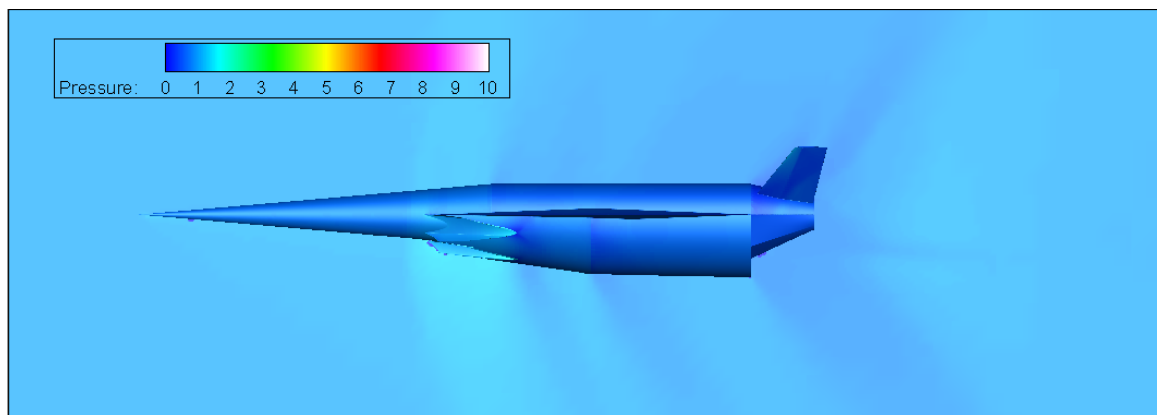


Figure A.3: CART3D flow result for the SPARTAN, at Mach 1.1, 6° angle of attack.

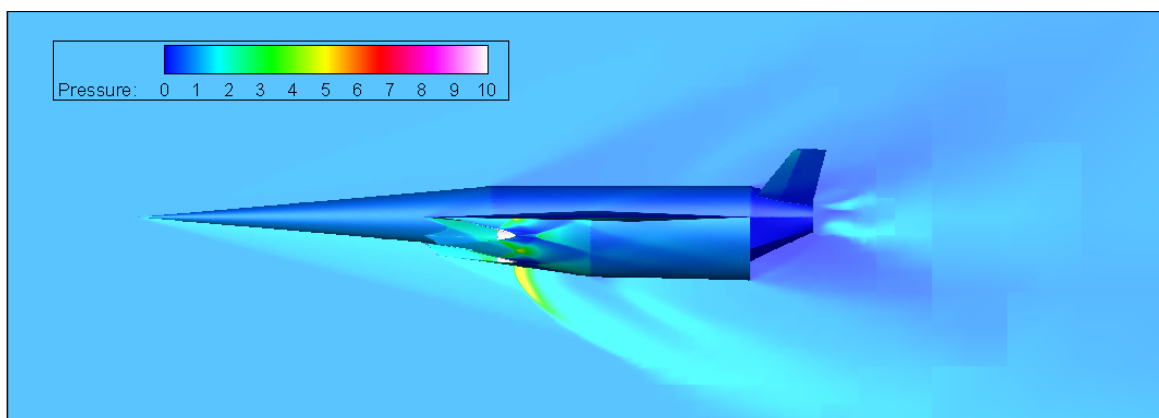


Figure A.4: CART3D flow result for the SPARTAN, at Mach 3, 6° angle of attack.